EVALUATING A MEAT AND BONE MEAL BIOCHAR AMENDMENT FOR IMMOBILIZATION OF ZINC IN A SMELTER IMPACTED SOIL

A Thesis submitted to the College of Graduate Studies and Research
in Partial Fulfillment of the Requirements
for the Degree of Master of Science
in the Department of Soil Science
University of Saskatchewan
Saskatoon

By
Aaron R. Betts

PERMISSION TO USE

In presenting this thesis in partial fulfilment of the requirements for a Postgraduate degree from the University of Saskatchewan, I agree that the Libraries of this University may make it freely available for inspection. I further agree that permission for copying of this thesis in any manner, in whole or in part, for scholarly purposes may be granted by the professor or professors who supervised my thesis work or, in their absence, by the Head of the Department or the Dean of the College in which my thesis work was done. It is understood that any copying or publication or use of this thesis or parts thereof for financial gain shall not be allowed without my written permission. It is also understood that due recognition shall be given to me and to the University of Saskatchewan in any scholarly use which may be made of any material in my thesis.

Requests for permission to copy or to make other use of material in this thesis in whole or part should be addressed to:

Head, Department of Soil Science
University of Saskatchewan
Saskatoon, Saskatchewan
Canada, S7N 5A8

ABSTRACT

Non-ferrous smelter emissions have prompted revegetation efforts near the border towns of Flin Flon, Manitoba and Creighton, Saskatchewan to facilitate regrowth of the surrounding boreal forest. Previously, several soil amendments were tested for plant response in soils from the smelter-impacted area and one amendment, a pyrolyzed meat and bone meal (MBM) biochar, was of particular interest because of its potential to immobilize Zn.

Hydroxyapatite (HAP), with a small degree of carbonate substitution, was identified as the major component of the MBM biochar. The solubility of this Ca-mineral was pH dependent, with dissolution occurring at pH 6.3; consequently, adsorption experiments were performed at a slightly lower pH (6.1 ± 0.1). Zinc adsorption kinetics were bi-phasic and could be modeled using the Elovich equation, suggesting a diffusion limited reaction likely related to material aggregation. Adsorption also was modeled using the Langmuir equation, which indicated a moderate affinity of the biochar for Zn and an adsorption maximum of 0.650 mmol Zn g^{-1}. Synchrotron-based Zn *K*-edge x-ray absorption spectroscopy (XAS) indicated an inner-sphere monodentate, tetrahedral bonding of Zn to phosphate groups in the MBM biochar. This was consistent with Zn adsorbed to a HAP standard, indicating that the same sorption mechanism was involved.

The ability of MBM biochar to affect Zn speciation in soils was investigated using four soils from four locations in the smelter-impacted region around Flin Flon. A 1:10 (w/w) mixture of the MBM and soil was suspended in 200-mL deionized water (pH 6.1 ± 0.1) and equilibrated for 30 d. Whereas all the soils showed a decrease in extractable Zn following equilibration, only one exhibited a change in Zn speciation—with ca. 25% of the Zn adsorbed onto the MBM biochar. Ore-derived minerals were present in all soils and strong backscattering made identification of minor Zn species difficult. However, using microprobe-based x-ray absorption near edge structure (XANES) spectroscopy, several minor Zn species were identified; including hopeite, a $ZnPO_4$ mineral. The presence of both hopeite and adsorbed Zn are indicative of a direct Zn-phosphate reaction. These results indicate that, under certain condition, MBM biochar can be an effective soil amendment.

ACKNOWLEDGMENTS

I am grateful for the guidance from each of my co-supervisors, Drs. Derek Peak and Richard Farrell both in the lab and in writing. They taught me much about the research process and professional development. I owe Dr. Derek Peak a great deal of appreciation for his expertise in soil chemistry and spectroscopy, without which, I would not have been able to learn so much about spectroscopic methods. I also would like to thank to my graduate advisory committee, Drs. Steve Siciliano and Fran Walley, and my external examiner, Dr. Alexey Klyashtorin, for their willingness to work under a tight deadline so that I could pursue an excellent job opportunity. I would also like to thank Dr. Siciliano for giving me the unique experience of a high-arctic fieldwork expedition in the summer of 2010.

I would like to thank HudBay Minerals, Inc. and the *Flin Flon/Creighton Green Project* for their cooperation on this research and for welcoming the Soil Science department to Flin Flon. Thank you to all of the grad students involved in the Flin Flon/Creighton revegetation project: Jen, Amanda, Catlan, Jordan, Cass and Kaitlin, for making the fieldwork fun and the exchange of research ideas. I would like to thank the 3D13, 5C13 and 5E19 lab groups and technicians, you made lab work more enjoyable and working in the department all the better. Thank you to my office-mates, particularly Zaho Matheos, Tom King and Samiran Banerjee, whose banter and coffee breaks made the office an enjoyable place to work. A special thanks to Jordan and Dr. Peak for their advice and aptitude at using the endstations of the CLS—and who kept me awake during long nights at the CLS.

I would like to thank Titan Clean Energy Inc., for providing the material used in this study. The project was supported by a Natural Science and Engineering Research Council (NSERC) Collaborative Research and Development (CRD) grant with HudBay Minerals Inc. (formerly Hudson Bay Mining and Smelting Co., Limited). Additional support was provided through the Saskatchewan Ministry of Agriculture Strategic Research Program—Soils and Environment and an Entrance Scholarship from the Department of Soil Science. I also acknowledge the financial support from the Department of Soil Science, the College of Agriculture and Bioresources and the College of Graduate Studies and Research at the University of Saskatchewan. Without their support, this project would not have been possible.

Dedication

I dedicate this work to my family. I could not have done this without them.

TABLE OF CONTENTS

LIST OF TABLES

LIST OF FIGURES

LIST OF ABBREVIATIONS

Å	angstrom
AAS	atomic absorption spectroscopy
ANOVA	analysis of variance
ATR-FTIR	attenuated total reflectance fourier-transform infrared reflectance
b	sorption maximum
BET	Brunauer-Emmett-Teller
BSE	bovine spongiform encephalopathy
c_f	final concentration of sorbate in solution (mmol L^{-1})
$CaHPO_4$	brushite
$Ca(H_2(PO_4)_2$	Calcium dihydrogen phosphate
$CaCO_3$	calcite
CLS	Canadian light source
CN	coordination number
DI	deionized
EXAFS	extended x-ray absorption fine structure
FT	Fourier transformation
HAP	Hydroxyapatite [$Ca_{10}(PO_4)_6(OH)_2$]
HIM	hydroxy-interlayered material
HSD	honestly significant difference
HXMA	hard x-ray micro-analysis
I_0	incoming x-rays
IAP	ion activity product
ICP-MS	inductively coupled plasma-mass spectrometry
IR	infrared
K_{sp}	solubility-product constant
k	Langmuir equation constant
LC	linear combination
MBM	meat and bone meal
$Pb_5(PO_4)_3Cl$	pyromorphite
pKa_1	acid dissociation constant, first proton loss
q	mass of sorbate per mass of sorbent (mmol g^{-1})
R^2	coefficient of determination
R	Fourier transform radial distance
VESPERS	very sensitive elemental and structural probe employing radiation from a synchrotron
XANES	x-ray absorption near edge structure
XAS	x-ray absorption spectroscopy
XRD	x-ray diffraction
XRF	x-ray fluorescence
Z	atomic number
Zn-Al LDH	Zinc-Aluminum layered double hydroxide mineral
Zn,CuS	sphalerite

$Zn_3(PO_4)_2$	Zn phosphate
Zn_2SiO_4	willemite
$Zn_4Si_2O_7(OH)_2 \bullet H_2O$	hemimorphite
$ZnFe_2O_4$	franklinite
α	primary Elovich model coefficient
β	secondary Elovich model coefficient
μXANES	micro x-ray absorption near edge structure
μXRD	micro x-ray diffraction
μXRF	micro x-ray fluorescence
σ^2	Debeye-waller factor
χ^2	residual from linear combination modeling
Ω	ohm

1.0 INTRODUCTION

In the boreal forest loss of vegetation and soil quality are common where industries mine and harvest valuable commodities. In Canada, one such area surrounds the provincial border towns of Creighton, Saskatchewan and Flin Flon, Manitoba, where mining for non-ferrous metals has occurred since the early 20th century. HudBay Minerals Inc., formerly Hudson Bay Mining and Smelting Co. Limited, has been operational in the Flin Flon/Creighton area since 1930. The smelting and refining complex extracted copper (Cu), zinc (Zn) and cadmium (Cd) through heating and chemical treatments of sulphide ore. Over the facility's life span, the smelting and refining operations have produced emissions of sulfur dioxide (SO_2) and particulates containing Zn, Cu, lead (Pb), arsenic (As), Cd and mercury (Hg). High metal concentrations have been observed in the surface organic layer within 5 km of the smelting stack (Zoltai, 1988), but smelter-derived metals have been identified in organic surface horizons as far as 100 km from the smelting facility (Henderson et al., 1999). However, the total metal concentration in surface soils decreases exponentially with distance from the stack and metal concentrations at depth (top of C horizon) only exceed natural concentrations within 10 km of the smelting stack (McMartin et al., 1997; Henderson et al., 1999). More recently, Cu-smelting operations were ceased in 2010 (HudBay Minerals Inc, 2010). Nevertheless, historic inputs have contributed enough stress to the surrounding forest that regrowth following natural forest fire disturbances has been retarded (Franzin et al., 1979).

Changes to the forest around Flin Flon/Creighton are similar to those surrounding many other non-ferrous smelting and metallurgy facilities around the world (Ginocchio, 2000; McMartin et al., 2002; Anderson et al., 2009). Kozlov and Zvereva (2007) have compiled a review of non-ferrous smelting and metallurgy facilities and found common historical patterns that result in vegetation loss and alteration of soil properties. Development of this phenomenon follows a common pattern beginning with a gradual decline in plant health from excessive pollution, accompanied by other human disturbances (usually clear

cutting) and concluded by a fire. Because vegetation recovery is suppressed by soil acidity and toxicity from smelter emissions, soils remain bare and suffer from erosion. This pattern may explain the ecosystem collapse in the Flin Flon/Creighton area. The forest was harvested for building material and fuel for early smelting operations in 1930. After nearly a decade of smelting activity, a severe fire cleared the forest in 1939 and since then, vegetation has been limited to stunted woody species and a metal-tolerant ecotype of colonial bent grass (*Agrostis capillaris*) (Winterhalder, 2003).

To prepare for eventual mine closure and facilitate forest revegetation across the Flin Flon/Creighton area, HudBay Minerals Inc. and the University of Saskatchewan Department of Soil Science developed a multi-disciplinary project to develop and assess options for revegetating the impacted land surrounding the smelter. The project, jointly funded by a Natural Science and Engineering Research Council (NSERC; Collaborative Research and Development program) with HudBay Minerals Inc., commenced in 2008 with a soil survey of the area and began to develop soil treatment strategies to increase revegetation success.

In 2010, soils were collected from three areas classified as: lime responsive with low total metals; lime unresponsive with high total metals; and lime responsive with high total metals. The soils were categorized by their responsiveness in terms of the quantity of plant growth following application of dolomitic limestone in the field. Soil amendments were tested for their plant growth response. Each amendment was applied with a base treatment of granular fertilizer and dolomitic limestone and included: montmorillonite; glauconite; zeolite; manure based compost; municipal compost; oat hull biochar; willow biochar; and a meat and bone meal (MBM) biochar. Treatments were applied to three soils and two separate plantings of tufted hairgrass (*Deschampsia cespitosa*) and American vetch (*Vicia americana*) grown from seed. Above ground biomass and root biomass of each species indicated a favorable and significant plant response from treatment with MBM biochar (Farrell, unpublished data, 2010). These results prompted the current study to determine if or how the MBM biochar was affecting metal speciation.

At high concentrations, and under acidic soil conditions, Zn can be highly toxic to plants due to its mobility in soil solution (Chaney, 1993). This along with high total soil Zn concentrations was a reason to suspect Zn as the strongest stressor on plant growth in Flin Flon/Creighton despite the common co-contamination of Cu, Cd, As, and Pb. Soil toxicity

studies weighed the influence of each contaminant in the smelter impacted soils and identified Zn toxicity as the primary restriction to plant growth (Sicilano, unpublished, 2010). Based on this finding, the guiding question for this thesis is: How does applying MBM biochar to soil affect Zn mobility and speciation?

Meat and bone meal (MBM) have been suggested for re-use as a readily available source of hydroxyapatite (HAP) mineral (Deydier et al., 2005)—a common calcium phosphate mineral that can immobilize multiple metals (Zn, Cu, Cd, Pb) in both contaminated soil and water (Hodson et al., 2001; Smiciklas et al., 2008; Dybowska et al., 2009). Many of these studies found immobilization via formation of metal phosphate minerals (Ma et al., 1994; Dybowska et al., 2009) or minor components of adsorbed Zn, which were attributed to a mixture of adsorbed and exchanged species (Ma et al., 1994; Xu et al., 1994; Cao et al., 2003; Sarret et al., 2004; Williams et al., 2011; Baker et al., 2012).

The overall objective of this study was to understand whether the MBM biochar directly influenced Zn speciation after a smelter-impacted soil was amended with MBM biochar. Methods are available to monitor Zn chemical forms, or species, indirectly through wet chemistry and directly through spectroscopy. The method of x-ray diffraction (XRD) spectroscopy has been used since the early 19th century and provides excellent information on structural changes of crystalline materials (Moore and Reynolds, 1989). The weakness of XRD is that it is only able to describe the structure of crystal species, whereas metal species in soils often occur as a mixture of solid and aqueous forms. Because both crystalline and non-crystalline forms of Zn can be directly observed by x–ray absorption spectroscopy (XAS), this method can potentially provide strong evidence of all Zn species in a soil. However, the interpretation for a heterogeneous sample is highly dependent on both quality of the data and ability of a library of standards to encompass all possible species.

This prompted the first two objectives: (i) confirm MBM biochar as a Zn sorbent and characterize its reactivity; and (ii) collect relevant species of Zn sorbed onto MBM biochar to add to the current library of Zn standards. This was achieved by first characterizing the physico–chemical properties of the MBM biochar. Given the composition, wet chemical sorption experiments provided pH, time, and sorbent conditions necessary for sorption to take place. Adsorbed MBM biochar solid was then recovered and Zn speciation after reaction

was detailed using Zn XAS. This combination of sorption experiments and XAS measurements has never before been used to characterize metal sorption with MBM biochar.

The MBM biochar was then applied in laboratory suspensions to a range of smelter impacted soils from the Flin Flon/Creighton area. The effect of MBM biochar was measured by observing the change in Zn species with x–ray absorption spectroscopy. The influence of amendment was monitored by determining the presence/absence of Zn-phosphate or Zn adsorbed to MBM biochar standards that had been collected in Chapter 4. By using Zn speciation, a cause and effect relationship between MBM biochar and Zn immobilization can be more clearly drawn in a heterogeneous soil system where many indirect factors could be influencing Zn mobility (e.g., soil pH; competing cations; CEC; solubility of different Zn precipitates).

The thesis begins with the Introduction (Chapter 1), which states the problem and provides background and rationale for the study. This is followed by a Literature Review (Chapter 2), which summarizes and evaluates the existing literature, provides a basis for the current research and highlights gaps in our knowledge base. This is followed by three research chapters that provide a characterization of the MBM biochar (Chapter 3), assess the effects of the MBM on Zn sorption and speciation (Chapter 4), and examine the impact of MBM biochar on Zn speciation in smelter-impacted soils from the Flin Flon/Creighton area (Chapter 5). Chapter 6 provides a synthesis of this research—highlighting conclusions and future research needs. A compilation of the references cited in Chapters 1–6 is provided in Chapter 7.

Additional information regarding a separate assessment of Zn reactivity with a willow biochar and characterization of a synthetic mineral standard is included in Appendix A. Site photos from field sampling positions and brief descriptions of each position are included in Appendix B.

2.0 LITERATURE REVIEW

2.1 Non-Ferrous Base Metal Smelting

Non-ferrous smelters are located where ore resources are rich in non-iron (Fe) metals such as copper (Cu), nickel (Ni), zinc (Zn), and lead (Pb) (Kozlov and Zvereva, 2007). The processing (smelting) of these ores, and especially sulphide ores, produces aerially-deposited sulphur dioxide (SO_2) and trace metals that can add stress to the surrounding landscape and reduce the ability of soil to sustain plant growth.

It is difficult to evaluate the effects of mining and smelting on the environment due to the complexity of factors involved and lack of consistent methodology (Dudka and Adriano, 1997). However, several trends are generally observed. The phenomenon of a barren landscape surrounding non-ferrous smelters is common at facilities operating in forest ecosystems (Kozlov and Zvereva, 2007). In Harjavalta, Finland, an area of 0.5–1.0 km surrounding the smelter had very little vegetation and biodiversity of the flora and fauna was reduced within 4 km (Kiikkila, 2003). In Anaconda, Montana, the impacted area contained mostly grasses in a naturally forested area (Anderson et al., 2009). Reduced vegetative growth was also observed in close proximity to a smelter at Kola Peninsula in Russia (Viventsova et al., 2005). The combined stress from smelter emissions (e.g., metal contamination, acidity), human induced disturbances (e.g., clear cutting) and natural disturbances (e.g., forest fires) have all been cited as causative factors to this phenomenon (Kozlov and Zvereva, 2007).

2.1.1 Mining and smelting in Flin Flon/Creighton

The Flin Flon, Manitoba and Creighton, Saskatchewan regions were first explored for ore deposits in the early 19th century and mining began in 1915 after Cu ore was discovered in the area (Stauffer, 1974). The area lies upon the Flin Flon greenstone belt, a metavolcanic deposit that contains multiple metals in a sulphidic ore (Syme et al., 1999). The rich quantity of transition metals prompted HudBay Minerals Inc., formerly Hudson Bay Mining and Smelting Co. Ltd., to construct a Cu, Zn, and Cd smelter to process mined ore in 1930. The

original emission stacks were 53-m (Zn plant) and 76-m (smelter) tall, which is relatively short and thus emissions were largely localized. An upgraded, single 251-m tall 'superstack' was constructed and began operation in 1974 (Franzin et al., 1979). This superstack was used until the Cu smelter was decommissioned in June 2010.

At the start of mining and smelting operations, the surrounding forest was logged for fuel. The boreal forest typical to the Flin Flon/Creighton area is characterized by a mixed jack pine (*Pinus banksiana*), trembling aspen (*Populus tremuloides*), black spruce (*Picea mariana*) and white spruce (*Picea glauca*) canopy with a lichen cover over the forest floor. Although the boreal forest ecosystem is dependent on frequent forest fires for cyclic disturbance and regrowth (Johnson et al., 1995), a severe (once in 150 years) fire swept through the area in 1939 (Peng and Apps, 1999). Since then regrowth has been largely limited to stunted woody species and a metal-tolerant ecotype of colonial bent grass (*Agrostis capillaris*) since this event (Winterhalder 2003).

After many years with little or no ground cover, the soils became heavily eroded, with exposed rock outcrops and soil pooling in depressions across the rolling Canadian-shield rocky parent material. Soils on the rock outcrops or fluvial plains have been classified as Orthic/Cumulic Regosols or Brunisols, while the depressions contain Organic soils (Mycock, 2011).

Soil pH in the area is very acidic (pH 3.5–4.5) due to the combination of naturally-acidic parent material (Johnson et al., 1995) and acid deposition from the smelter emissions. At a similar smelter in Sudbury, ON, the manual surface-spreading of ground limestone was able to detoxify the soil sufficiently for spontaneous colonization by seedlings of birch, poplar and willow (Gunn et al., 1995; Winterhalder 1995). In 1999, a community-based greening program was initiated to test whether the same technique would work in the Flin Flon/Creighton area. This approach led to varying degrees of success and provided the impetus for further research into other factors limiting natural revegetation of the forest.

2.1.2 Metal releases in the Flin Flon/Creighton area

The mined and processed sphalerite ore at the smelter contains primarily Cu and Zn but also impurities of As, Cd, Ni and Pb (Syme et al., 1999). Byproduct emissions of the smelting process include sulphur dioxide (SO_2) and particulates containing several metals including Zn, Cu, Pb, As, Cd and Hg (Jones and Henderson, 2006) and smelter-derived metal

deposition has been observed as far as 100 km from the smelting stack (Zoltai, 1988; Henderson et al., 1998; McMartin et al., 1999).

However, metal accumulation in soil is not as simple a function of proximity to the exhaust stack. In the Flin Flon/Creighton area, trace metal concentrations cover a wide range and correlate with both slope position and proximity to the stack, partially due to erosive transport (Bentz and Farrell, unpublished data, 2010). Soil contamination is localized in the surface organic layer or A horizon, though weathering can leach metals into the subsurface, and erosion can move contaminated topsoil into depressional areas (Bentz, unpublished data, 2010). Indeed, Roberts et al. (2002) and Voegelin et al. (2011) demonstrated that weathered species of smelter-sourced minerals elute into the subsoil and re-partition. The highest metal concentrations were found in concave positions, intermediate in poorly developed mineral soil on upper and mid-slope positions and lowest concentrations occur in developed mineral soils with a B horizon on upper and mid slopes.

Metal toxicity has been known to limit plant growth around industrial areas. The most commonly phytotoxic metals are Zn, Cu and Ni (Adriano, 2001). Zinc phytotoxicity has been linked with Zn smelting activities, as thermal decomposition of sulphides produces both acidity and high Zn concentrations in soil (Chaney, 1993). The focus of revegetation research in the Flin Flon/Creighton area is focused on reducing Zn phytotoxicity due to its recognized role in retarding plant growth when in high concentration and under acidic conditions (Chaney, 1993; Adriano, 2001) that are typical of the Flin Flon/Creighton area (Jones and Henderson, 2006).

2.2 Zinc and Plant Health

Zinc is the most commonly deficient micronutrient and extremely important in plant nutrition (Adriano, 2001). Zinc is involved in a number of metallo-enzymes such as dehydrogenases, proteinases, peptidases and phosphohydrolases (Kabata-Pendias, 2004). Yet despite the necessity of Zn for plant function, it becomes highly toxic when available Zn levels greatly exceed plant needs (Chaney et al., 1993).

While the effects of Zn toxicity are well characterized, the fraction of soil Zn available for plant uptake is less known. Zinc in soils can form a wide variety of minerals or adsorb onto many soil solid phases, having varying degrees of plant accessibility. This

emphasizes the need for knowledge of Zn speciation in soils as total concentration of Zn may not be useful in predicting plant toxicity or deficiency (Adriano, 2001).

2.3 Influences on Soil Zinc Mobility

The terms 'immobilization', 'sorption' and 'adsorption' are used to describe processes that control Zn mobility. Immobilization is a general term that can refer to any reaction mechanism that prevents Zn from becoming aqueous at common soil conditions (e.g., precipitation, surface exchange, or adsorption). Sorption is a general term that refers to the process by which one substance becomes attached to another (e.g., aqueous Zn^{2+} attracted to a clay surface by charge differences). Adsorption specifically refers to the process by which atoms, molecules or ions are retained on a solid surface through a chemical or physical bond (Sposito, 1984). Soil pH is the most important soil variable affecting Zn mobility and phytotoxicity (Chaney et al. 1997). In fact, for every unit increase in pH, Zn solubility is decreased 100-fold (Lindsay, 1979). Hydrolysis of Zn in water increases as pH increases and this reduces Zn activity (Table 2.1). The sorption of Zn onto organic or inorganic surfaces is also affected by pH, due to the pH dependent charge of many soil surfaces (e.g., clays, metal (hydr)oxides, and organic matter). Cation sorption generally increases with soil pH, as there is reduced competition with H^+ ions for sites of negative charge on organic matter and clay.

Table 2.1. Zinc hydrolysis/oxide constants

Reaction	Hydrolysis Constant †
	$Log_{10}[K_{25°C}]$
$Zn^2 + H_2O \leftrightarrow Zn(OH)^+ + H^+$	-8.96
$Zn^2 + 2H_2O \leftrightarrow Zn(OH)_2^0 + 2H^+$	-16.9
$Zn^2 + 3H_2O \leftrightarrow Zn(OH)_3^- + 3H^+$	-28.4
$Zn^2 + 4H_2O \leftrightarrow Zn(OH)_4^{2-} + 4H^+$	-41.2

† Adapted from Baes and Mesmer, 1967

2.3.1 Zn mineral types and stability

Much of the Zn produced in Canada and globally is sourced from ores containing the Zn sulfide minerals sphalerite and wurtzite; these minerals are abundant and rich in Zn, containing 64% and 61% Zn by weight, respectively (Canadian Mining Association, 2011). In oxidized environments, Zn sulfides are readily transformed into Zn silicate, hydroxide, oxide, sulfate, carbonate, and phosphate minerals during sulphide oxidation. Soil pH directly

controls Zn dissolution/precipitation, reduction/oxidation, and sorption/desorption reactions as observed in the empirical formulas in Table 2.2.

Table 2.2. Equilibrium reactions of various Zn minerals at 25°C (adapted from Lindsay, 1979)

Reaction No.	Equilibrium Reaction	log K^0
1	$Zn^{2+} + 2e^- \leftrightarrow Zn(s)$	-25.80
2	$Zn(OH)_2$ (amorphous) + $2H^+ \leftrightarrow Zn^{2+} + 2H_2O$	12.48
3	α-$Zn(OH)_2$ (s) + $2H^+ \leftrightarrow Zn^{2+} + 2H_2O$	12.19
4	β-$Zn(OH)_2$ (s) + $2H^+ \leftrightarrow Zn^{2+} + 2H_2O$	11.78
5	γ-$Zn(OH)_2$ (s) + $2H^+ \leftrightarrow Zn^{2+} + 2H_2O$	11.74
6	ε-$Zn(OH)_2$ (s) + $2H^+ \leftrightarrow Zn^{2+} + 2H_2O$	11.53
7	ZnO (zincite) + $2H^+ \leftrightarrow Zn^{2+} + H_2O$	11.16
8	$ZnCO_3$ (smithsonite) + $2H^+ \leftrightarrow Zn^{2+} + CO_2(g) + H_2O$	7.91
9	Soil-Zn + $2H^+ \leftrightarrow Zn^{2+}$	5.80
10	$ZnFe_2O_4$ (franklinite) + $8H^+ \leftrightarrow Zn^{2+} + 2Fe^{3+} + 4H_2O$	9.85
11	Zn_2SiO_4 (willemite) + $4H^+ \leftrightarrow 2Zn^{2+} + H_4SiO_4^0$	13.15
12	$ZnCl_2$ (s) $\leftrightarrow Zn^{2+} + 2Cl^-$	7.07
13	$ZnSO_4$ (zinkosite) $\leftrightarrow Zn^{2+} + SO_4^{2-}$	3.41
14	$ZnO \bullet 2ZnSO_4(s) + 2H^+ \leftrightarrow 3Zn^{2+} + 2SO_4^{2-} + H_2O$	19.12
15	$Zn(OH)_2 \bullet ZnSO_4(s) + 2H^+ \leftrightarrow 3Zn^{2+} + SO_4^{2-} + 2H_2O$	7.50
16	$Zn_3(PO_4)_2 \bullet 4H_2O$ (hopeite) + $4H^+ \leftrightarrow 3Zn^{2+} + 2H_2PO_4^- + 4H_2O$	3.80

Zinc mineral solubilities are plotted in an activity diagram in Fig. 2.1. Franklinite is generally considered the least soluble of Zn minerals, but this is dependent upon the Fe(III) oxides present that control Fe^{3+} activity. Although Zn has two oxidation states, Zn^0 and Zn^{2+}, only Zn^{2+} is important in soil environments. Redox is important to Zn in mine and smelter contamination because the exposure of sulphide minerals to surface water and soil conditions can create unstable conditions for sulphides and increase the solubility of these species (Carroll et al., 1998).

Zinc carbonates, oxides, sulfates (not shown), and hydroxides (not shown) are far more soluble than franklinite, willemite (a Zn-silicate), and the Zn-phosphate mineral hopeite. Willemite solubility is highly dependent on the activity of H_4SiO_4, which in soils is commonly controlled by quartz (SiO_2) (Lindsay, 1979). It should be noted that all Zn concentrations are highly influenced by pH.

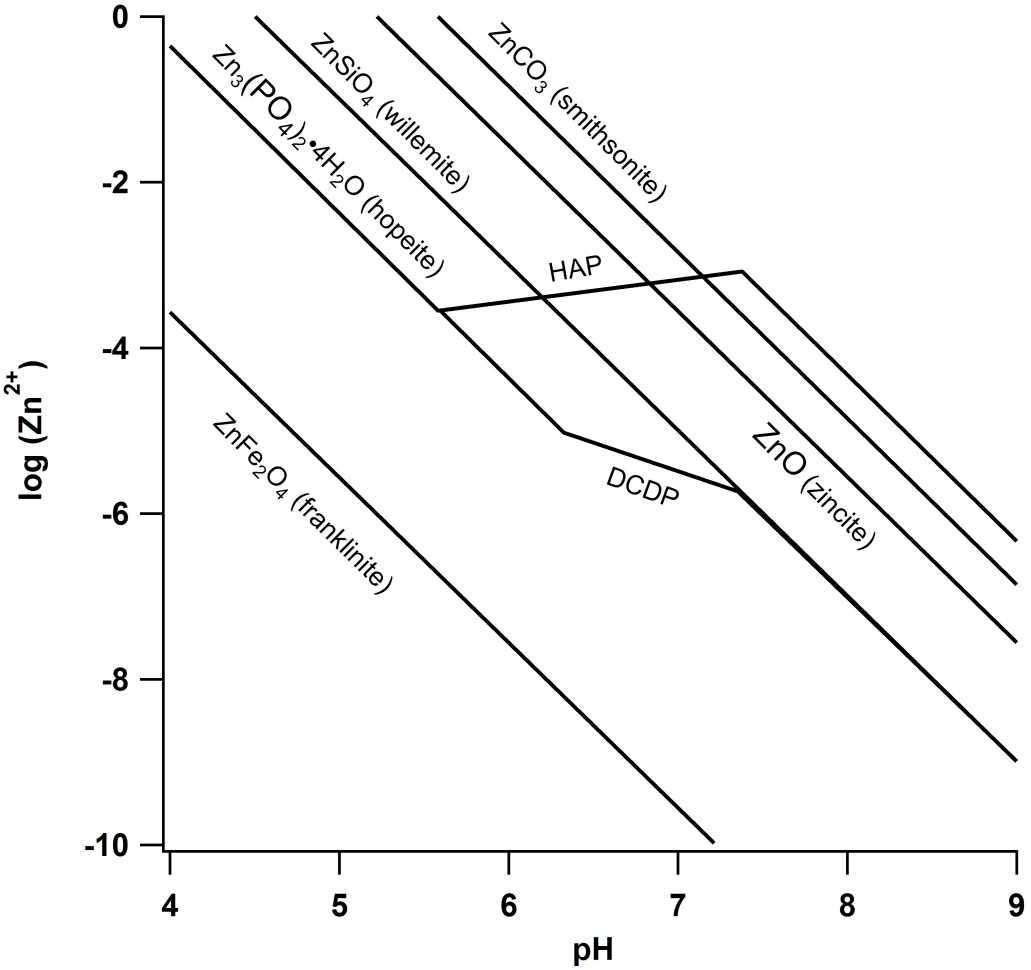

Figure 2.1 Activity diagram of several Zn minerals as a function of Zn^{2+} activity and pH. This graph was developed using the reactions in Table 2.2 with H_4SiO_4 controlled by quartz, Fe controlled by soil-Fe, PO_4^{3-} controlled by hydroxyapatite (HAP) or dicalcium phosphate dehydrate (DCDP), Ca = $10^{-2.5}$ M, and CO_2 = 0.003 atm. Adapted from Lindsay (1979).

Hopeite, [$Zn_3(PO_4)_2$•$4H_2O$], formation/dissolution has an important influence on the availability of Zn in soils (Nriagu, 1973), particularly when soil phosphate is in excess and mobile (Lindsay, 1979). The enthalpy of formation for hopeite is 4093.5 ± 3.3 kJ mol^{-1} (at 25ºC), making its formation an exothermic reaction (Al-Maydama et al., 1992). Nriagu (1973) found the solubility product constant (K_{sp}) of hopeite to be $10^{-35.3 \pm 0.1}$, making hopeite formation favorable. According to the Gibbs free energy, this would result in a favorable, spontaneous reaction, depending on solution saturation of constituent ions. The formation of

Zn-phosphate minerals, such as hopeite, is known to occur across many soil conditions and can be a limit on trace metal plant-availability in agricultural soils (Adriano, 2001)

Lindsay (1979) has considered hopeite formation to be highly dependent on the activity of PO_4^{3-}. The activity of PO_4^{3-} is in soils is pH-dependent, either controlled by fixation to strengite-soil-Fe at low pH or by highly insoluble Ca-phosphates at high pH, resulting in the hopeite solubility line shift in Figure 2.1. According to the activity diagram, hopeite becomes soluble if hydroxyapatite (HAP) is controlling PO_4^{3-} activity (i.e., if pH > 5.5), but if pH is < 5.5, hopeite remains insoluble.

According to the activity diagram, Zn-containing minerals are more soluble than soil sorption complexes (e.g., sorption to clays or humic matter) in natural systems and therefore, can be expected to supply Zn to plants (Fig. 2.1). This also suggests that in systems where PO_4^{3-} is controlled by HAP, hopeite becomes soluble above pH 5.5 and Zn partitioning between mineral and sorbed species becomes difficult to predict with solubilities alone.

2.3.2 Sorption of zinc in soils

Cationic zinc (Zn^{2+}) can potentially form many sorption species in soils, either with humic matter or clays (Cances et al., 2003; Bradl, 2004; Kumpiene et al., 2008; Voegelin et al., 2011). In organic topsoil contaminated by a Zn smelter, Zn speciation was dominated by Zn-organic matter complexes (Sarret 2004) and cation exchange and organic ligand complexation were the main mechanisms to limit Zn mobility in acidic soils (Kabata-Pendias and Pendias, 2000). Alternatively, it has been observed that Zn mobility in soil solution is decreased in heavy-textured soil when compared to light-textured soil at equal pH (Chaney, 1993). Several studies investigating the clay fraction of historic smelter sites have found attenuation of high temperature Zn minerals in acidic soils occurring naturally by (i) adsorption onto Mn and Fe (i.e., oxyhydroxides) (Feng et al., 2007), (ii) incorporation into phyllosilicates (Schienost et al. 2002), (iii) Zn formation of layered double hydroxides with Al (Zn-Al LDH) (Manceau et al., 2004; Vespa et al., 2010) and (iv) formation of Zn bearing hydroxyl-interlayered phyllosilicate mineral (Zn-Al HIM) (Manceau 2000; Manceau et al., 2002; Roberts et al., 2002; Van Damme et al., 2010; Degryse et al., 2011). Zinc will sorb onto Mn-O, Fe-OH, Al-OH, aluminosilicates and can adsorb to humic substances, though other trace metal cations may out-compete Zn for sorption sites.

Several conceptual models have been proposed to explain the specific adsorption of metal cations in soils. Sposito (1989) predicted the tendency of metals to form covalent bonds, based on their ionic radius and ionization potential, in the order: Pb > Cd > Cu > Co > Ni > Zn. According to McBride (1994), electronegativity is an important factor and the strongest bond should be formed by the metal with the highest charge to radius ratio, re-ordering the metal sorption preferences to: Ni > Mg > Cu > Co > Zn > Cd > Sr > Pb. Regardless of the model chosen, Zn is out-competed for specific adsorption by a majority of the other cationic metals, making Zn very mobile in soils. This phenomenon has been widely observed, showing reduced selectivity of Zn sorption in the presence of competing cations in humic matter (Schnitzer, 1969), clays (Atanassova, 1999; Bradl, 2004) and apatite surfaces (Cao et al., 2003; Sheha et al., 2007).

2.4 Inducing Zn Immobilization in Smelter Contaminated Soils with Amendments

Feasibility testing of soil amendments to control metal solubility and toxicity in shorter time frames than natural attenuation processes has been a topic of intense study. A USEPA report (2007) offered general suggestions for best management practices related to applying soil amendments to contaminated sites. The general recommendation for all mixed metal contamination is to lime soil to a final pH of 5.5–6.6 and to supplement phosphorus (P) nutrition because soils are commonly acidic and P deficient.

2.4.1 Liming

Because Zn solubility decreases 100-fold with each pH unit increase (Lindsay, 1979), increasing the soil pH is a well-supported initial step for revegetation. Liming (i.e., the application of carbonates as limestone or dolostone to soil) is the most common strategy used to neutralize non-ferrous smelter contamination (USEPA, 2007). This reflects the fact that carbonates neutralize the acidic deposition common to smelter-impacted soils, increasing the soil pH and, in turn, immobilizing and detoxifying metals. In calcareous and alkaline conditions, Zn will sorb onto carbonates, precipitate as Zn hydroxide, Zn carbonate or calcium zincate (Bradl, 2004; Jacquat et al., 2009). Liming has been successful in revegetating the Ni/Cu smelter in Sudbury, ON (Gunn et al., 1995). Due to the mixed results of liming in the Flin Flon/Creighton area, it is believed that the use of additional amendments should be explored.

2.4.3 Biochars

Biochars are biological residues combusted under low-oxygen conditions that produce a porous, low-density, carbon-rich material (Sohi et al., 2010; Beesley et al., 2011). The typically large surface area and cation exchange capacity of biochars facilitate sorption of both organic and inorganic contaminants, depending in large part on the source material and pyrolysis temperature. Sorption of contaminants onto biochars may reduce contaminant mobility in contaminated soils. The specific mechanisms of contaminant-biochar sorption and long-term release remain unclear and should be characterized to ensure that these materials are appropriate for long-term contaminant management.

Limited information is available on the factors controlling the surface complexation of inorganic contaminants onto biochar. Transition metals can sorb to negatively-charged functional groups (depending on whether pH is above the point of zero charge) on biochar surfaces by metal-ligand complexes or static attraction (Joseph et al., 2010). Either permanent or variable surface charge produced by oxidation of surface carbon can provide a high-surface reactivity to the biochar (Joseph et al., 2010). There is evidence that when char is oxidized, surface functional groups play a dominant role in metal adsorption (Uchimaya et al., 2011). Inorganic contaminants most consistently sorbed by biochar amendments are Cd, Cu, Pb and Cr and to a lesser degree Zn (Beesley et al., 2010; Beesley and Marmiroli, 2011; Fellet et al., 2011).

2.4.4 Phosphate amendments

Many transition metals have a low solubility with aqueous phosphate (PO_4^{3-}) and can form metal-phosphate precipitates under a wide range of aerobic soil conditions (Nriagu, 1984; Cotter-Howells and Caporn, 1996; Chen et al., 1997a,b; Lanfranco et al., 2003; Porter et al., 2004). Because of this, phosphate-containing materials are commonly applied to metal contaminated soil to induce *in situ* metal immobilization (Cotter-Howells and Caporn, 1996; Li et al., 2000; Kumpiene et al., 2008). Lead has been extensively studied and the formation of the insoluble pyromorphite, [$Pb_5(PO_4)_3Cl$], is known to consistently occur when phosphate is applied to contaminated soil (Ruby et al., 1994; Cao et al., 2002; Porter et al., 2004; Chen et al., 2006; Hashimoto et al., 2011). Reaction of Zn with phosphate is also highly favorable and can reduce Zn mobility in soils by forming insoluble minerals (Nriagu, 1984; Kumpiene et al., 2008; Waterlot et al. 2011) or adsorption complexes (Chen et al., 1997; Boisson et al.,

1999; Basta et al., 2001). For this reason, sources of phosphorus are valuable soil amendments that can induce *in situ* soil sequestration of multiple transition metals.

Phosphate (PO_4^{3-}) can be applied to soil in many forms (e.g., phosphoric acid, diammonium phosphate); however, excess P leaching can become an issue and highly-soluble P sources are to be avoided. Apatites are sparingly soluble in soils and, as such are of interest as a slow-release phosphate.

Comparisons of different apatite minerals have been conducted to assess their suitability as a soil amendment for Zn. Solubility of apatites follow the general trend: synthetic > bone-based > rock phosphate (Dybowska et al., 2009). Synthetic apatites are expensive and have limited use as a soil amendment; rock phosphate is readily available and relatively inexpensive, but its low solubility may result in low reactivity in soil (Basta et al., 2001; Baker et al., 2012). Consequently, focus has shifted to bone-based products because of their moderate solubility and ample supply (Deydier et al., 2005; Knox et al., 2006; Chrysochoou et al., 2007; Kumpiene et al., 2008). Hydroxyapatite (HAP) is a major component of bones (~40% w/w), with the empirical formula $[Ca_{10}(PO_4)_6(OH)_2]$ (Narasaraju and Phebe, 1996; Moreno-Pirajan et al., 2011).

Meat and bone meal (MBM) is solid material derived from rendering waste and can be pyrolyzed, or incinerated, to remove biohazards and reduce weight. Some researchers have proposed that MBM thermal residue (i.e. biochar) can be a readily accessible source of HAP (Deydier et al., 2005; Coutand et al., 2008; Sobczak et al., 2009). Despite extensive research on the sorption of metals by HAP (Xu et al., 1994; Ma et al., 1994; Basta et al., 2001; Terra et al., 2002; Lee et al., 2005; Corami et al., 2007) the adsorption capacity and mechanisms of metal sorption by MBM and its charred residue have received relatively little attention (Deydier et al., 2003; Coutand et al., 2009; Dybowska et al., 2009).

Regardless of source, it is highly recommended that apatites be applied under acidic conditions, making them suitable for smelter-impacted soils (Chen et al., 1997; Sneddon et al., 2008; Warren et al., 2009). The acidity causes dissolution of the HAP mineral and induces hopeite formation through the following reaction (Jaynes et al., 1999):

$$3Zn^{2+} + 2H_2PO_4^- + 4H_2O \leftrightarrow Zn_3(PO_4)_2 \bullet 4H_2O(s) + 4H^+ \quad [2.1]$$

Hopeite has been suggested to influence the availability of Zn in soils (Nriagu, 1973). Indeed, several studies have found hopeite precipitation after reacting HAP with Zn in both soil and batch sorption experiments (Ma et al., 1994; Chen et al., 1997; Dybowska et al., 2009; Williams et al., 2011; Baker et al., 2012).

2.5 Techniques to Assess Zinc Mobility

The speciation (i.e., chemical form) of an element gives detailed information about its mobility and bioaccessibility in the environment. Evaluation of health risks from metal contamination depends on the accurate determination of chemical species because metal toxicity and mobility depend on both concentration and chemical form. Common methods of studying chemical speciation include (i) laboratory based sorption experiments and sequential chemical extractions, and (ii) molecular-scale spectroscopic analysis of samples.

2.5.1 Adsorption experiments

Adsorption is the net accumulation of a substance at the common boundary of two contiguous phases (Sposito, 1984). The adsorbate is the accumulating substance at the surface of an adsorbent and the adsorptive is the concentration of substance remaining in solution. Adsorption experiments test the properties of an adsorbent by varying one reaction condition (e.g., temperature, pH, ionic strength, or sorbate concentration) and observing the effect it has upon adsorbate concentration in solution. The study of adsorption phenomena in soils and solids can provide a macroscopic, quantitative description of the reactivity of an adsorbent with an adsorbate of interest. Adsorption experiments are characterized by three operations: (i) reaction of the solid with a liquid of prescribed composition for a prescribed period of time, (ii) isolation of the solid from the reactant liquid phase, and (iii) chemical analysis of the solid and/or the reactant liquid phase. Results from adsorption experiments are typically modeled as either a single or, more often, a mixture of mechanisms (adsorption, polymerization, or precipitation) that can co-occur (Sposito, 1984; Sparks, 2003). However, although adsorption techniques can infer reaction processes, more direct spectroscopic techniques such as synchrotron-based XAS are required to conclude adsorption mechanisms.

2.5.2 Synchrotron-based speciation techniques

2.5.2.1 X-ray absorption spectroscopy (XAS). Synchrotron-based, hard x-ray absorption spectroscopy involves exciting the core electrons of an element to probe its oxidation state, coordination number, and short-range local bonding environment (Henke et al., 1993). Every element has known excitation and fluorescence energies based on the binding energies of its electrons. Once the excitation energy (i.e., equal to the binding energy of the electron) is exceeded, electrons in the atom strongly absorb incoming x-rays and the excited core electron is ejected from the atom as a photoelectron. A temporary vacancy in the orbital is created and filled by a higher-energy electron of the atom. As the high-energy electron decays (i.e., sheds its excess energy to reach the lower energy state), the excess energy is released as a photoelectron, which is measured as counts by a detector near the irradiated sample. This photoelectron measurement is the phenomenon that gives the characteristic 'edge' feature in XAS. It is preferable to excite an element at its K-edge to get the most intense fluorescence from the sample (i.e., the largest energy difference between outer shell electron and 1s electron).

The spectrum contains characteristic features including an 'edge jump' or main peak feature at the fluorescing energy and the subtle oscillations of constructive and destructive interferences of the photoelectric wave at higher energies. An XAS spectrum can be divided into three regions: pre-edge, the X-ray Absorption Near Edge Structure (XANES) and the Extended X-ray Absorption Fine Structure (EXAFS), as shown in Figure 2.2 for smithsonite.

XANES spectroscopy is sensitive to an element's oxidation state and coordination number of the first shell of atoms surrounding the element. Differences between nearest neighbor elements are seen most clearly in the EXAFS region. In a simple species such as fully-hydrated, aqueous zinc [$Zn(H_2O)_6^{2+}$], the EXAFS have simple backscattering that resemble a sine wave from the equidistant six oxygen neighbors. If other neighboring atoms are close and/or backscatter strongly, they will emit additional photoelectrons whose oscillation combine with that of the original Zn atom and give a more complicated, combined spectrum with constructive and destructive interference.

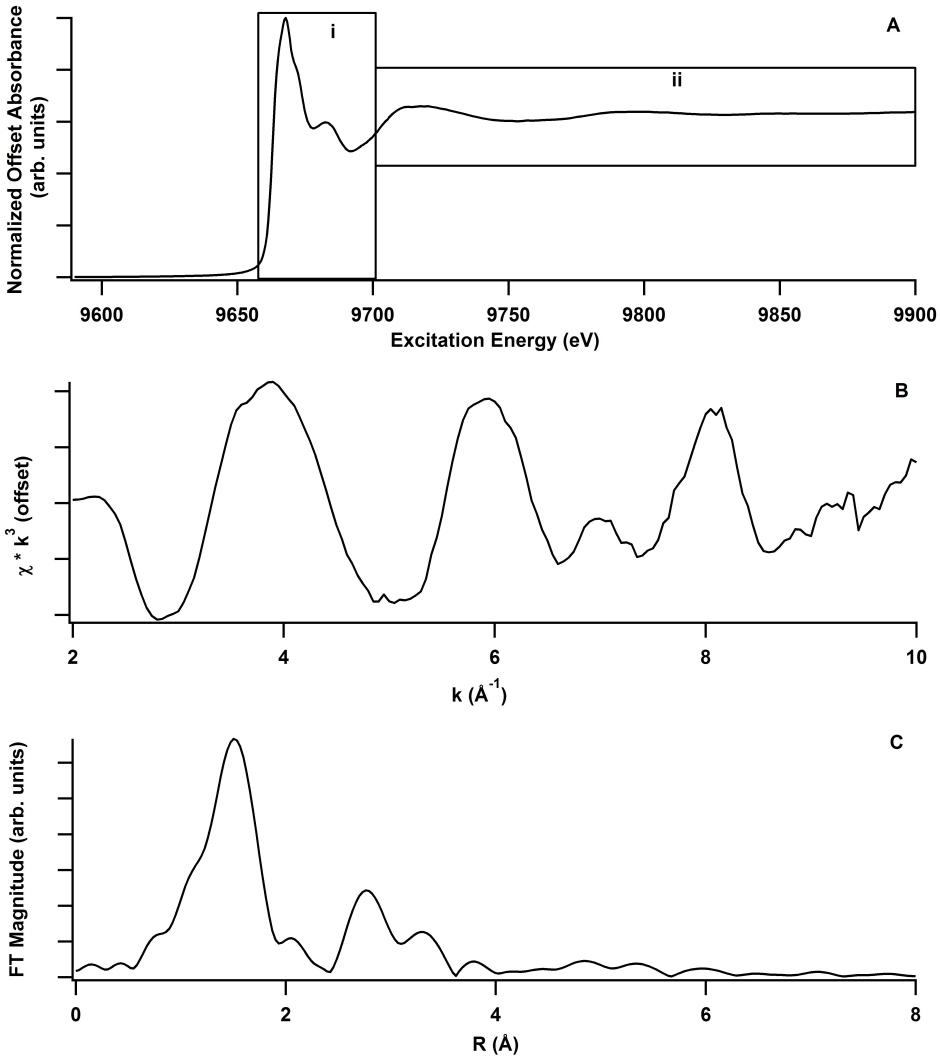

Figure 2.2. Example of an x-ray absorption (XAS) spectrum from a smithsonite ($ZnCO_3$) standard. The spectrum of smithsonite (A) contains the entire data range. The x-ray absorption near edge structure (XANES) begins at the Zn K-edge (9659 eV) (i) and features range up to 30 eV relative to the "edge jump" and the extended x-ray absorption fine structure (EXAFS) region contains features at energies > 30 eV from the edge. The EXAFS region (ii) is typically transformed and replotted (B) as absorbance (X) as a function of the photoelectron wavenumber (k). The absorbance is often weighted to amplify the oscillations by a power of k (k^3) as shown in the figure (B). The oscillations in the EXAFS can then be Fourier transformed (FT) to generate a plot of the radial interatomic distances (in Å) from the fluorescing atom.

Bulk XAS can be measured on reference materials, (known single species samples) or unknown heterogeneous samples (typically multiple species). Heterogeneous samples can be difficult to analyze if many species are present, so interpretation is greatly enhanced by complementary techniques, particularly spatially-resolved measurements.

2.5.2.2 Synchrotron x-ray microprobe techniques. Additional microprobe techniques such as micro x-ray fluorescence (μXRF) mapping, micro x-ray diffraction (μXRD) and micro x-ray absorption spectroscopy (μXANES), can be performed at a synchrotron microprobe beamline using a smaller spot size beam (typically 5-μm^2) than bulk XAS measurements (typically 0.5-mm^2). The smaller beam size allows spectral information in the sample on smaller areas to reduce the likelihood of multiple species. Micro scale XRF mapping can be used to raster across an area in 5-μm^2 pixels to describe spatially-resolved, semi-quantitative elemental associations in a heterogeneous sample. This can identify points of interest where single species may exist, after which μXANES is employed to directly measure the point of interest and confirm speciation.

2.5.3 Common methods for analyzing XAS analysis

Regardless of beam-size resolution, further analysis is necessary to elucidate speciation in unknown samples. Interpretation of the unknown sample data relies on theoretical or experimentally collected samples.

2.5.3.1 Multi-shell theoretical EXAFS modeling. This method is a precise method of analysis that requires excellent quality data and a relatively few number of species in the sample to be successful. In this approach, theoretical scattering paths are computed using computer code such as ATOMS and FEFF (Ravel, 2001) and then combined to reproduce the major features of the measured spectra using the EXAFS equation (Newville, 2001). Major variables of the EXAFS equation include coordination number (CN), Fourier transformed radial distance (R), and Debeye-Waller bond disorder (σ^2) (Newville, 2001). The models should be constrained to be physically realistic and be well-fit to the observed spectrum (Henke et al., 1993).

2.5.3.2 Linear combination modeling. Linear combination (LC) modeling is commonly referred to as a 'fingerprinting' method for use in quantifying species of more heterogeneous samples. It involves interpreting an unknown, multi-species spectrum as a linear combination of known single species spectra (Ravel, 2001). Linear combination model error for each

component ranges between 5 and 10%. This procedure is highly dependent on the standards used and the choice of standards which has the potential to bias the outcome of the LC modeling (Ravel and Newville, 2005). Supplementary experiments such as wet chemistry or synchrotron-based microprobe techniques can greatly justify and strengthen model choices (Manceau et al., 2000).

The measure of "wellness of fit" for LC analysis is the chi-square (χ^2) value; however, this can only be interpreted as the wellness between models for a single sample because this parameter is sample specific. The limited inference space results from difficulty in quantifying the number of independent measurements in an XAS spectrum. Because of this, the number of measurements is estimated as the number of data points in a spectrum using Athena software. The best metric of how well a LC model fits the data is the chemical likelihood of component species proposed to be in the sample, which depends on the supporting data gained from wet chemical or spectroscopic methods (Manceau et al., 2000).

A MBM biochar soil amendment is a relatively unknown sorbent. These techniques will be used to assess Zn mobility and determine whether a MBM biochar will act as a sorbent for Zn in adsorption experiments and in smelter-impacted soils of the Flin Flon/Creighton area.

3.0 MEAT AND BONE MEAL BIOCHAR CHARACTERIZATION

3.1 Preface

The physicochemical data collected in this chapter characterized the mineral and organic components of the unknown, novel adsorbent, MBM biochar. The characteristics of MBM biochar will provide mineralogical, structural and chemical information required to effectively interpret the results of adsorption experiments with Zn described in Chapter 4.

3.2 Introduction

Biologically-stressed landscapes such as the forest surrounding the HudBay Minerals Inc. (formerly Hudson Bay Mining and Smelting Co. Ltd.) often require external inputs to support revegetation. *In situ* amendment spreading involves applying reactive materials to soils to improve fertility and/or decrease contaminant toxicity to plants (Kumpiene, 2008). Products generated from waste materials are well-suited for use as soil amendments due to their excess supply and low cost (Babel et al., 2003). Biochars represent a particularly promising development in waste material-based soil amendments.

Meat and bone meal (MBM) is a processed animal-rendering waste consisting of animal parts (e.g., skin, blood, horns, bones etc.) that have been steam heated at >125°C to remove moisture and fat, and sterilize the end-product (Deydier et al., 2005; Etok et al., 2007). The use of this animal by-product as animal feed is banned due to the risk of Bovine Spongiform Encephalopathy (BSE), and it therefore needs to be destroyed or recycled. Thermal treatments, mainly combustion and pyrolysis are being investigated because the heating value of MBM (about 5,000 kcal kg^{-1}) may make the material appropriate for energy recovery (Ayllon et al., 2004). Pyrolysis involves adding heat from an external source in the absence of oxygen, which can produce a larger quantity of tar/oil and solid char relative to incineration (Chaala and Roy, 2003; Ayllon et al., 2006). Pyrolysis of MBM can have the benefits of generating fuel or adding value to MBM residue as a potential source of calcium phosphate (i.e., hydroxyapatite; HAP) from the residue (Deydier et al., 2005).

The composition and reactivity of MBM biochars—hence, its suitability as a soil amendment—are often unknown and can vary widely depending upon production conditions (Etok et al., 2007). The strongest influence on MBM residue properties is the temperature, which affects changes to the crystalline structure of the bone and its associated organic components (Ayllon et al., 2006; Etok et al., 2007). A study by Etok et al. (2007) detailed the physicochemical changes when MBM was incinerated under laboratory conditions. They found that (i) all loosely bound and structurally-bound water is lost at temperatures above 250°C, (ii) the largest reduction in mass occurs as organic material is combusted at temperatures between 300–500°C, with some production of char (iii) all organic material including any char is burnt off at temperatures >500°C, which leaves calcium phosphate minerals and salts to re-organize, and (iv) at temperatures >700°C, pores in the HAP collapse and sintering significantly reduces the surface area (Etok et al., 2007). This loss of surface area and increase in cyrstallinity also has been seen with synthetic nano-particle size HAP (Pang and Bao, 2003).

The surface area and mean crystallite size are strong controls on how much HAP surface is available to react with soluble ions (Stoetzel et al., 2009) or dissolve by releasing its constituent ions into solution. For example, Dybowska et al. (2009) found that incinerated MBM residue (e.g., 725°C and 850°C) had a greatly reduced capacity to remove Zn and other metals from an acidic solution (initial pH 3.0).

In an industrially-produced material, the composition of the final pyrolyzed product will be more variable than any material prepared in a laboratory—highlighting the need for an accurate characterization of the product's physico-chemical properties. The purpose of this study was to characterize the physico-chemical properties of a commercial MBM biochar as a first step in assessing its potential as a soil amendment to reduce Zn toxicity in smelter-impacted soils.

3.3 Materials and Methods

3.3.1 Meat and bone meal (MBM) biochar

Meat and bone meal biochar was obtained from Titan Clean Energy Projects Corporation (Craik, SK). Animal rendering wastes were ground by passing through a thermal extruder and then heated at 20°C min^{-1} under an N_2 atmosphere to a final temperature of

900°C. Upon reaching 900°C, temperature was reduced at 40°C min^{-1} by passing cold water through pipes adjacent to the pyrolyzed residue (personal communications, Titan Clean Energy Projects Corporation). Willow (*Salix* spp.) biomass was chipped into pieces <5-mm in diameter and pyrolyzed separately at 600°C under an N_2 atmosphere. The resulting willow biochar was added to the pyrolyzed rendering waste, so the resulting product is a 90:10 (v/v) mixture of meat and bone meal biochar and willow biochar. For simplicity, this final product will be referred to as 'MBM biochar'.

3.3.2 Sample preparation

The MBM biochar was passed through a 2-mm sieve for all analyses. A sub-sample of the sieved biochar was processed by ball grinding using a Mixer/Mill 8000M at 1060 cycles min^{-1} for 5 min, passed through a 40-μm sieve and stored in a bell jar desiccator (Rogers et al., 2002). For adsorption experiments, it was necessary to use the MBM biochar in a liquid suspension of 0.1 M $NaNO_3$. This background electrolyte maintains a constant ionic strength, provides a source of non-specific ions (Na^+ and NO_3^-) as competitors during sorption reactions and allows pH adjustment using a strong acid/base without altering the overall ionic strength of the suspension (Sigg and Stumm, 1981). A mass of 3.5 g (<2 mm) MBM biochar was suspended in 150 mL 0.1 M $NaNO_3$ in a 250-mL polypropylene bottle (n=4) and shaken at 160 rpm for 1 h on a gyratory shaker (New Brunswick Scientific, Model G10, Manasquan, New Jersey, USA). The suspensions were then centrifuged at 6,000 g for 2 h (Heraeus Megafuge 1.0, Langenselbold, Germany) and the supernatant decanted and discarded; the biochar was then resuspended in 0.1 M $NaNO_3$ and the procedure repeated a total of three times.

The MBM biochar suspension was then transferred to a 1.0 L screw-top glass bottle and brought to a final volume of 1.0 L with 0.1 M $NaNO_3$. The final suspension density was measured as follows: 5.0-mL aliquots of suspension were pipetted into weighing tins and oven evaporated at 105°C. The dry weight of the residue (corrected for the mass of $NaNO_3$ present) was used to provide suspension density (in g L^{-1}) of the char suspension. The stock suspension (1.0 L) was kept at 10°C to slow microbial decomposition.

3.3.4 Attenuated total reflectance Fourier-transform infrared (ATR-FTIR) spectroscopy

Attenuated total reflectance Fourier transform infrared spectra were collected using an FT-IR spectrometer (Bruker Equinox 55, Karlsruhe, Germany) equipped with a liquid N_2-cooled Mercury–Cadmium–Telluride detector operated under continuous instrument purging with CO_2-and H_2O-free air. All spectra were collected in attenuated total reflectance (ATR) mode using a Bruker PlatinumIR accessory that contains a single bounce diamond coated ZnSe crystal for optics.

Samples and standards were either drop-coated onto the ATR-FTIR window or pressed as a fine powder. Samples and standards included: MBM stock suspension; hydroxyapatite [$Ca_{10}(PO_4)_6(OH)_2$]; Zn phosphate [$Zn_3(PO_4)_2$]; brushite [$CaHPO_4$]; calcium dihydrogen phosphate [$Ca(H_2(PO_4)_2$]; and calcite [$CaCO_3$]. Measurement of air and DI water were collected and subtracted from all spectra for background correction using Opus 6.5 software (Bruker). All samples were measured with 100 scans from 500–4000 cm^{-1} with a resolution of 4 cm^{-1}. A detailed description of the methods can be found in Peak et al. (2003).

3.3.5 X-ray diffraction (XRD)

Meat and bone meal biochar samples and mineral standards were ground with an agate mortar and pestle and passed through a 75-μm sieve (Klug and Alexander, 1974). The samples were then mounted on glass slides as a methanol slurry and allowed to air-dry. X-ray diffraction spectra were measured on an x-ray diffractometer (PANalytical Empyrean, Almelo, The Netherlands) using Co radiation at 40kV and 45 mA. Diffracted x-rays were measured in 2θ mode between 10 and 80° at a scan rate of 2.5° min^{-1}. Samples and standards included: MBM stock suspension; hydroxyapatite [$Ca_{10}(PO_4)_6(OH)_2$]; Zn phosphate [$Zn_3(PO_4)_2$]; brushite [$CaHPO_4$]; calcium dihydrogen phosphate [$Ca(H_2(PO_4)_2$]; and calcite [$CaCO_3$]. Mineral standards were used to identify peaks in the MBM biochar sample.

3.3.6 Specific surface area and total elemental analysis

The external surface area (excluding micropores) of unwashed MBM biochar (<2 mm) was measured at atmospheric pressure with a NOVA 2200e instrument (Quantachrome, Boynton Beach, FL USA). An N_2 adsorption isotherm was modeled with an 11-point curve (Das and Hendry, 2011) was used to perform Brunauer-Emmett-Teller (BET) analysis. Meat

and bone meal biochar (0.2 g) was degassed at 24°C for 24 h with N_2 prior to conducting the analyses (n=4).

Total carbon analysis was performed by combustion of C in samples at 1100°C using a C 632 Carbon Determinator (LECO corporation, St. Joseph, Missouri, USA). Sucrose standard was weighed into ceramic boats and used in a four-point calibration curve of a high-C standard (0.421 mg C mg^{-1}). Calibration was used to linearly correlate CO_2 absorption by a detector with quantity of C in the sample. A 0.20 to 0.40-g subsample of ball-ground (<40-μm), unwashed MBM biochar was weighed into ceramic boats and combusted at 1100°C for 2 min (n=5).

Digestions were performed using standard methods with HF, HNO_3 and heat, (Jenner et al., 1990). A Teflon jar was placed on an analytical balance, 100 mg of sample (<40 μm) was added, and the exact weight recorded; 5 mL of double distilled concentrated HF (10 M) and 5 mL of double distilled concentrated HNO_3 (16 M) was then added and the cap secured onto the jar. The jar was then placed on a hot plate at 100–150 °C for 4 d. After all solid phases were dissolved, the lid was removed and the solution evaporated until dry. After cooling, 2 mL of 16 M HNO_3 and 2 mL 10 M HF were added, and the sample refluxed again for an additional 3 d to ensure complete dissolution of recalcitrant minerals. Next, 2.5 mL HNO_3 (8 M) and 0.5 mL H_2O_2 were added and warmed gently to dissolve the remaining residue. The samples were then transferred into sample bottles, lids were rinsed into the bottles as well (using Milli-Q water) to transfer any residues, and brought up to a final weight of 100 g using Milli-Q water. The sample was filtered and then the filtrate analyzed by ICP-MS (Perkin Elmer NexIon 300D, Waltham, MA USA). Results were reported in mg kg^{-1} for a range of elements (Atomic number (Z)=3, 11–13, 15, 19–34, 37–42, 47–51, 55–60, 62–73, 81–82, 90–92) according to published procedures (Longerich et al., 1990; Stefanova et al., 2003). Elements measured in MBM biochar of concentration <100 mg kg^{-1} were not reported.

3.4 Results and Discussion

3.4.2 Attenuated total reflectance Fourier-transform infrared reflectance (ATR-FTIR)

Representative ATR-FTIR spectra for the MBM biochar, HAP and calcite are shown in Fig 3.2. The ATR-FTIR spectra of the MBM biochar contains a combination of species, as

evidenced by the combination of features characteristic of both calcite and HAP (Fig. 3.2). However, the highest intensity peak positions are consistent with the HAP standard (Panda et al., 2003).

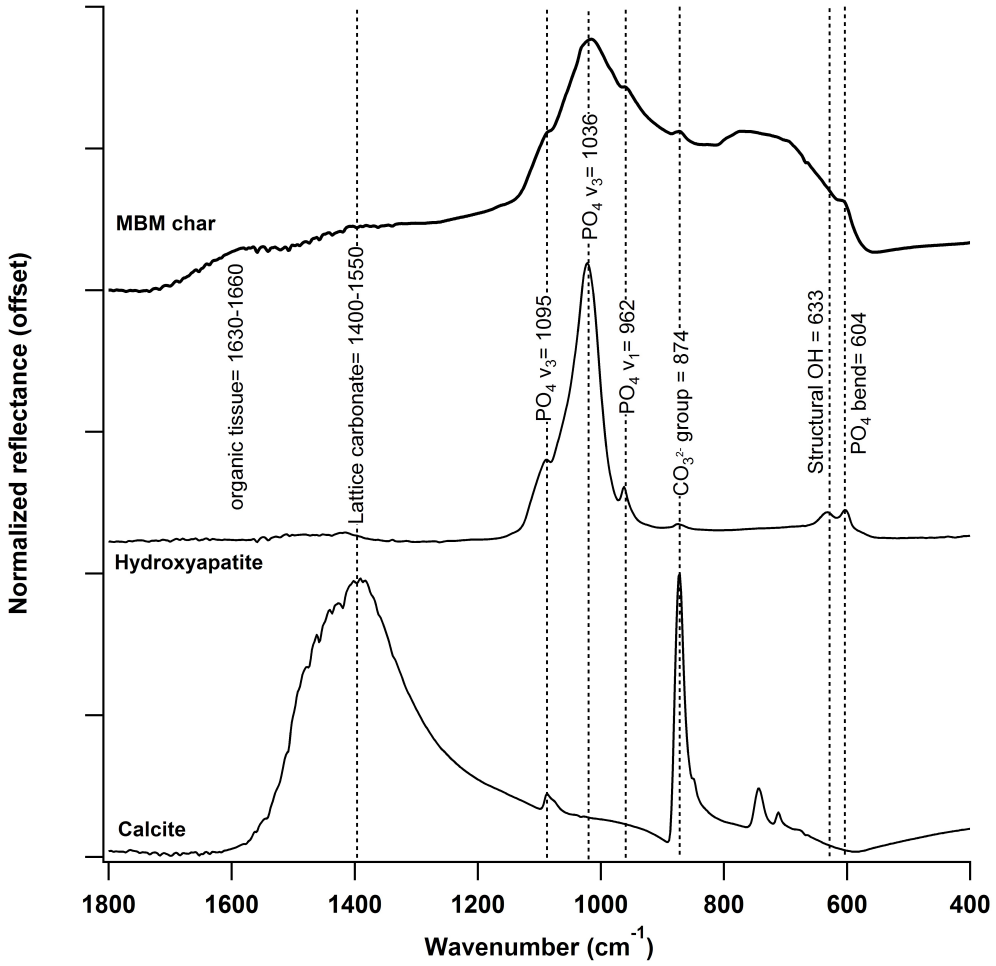

Figure 3.2. Attenuated total reflectance-Fourier transform infrared (ATR-FTIR) spectroscopy shows that meat and bone meal (MBM) biochar has identical v_3 mode P-O bond vibrations (at 1035 and 975 cm^{-1}) as the hydroxyapatite standard. MBM biochar has additional bands associated with carbonate.

The MBM biochar shows broad bands between 1700–1400 cm^{-1} that are associated with proteins, which includes the band reported for organic tissue in bone (i.e., 1630–1660 cm^{-1}) (Thompson et al., 2013). This can be seen in the MBM biochar spectrum (Fig. 3.2) but is absent in the HAP spectrum (Fig 3.2). Although this band may arise from the organic component of the bone, it may also arise from the willow component of the MBM biochar.

The 1400–1550 cm^{-1} range vibrations likely arise from carbonate, either as a substituted anion in the apatite or as a separate mineral (Rey et al., 1991).

Carbonate substitution can occur at either the OH^- or PO_4^{3-} sites (referred to as A and B substitution, respectively) and have characteristic infrared (IR) signatures. Type A carbonate has doublet bands at about 1540 and 1450 cm^{-1} and a singlet band at 880 cm^{-1}; Type B carbonate has these bands at about 1455, 1410 and 875 cm^{-1}, respectively (Fleet et al., 2004; Rey et al., 1991). The MBM biochar has additional bands associated with carbonate but the resolution of the peaks is not sufficient to distinguish between substituted carbonates and a separate calcite phase (Fig. 3.2).

Observing carbonate in calcium phosphates is difficult because two of the four vibrational bands of CO_3^{2-} overlap with phosphate bands (Rey et al., 1989). The v_1 mode is masked by the v_3 phosphate band, and the v_4 is very weak and could be misinterpreted as a baseline irregularity. The v_3 mode (1400–1600 cm^{-1}) is the strongest IR band but is obscured in MBM by several overlapping absorption bands of proteins (Rey et al., 1989). These regular interferences in calcium phosphates make the v_2 mode the most easily accessible IR peak in our char samples.

The broad vibration at 865–877 cm^{-1} can be seen in the MBM biochar sample, but not the HAP standard. Subtle energy differences in band location can either indicate a separate calcium carbonate mineral (874 cm^{-1}) or CO_3^{2-} ions substituted into the apatite by type A-substitution (879 cm^{-1}) or type B substitution (873 cm^{-1}) with a small shoulder at 866 cm^{-1} (Rey et al., 1989). The data quality in this study is not sufficient to distinguish between the two possible band locations; however, because carbonate substitution is common in bone samples, both should be considered likely to exist in the MBM biochar (Narasaraju and Phebe, 1996).

A shift of the PO_4^{3-} v_3 mode down to 1025 cm^{-1} and 1045 cm^{-1} is also indicative of Type B substitution of CO_3^{2-} for PO_4^{3-} (LeGeros et al., 1969). If both apatite structures are components of the MBM biochar, this would result in an average of the two bands and explain the broadness of the band observed in the MBM biochar between 1050 and 1000 cm^{-1}.

3.4.3 X-ray diffraction (XRD)

The XRD pattern for stock suspension MBM biochar shares most of the same crystal structure as the hydroxyapatite standard (Fig. 3.3). The shows that the mineral structure in MBM biochar is consistent with a moderately-crystalline hydroxyapatite (Peters et al., 2000). Other peaks are present in the MBM biochar XRD pattern that could not be identified using the standards measured, which include: aragonite [$CaCO_3$], calcite [$CaCO_3$], brushite [$CaHPO_4 \bullet 2H_2O$], and calcium dihydrogen phosphate [$Ca(H_2PO_4)_2$] (Fig 3.3).

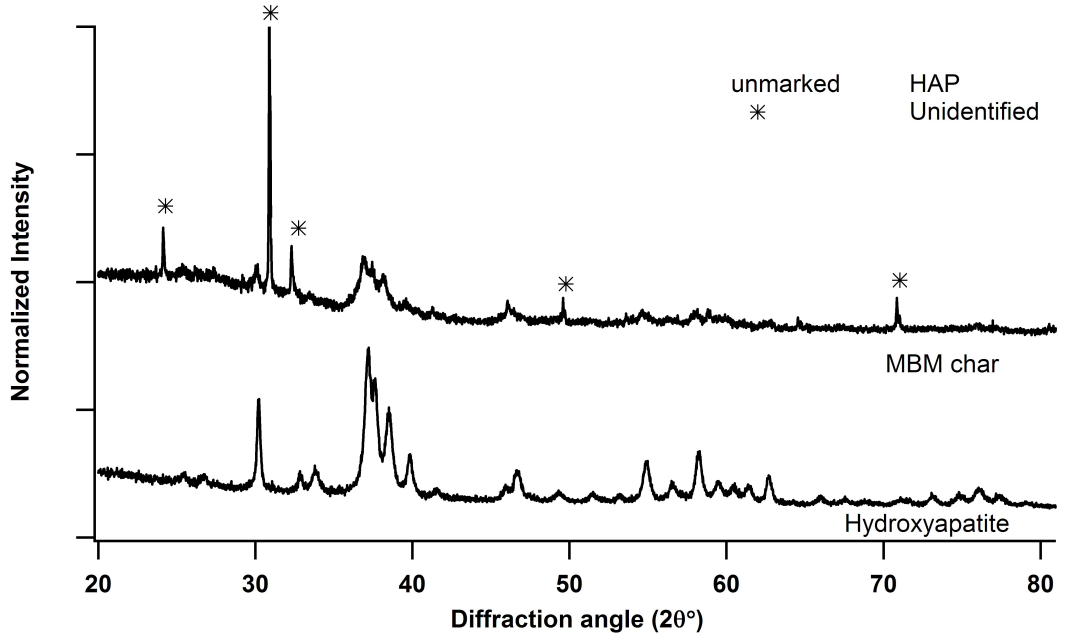

Figure 3.3. X-ray diffraction (XRD) spectra of meat and bone meal (MBM) biochar after washing and storage in 0.1 M $NaNO_3$ and a hydroxyapatite (HAP) standard. All unmarked peak positions of MBM biochar match with the peak positions of HAP.

3.4.4 Specific surface area and total elemental analysis

External surface area of MBM biochar was found to be 35.3 ± 0.6 m^2 g^{-1} (Table 3.1). Other studies of pyrolyzed meat and bone meal are consistent with this result. For example, Ayllon et al. (2006) found an increase in surface area with temperature, peaking at 37.7 m^2 g^{-1} at 900°C. The surface area and crystallinity are consistent with a previously reported MBM biochar with a maximum heating temperature of 700°C (Dimovic et al., 2009). It is possible that a 'thermal shielding effect' as well as the short heating time prevented interior

meat or bones from reaching the full oven temperatures; this has been observed in other laboratory studies involving pyrolysis (Etok et al., 2007; Coutand et al., 2008).

Table 3.1. Meat and bonemeal (MBM) biochar total elemental composition.

SA † (m^2 g^{-1})	35.3 ± 0.6
TC‡ (g kg^{-1})	346.0 ± 0.6
Ca§ (g kg^{-1})	134.8 ± 0.05
P	72.6 ± 0.1
K	18.2 ± 0.7
Na	10.7 ± 0.9
Fe	9.6 ± 1.0
Mg	5.3 ± 0.2
Al	4.4 ± 0.2
Mn	0.2 ± 0.006
Ti	0.1 ± 0.05
Zn	0.1 ± 0.001
Sr	0.1 ± 0.001
Ba	0.1 ± 0.001

† External surface area (SA) measured by Quantachrome (n=3)

‡ Total carbon (TC) measured by LECO method at 1100 °C (n=5)

§All other measurements are HF digest of MBM and measurement on ICP-MS

Pure HAP has a Ca:P elemental ratio of 1.65–1.67 (Narasaraju and Phebe, 1996; Peters, 2000), whereas the MBM biochar has a higher ratio of 2.01 (Table 3.1). One possible explanation for this elevated Ca:P ratio is the presence of other calcium compounds that do not include P. Attenuated total reflectance Fourier transform infrared spectroscopy suggested a carbonate component as carbonate substitution for phosphorus; this may affect the Ca to P ratio by reducing the phosphate content of the apatite relative to Ca. Although XRD did not match calcite or aragonite with the peak patterns of MBM biochar, amorphous calcium minerals may be components of MBM biochar.

Other elements such as K and Na are also present in high concentration. The XRD analysis indicates other unidentified, highly-crystalline minerals could possibly be soluble salts (e.g., KCl), these elements are associated with the soluble ash fraction of MBM char (Deydier et al., 2005). Given apatites' natural tendency to form cationic and anionic

substitution, non-stoichiometry is common (Ishikawa et al., 1993; Narasaraju and Phebe, 1996). Natural apatites such as those in bone commonly have Mg substitution for Ca, which may contribute to this element's abundance (Narasaraju and Phebe, 1996). Meat and bone meal biochar also contained 346 g kg^{-1} carbon, which has been found in other studies on similar meat and bone meal char (Deydier et al., 2005; de Jong et al., 2007). Other elements such as Na, K, Fe, Mg and Al are commonly associated with organic meat waste and have been cited as occurring in meat thermal decomposition end-products (Coutand et al., 2008).

3.5 Conclusions

Production of MBM biochar resulted in a residue with a surface area of 35.3 ± 0.6 m^2 g^{-1}. The MBM biochar material contains 346 g C kg^{-1}, which includes charred organics. The mineral portion of the MBM biochar is dominated by HAP. The major elements in MBM biochar are Ca, and P at 134 and 72 g kg^{-1}, respectively. Other major components (e.g., K, Na, Fe, Mg, Al) have been attributed to the organic portion of MBM biochars (Deydier et al., 2005).

X-ray diffraction and ATR-FTIR evidence indicate carbonate substitution into the HAP structure for some of the PO_4^{3-} groups and some of the OH^- groups. The ratio of Ca:P (2.01) is higher than those reported for HAP (1.65), which is consistent with HAP and Ca from other phases. The proposed formula for the carbonated apatite found in the MBM biochar is given by [Eqn. 3.1]:

$$Ca_{10}(PO_4)_{6-x}(CO_3)_xOH_{2+0.4x} \qquad [3.1]$$

In summary, a carbonated HAP with a moderately-high surface area was identified as the major mineral component of MBM biochar.

4.0 MACROSCOPIC AND SPECTROSCOPIC EVALUATION OF ZINC SORPTION ONTO MEAT AND BONE MEAL (MBM) BIOCHAR

4.1 Preface

After characterizing the physicochemical properties of meat and bone meal (MBM) biochar in Chapter 3, results confirmed that it contains a carbonate-substituted hydroxyapatite when suspended in solution. To determine the extent and mechanism of Zn adsorption onto MBM biochar, adsorption experiments were performed by varying the time of reaction, pH, and Zn concentration. Zinc *K*-edge x-ray absorption spectroscopy (XAS) were performed on the resulting adsorbent and Zn species detailed. The combination of macroscopic adsorption experiments and molecular-scale Zn XAS, provide compelling evidence for the mechanism of Zn adsorption. This provided the first XAS-based evidence of Zn bonding mechanisms with a MBM biochar material, and will also provide the potentially important standard to use in modeling the XAS of MBM biochar-amended soils in Chapter 5.

4.2 Introduction

Because many metals, such as Pb, Zn, and Cd, are extremely reactive with phosphorus (Ma, 1994; Chen et al., 1997), bone and its major mineral component hydroxyapatite (HAP) have been studied as metal sorbents in both wastewater filtration (Cheung et al. 2000; Carlos Moreno et al., 2010) and contaminated soils (Boisson et al., 1999; Hodson et al., 2000). Meat and bone meal (MBM) biochar is a waste material with a high HAP content that is sourced from animal rendering plants and can provide a cost-effective source of phosphate. Meat and bone meal is commonly incinerated or pyrolyzed as a treatment method to allow for its safe disposable, but it has been suggested that the charred residue could be repurposed as an alternative source of HAP for agronomic and/or environmental purposes (Chaala and Roy, 2003; Deydier et al., 2005; Etok et al., 2007; Coutand et al., 2008).

HudBay Minerals Inc. operates a mining and Cu/Zn processing facility near Flin Flon, MB. The native forest has been reduced by fires, and native vegetation has been

extremely slow to recover. This slow recovery has been attributed to an increase in soil acidity and metals concentration originating from the Cu/Zn smelter complex. The soils are generally acidic (pH 3.5–4.5) due to a combination of sulfuric acid deposition and naturally acidic parent materials, and Zn concentrations in soils near the smelter can be as high as 10,000 mg kg^{-1} soil (Jones and Henderson, 2006), suggesting that this element may be limiting revegetative success. Indeed, at high concentrations, Zn is one of the most phytotoxic metals (Chaney 1994; Paschkle et al., 2000). Thus to stimulate revegetation, a variety of *in situ* soil amendments are being considered to alleviate acidity and immobilize Zn.

The expense of an amendment, as well as transportation costs can severely limit the options available to remediation projects in remote or northern areas such as Flin Flon. Waste materials, when available, are often more cost effective for use as soil amendments than synthesized or mined products (Kumpiene, 2008), but their reactivity and suitability may vary depending upon source and material handling practices (Babel and Kurniawan, 2003). For this reason, it is important to test the reactivity of any waste material prior to application to determine whether it is a suitable amendment for the site. Meat and bone meal (MBM) biochar is one such material that could be sourced locally and has a high apatite content (Chapter 3), which indicates potential for Zn immobilization.

Studies that investigate Zn sorption on bone or its major component (hydroxyapatite) commonly find dissolution of the bone accompanied by precipitation of the Zn phosphate mineral, hopeite (Ma et al., 1994; Dybowska et al., 2009). Both bones and HAP have solubilities that depend on factors that change with heat such as mineral crystallinity, non-stoichiometry, and co-existing minerals affecting the ion activity of dissolution products (Narasaraju and Phebe, 1996; Baig et al., 1999; Etok et al., 2007). When conditions (primarily pH) favor HAP stability in solution, other sorption mechanisms have been reported to occur as well; e.g. Zn substitution for Ca (Terra et al., 2002; Barrea et al., 2003), surface complexation (Xu et al., 1994). Most often, a combination of mechanisms is interpreted to occur between Zn and HAP (Xu et al., 1994; Smiciklas et al., 2008).

Recent direct spectroscopic studies using extended x-ray absorption fine structure (EXAFS) spectroscopy probed the bonding environment after sorption of Zn onto a synthetic HAP mineral (Lee et al., 2005). It was interpreted from multi-shell theoretical EXAFS

modeling that the mechanism of Zn adsorption had been primarily bidentate inner-sphere bonding to phosphate in the synthetic HAP. To my knowledge, however, sorption reactions on industrially produced bone material such as MBM biochar have not been characterized using EXAFS or multi-shell theoretical EXAFS modeling.

The purpose of this study was to determine the extent and mechanism of Zn adsorption onto MBM biochar as a function of time, pH, and Zn concentration in laboratory-based adsorption experiments. In conjunction with these macroscopic studies, the Zn speciation was determined using x-ray absorption spectroscopy (XAS) on solid residues recovered from adsorption experiments.

4.3 Materials and Methods

4.3.1 Meat and bonemeal (MBM) biochar

Meat and bonemeal biochar was obtained from Titan Clean Energy Projects Corporation (Craik, SK). The MBM and willow *(Salix spp.)* wastes were each pyrolyzed separately before being combined and consisted of a 90:10 (v/v) mix of pyrolyzed MBM and willow. The end-product, hereafter refered to as 'MBM biochar', contains carbonate-substituted HAP as the main mineral component (see Chapter 3).

The 'willow biochar' alone (sourced from the same producer) was also tested for in Zn adsorption experiments. Following the methods used for MBM biochar, willow biochar was prepared as a 'stock suspension' by sequential washing with 0.1 M $NaNO_3$ prior to adsorption experiments.

4.3.2 Stock suspension preparation

Meat and bone meal biochar was prepared as a suspension in a background electrolyte of 0.1 M $NaNO_3$. Use of a background electrolyte provides non-specific, weak competitor ions (e.g., Na^+ and NO_3^-) during sorption reactions and makes it possible to adjust pH with a strong acid/base without altering the ionic strength of solution (Sigg and Stumm, 1981). Meat and bone meal biochar was chosen to be studied as the < 2-mm size fraction to better represent typical soil amendments.

Procedure for repeated washing of MBM biochar to create a 'stock suspension' of constant ionic strength is as follows: A mass of 3.5 g (<2-mm particle size) MBM biochar

was suspended in 150 mL 0.1 M $NaNO_3$ in a 250-mL polypropylene bottle (n=4) and shaken at 160 rpm for 1 h on a gyratory shaker (New Brunswick Scientific, Model G10, Manasquan, New Jersey USA). The suspensions were then centrifuged at 6,000 g for 2 h (Heraeus Megafuge 1.0, Langenselbold, Germany), the supernatant decanted and discarded. The MBM biochar was then re-suspended with 150 mL and the procedure was repeated a total of three times.

The washed MBM biochar solid was then transferred to a 1.0 L screw-top glass bottle and brought to a final volume of 1.0 L with 0.1 M $NaNO_3$. The final suspension density was measured as follows: 5.0-mL aliquots of suspension were pipetted into weighing tins and oven evaporated at 105°C. The dry weight of the residue (corrected for the mass of $NaNO_3$ present) was used to provide suspension density (in g L^{-1}) of the char suspension. The 1.0 L of stock suspension was kept at 10 °C to slow microbial decomposition. This method was used to for all stock suspensions used in this project. Multiple stock suspensions were necessary to provide sufficient material for all sorption experiments.

4.3.3 Adsorption experiments

Adsorption experiments were conducted using a modified method from Zasoski and Burau (1978). Experiments were initiated in 500 mL reactors to establish and homogenize reaction conditions (e.g., temperature, pressure, pH, adsorbate concentration, adsorptive concentration) under well-mixed conditions on a magnetic stir plate. After a short time (10 min) in this stirred-batch reactor, a 10-mL aliquot was transferred into a 15-mL polypropylene centrifuge tube and mixed via shaking. The multi-tube technique comprises the majority of adsorptive/adsorbent reaction time (i.e., 72 h) in which the Zn reacts with MBM biochar. When necessary, pH was adjusted in the tubes, and minor changes in volume following acid/base additions were accounted for and adjusted concentrations were calculated (Microsoft Excel, 2011). All experiments were performed at room temperature (24 ± 0.3 °C).

At the end of the experiment, suspensions were filtered with disposable 25-mm, 0.45-µm pore size disposable filters (Whatman, Inc, Clifton NJ, USA) and filtrate was collected in a separate 15-mL centrifuge tube, acidified with 10 µL of 8.0 M HNO_3 and stored at 4°C until elemental analysis via atomic absorption spectrometry (AAS). Zinc and/or Ca were measured separately in the filtrate using a SpectrAA 220 Atomic Absorption Spectrometer

(Varian Australia Pty Ltd., Mulgrave, Victoria, Australia). Standard operating methods were used for Zn or Ca measurement (Varian Inc., 1989). Prior to Flame-AAS measurement, the samples were diluted with $LaCl_3$ (0.72 mmol L^{-1}) to ensure that Zn concentration was within the linear range of absorbance measured on calibration standards. Lanthanum solution was used to prevent phosphate mineral precipitation when measuring Ca or Zn (Baker and Amacher, 1982; Cantle, 1982).

A stock 1.0 M Zn spiking solution for all adsorption experiments was prepared by weighing 14.87 g $Zn(NO_3)_2 \bullet 6H_2O$ into a 500-mL volumetric flask, acidified with 50 μL 8 M HNO_3 and filling to volume with double-distilled water (18 Ω). Final pH of solution was measured with accuTupH rugged-bulb, pH electrode with KCl internal solution and double-junction reference (Fisher Scientific, Singapore, Singapore). Actual Zn concentration in solution was determined by replicated measurement (n=5) with a mean value of 1.05 mM using AAS.

4.3.3.1 Adsorption pH envelopes. Adsorption experiments where only the pH was adjusted and zinc concentration and reaction time are constant are referred to as pH envelopes. The purpose of this experiment is to observe the pH at which an 'adsorption edge' occurs and dissolved Zn concentration markedly decreases.

The stirred-batch envelope experiment was initiated by transferring a 50 mL aliquot of the MBM biochar 'stock suspension' to a 500-mL Erlenmeyer flask and diluted with 0.1 M $NaNO_3$ measured with 50-mL and 200-mL volumetric flasks. The solution was well-mixed with a Teflon magnetic stir bar on a stir plate and sparged with N_2 for 12 h prior to pretreatment. The actual mass of MBM biochar in each stirred-batch reactor was determined by measuring the mass of solid retained after filtrate separation in the experimental blank (10 mL). This mass was defined as the difference in dry paper weight before and after sample filtration and correction for the presence of 0.1 M $NaNO_3$ in the entrained solution volume.

Two distinct MBM biochar pH adsorption envelope experiments were performed: (1) no pre-treatment of MBM biochar and an initial reaction pH of 8.6 or (2) pre-treatment of MBM biochar in stirred-batch reactor by acidification to pH 3.5. In both cases, the stirred-batch suspension was maintained for 72 h prior to a 1.0 mM Zn spike at which point pH was measured and adjusted with either 0.1 M HNO_3 or 0.1 M NaOH using a Metrohm 716 Stat Titrino autotitrator (Metrohm, Herisau, Switzerland) depending on the starting conditions.

The untreated pH experiments began at pH 8.6, and after Zn spike were readjusted to this pH with 0.1 M NaOH, allowed to mix for 10 min, and then 10-mL aliquot of sample was pipetted into a 15-mL falcon tube and placed on a Rugged Rotator Model 099A carousel shaker (Glas-Col, Terre Haute, Indiana, USA). Solution pH was adjusted to 8.0 with 0.1 M HNO_3, at which point the stirred-batch reactor was allowed to mix for 10 min, a 10-mL aliquot pipetted into a 15-mL falcon tube that was placed on a carousel shaker at 10 rotations min^{-1}. These steps were repeated for each pH half unit increment (i.e. 8.5, 8.0, etc.), ending at pH 3.5. All centrifuge tubes were then mixed under constant agitation for 72 h on a carousel shaker. This procedure was performed in triplicate (n=3). Solution pH was measured every 24 h and adjusted with 0.1 M HNO_3 or 0.1 M NaOH accordingly within ± 0.1 pH unit of each sample's initial pH. Volume changes due to acid or base addition were recorded and suspension density and concentration were adjusted when necessary.

The acidified pre-treatment followed the same methods except an initial adjustment of the stirred-batch reactor to pH 3.5 by addition of 2 M HNO_3. The experiment began at pH 3.5 and was titrated upwards with 0.1 M NaOH. At each pH half unit increment (i.e., 3.5, 4.0, etc.) suspension was allowed to equilibrate for 10 min and then a 10-mL aliquot was transferred to 15-mL centrifuge tubes. This procedure was performed in duplicate (n=2).

For both types of envelopes, final pH was measured after 72 hours; the solid was then separated by filtration through a Whatman 25 mm, 0.45-µm pore size disposable filter, and filtrate was stored in 15-mL polypropylene falcon tubes at 4°C prior to AAS analysis for dissolved Zn and Ca using previously described methods (Section 4.3.3).

4.3.3.2 Adsorption kinetics. Adsorption kinetics can describe the reaction rate as mass of sorbate per sorbent (q) as a function of time (t). Suspension pH for kinetics experiments was maintained at 6.0 ± 0.05 (under constant sparging with N_2) using a Metrohm 716 autotitrator and 0.1 M NaOH. The MBM biochar sorbent was pre-equilibrated at pH 6.0 for 24 h, and then a blank (time=0) subsample was removed. Zinc was next added by pipetting 5.0 mL of 1.0 M $Zn(NO_3)_2$, resulting in a final Zn concentration of 1.0 mM Zn^{2+}. After Zn addition, 10-mL aliquots were periodically removed and immediately filtered (via 0.45-µm disposable filters), the filtrate acidified with 10 µL 8.0 M HNO_3 and stored at 4°C prior to analysis. Samples were removed from stirred-batch reactor at 15-min intervals during the first hour of

reaction, at 30-min intervals for the next 3 h, and additional sampling at 16, 18, 24, 26, 48, and 72 h was performed. This kinetics experiment was performed in triplicate (n=3).

Samples were measured for Zn concentrations using previously described methods (Section 4.3.3) by AAS (SpectrAA 220 Atomic Absorption Spectrometer, Varian Australia Pty Ltd., Australia).

4.3.3.3 Adsorption isotherms. An adsorption isotherm is the graphical representation of the activity or equilibrium concentration of the sorbate (c; mmol L^{-1}) and the quantity of sorbate on the sorbent at constant temperature (q; mmol g^{-1}). The reaction of Zn with MBM biochar at pH 6 without sample pretreatment and with two sorbent pre-treatments studied. The two pre-treatments were: (i) acidification by pre-equilibriation at pH 5.0 for 24 h and (ii) sonication by disruption of aggregated MBM biochar using 15 W of vibration for 10 min with a W350 sonifier cell disruptor (Branson Sonic Power Co., Danbury, Connecticut USA). The rationale for acidification is to dissolve any carbonate (observed in the MBM biochar stock characterization in Chapter 3), which is more soluble at this pH than HAP. The choice of pH 5.0 is based on the work of Cheung and co-workers (2002) to remove carbonates without dissolving HAP. The sonication effect was tested because the particle size of MBM biochar used in these experiments was <2-mm and as a result, aggregated particles are likely to persist. This aggregation may decrease the adsorption capacity of the biochar.

The adsorption experiments were performed in stirred-batch reactors at pH 6.1, 0.1 M ionic strength ($NaNO_3$). The stirred-batch suspension was N_2 sparged for 12 h prior to Zn addition, and a 10-mL blank was removed prior to addition of the first Zn spike. The acidification pre-treatment method was maintained at pH 5.0 for 24 h prior to Zn spiking The methods using untreated adsorbent and sonication pre-treated adsorbent were each performed in five replicates (n=5); the method using acidification pre-treated sorbent was performed in triplicate (n=3).

In all cases, the stirred-batch reactors were successively spiked with increasing amounts of 0.1 M $Zn(NO_3)_2$ to produce Zn concentrations ranging from 0 to 2.5 mmol Zn L^{-1}. At each concentration, the stirred-batch reactor was allowed to mix for 10 min and a 10-mL aliquot was taken at each concentration and allowed to react in polypropylene tubes (15-mL) for 72 h on a vertical carousel shaker Rugged Rotator Model 099A (Glas-Col, Terre Haute, Indiana, USA) at 10 rotations min^{-1}. Suspension pH was measured every 12 h and

adjusted to pH 6.1 ± 0.1 by pipetting either 0.1 M NaOH or 0.1 M HNO_3; volume changes due to acid or base additions were adjusted in calculations accordingly.

After the reaction was complete (i.e., after 72 h), each sample was passed through a Whatman 25 mm, 0.45-µm pore size disposable filter. Filtrate was stored in 15-mL polypropylene falcon tubes at 4°C until analysis by atomic absorption spectrometry via SpectrAA 220 Atomic Absorption Spectrometer (Varian Australia Pty Ltd., Mulgrave, Victoria, Australia). Methods are described in Section 4.3.3.

4.3.4 Synthesis of standards and samples for XAS

Methods for synthesizing the hydroxyapatite (HAP) used in this study can be found in Tang et al. (2009). X-ray diffraction spectra of the synthetic HAP matched a commercial HAP, shown in Appendix A. Hydroxyapatite was synthesized under N_2-atmosphere in a glovebox (PlasLabs, Lansing, Michigan, USA). Solutions (100 mL each) of 0.2 M $Ca(NO_3)_2$ and 0.12 M $(NH_4)_2HPO_4$ were added slowly into a 250-mL screw-top Pyrex bottle with constant stirring and while maintaining a pH >8.0 using 14 M NH_4OH. The sealed 250-mL screw-top Pyrex bottle was then removed from the glovebox and heated with stirring at 90°C for 5 h. The sample was then transferred to a 50-mL polypropylene centrifuge tube, centrifuged at 6,000 g for 10 min, and the resulting material was washed three times by addition of 40 mL DI water, 15 W of ultrasonic vibration for 10 min using a W350 sonifier cell disruptor (Branson Sonic Power Co., Danbury, Connecticut USA), and separation via centrifugation. The solid residue was then dried at 105°C in a convection oven for 10 h to produce synthetic HAP.

Using the synthetic HAP, a Zn/HAP adsorption sample was prepared for XAS measurement by suspending 3.0 g of synthetic HAP in 40 mL of 0.1 M $NaNO_3$ containing 1.0 mM $Zn(NO_3)_2$ and adjusted to 6.1 ± 0.1 with 0.1 M NaOH, and shaken for 2 h. This sample was centrifuged at 6,000 g for 30 min, the supernatant was filtered, acidified, and stored at 4°C AAS analysis as described previously in Section 4.3.3.

Each MBM biochar adsorption XAS sample was synthesized by reacting MBM biochar and Zn in a stirred-batch suspension as described in Section 4.3.3. Four samples of separate reaction conditions (e.g., reaction time and Zn concentration) were synthesized to test for their effect on the species of adsorption. Stirred-batch reactors were reacted for either 2 h or 48 h in the presence of either 1.45 or 2.25 mM Zn at pH 6.1 under constant N_2 gas

sparging. The solid was recovered onto 0.45-μm pore-size filter paper by vacuum filtration; pastes were pressed into Teflon XAS sample holders that were sealed with Kapton tape until Zn *K*-edge XAS spectra were measured. Filtrate was acidified with 10 μL of 8.0 M HNO_3 and stored at 4°C for measurement by Flame atomic absorption spectrometry as discussed previously in Section 4.3.3.

4.3.5 Zinc *K*-edge x-ray absorption spectroscopy

Zinc *K*-edge XAS were measured into the EXAFS region at the HXMA beamline (06-ID1) of the Canadian Light Source, Inc. in Saskatoon, SK, Canada. Spectra were collected using a Si (220) monochromator with detuning of 40–50% at 12k to remove higher order harmonics. The beamline was calibrated to the Zn K-edge (9659 eV) using a reference Zn metal foil located behind the sample, allowing for continual calibration and alignment of data throughout the measurements. Multiple EXAFS scans were collected in partial fluorescence mode using a solid-state liquid nitrogen-cooled 32-element germanium (Ge) detector (Canberra) with a 6 μm Cu filter and Sollar slits to remove fluorescence arising from other elements and scattering effects. Individual spectra were calibrated, aligned, and then averaged for analysis using the program Athena (Ravel and Newville, 2005).

Multi-shell theoretical EXAFS modeling was performed using the program WinXAS v. 311 (Ressler et al., 1998). The amplitude reduction factor was held constant for all models, and was estimated to be 0.87 based on results from modeling a dilute zinc nitrate solution with constrained coordination number of 6.0. Coordination number and shell distance errors of this study are based on the errors found in modeling of Zn *K*-edge EXAFS in comparable systems (Scheidegger et al., 1997; Lee et al., 2005; Nachtegaal et al., 2005; Ryser et al., 2006). Shell distances had an error of ±0.02 Å for the first shell, ±0.03–0.05 Å for more distant shells. Coordination number (CN) error is ±15% for the first O shell and ± >25% for the more distant shells.

4.4 Results and Discussion

4.4.1 Adsorption experiments

4.4.1.1 Adsorption pH envelopes. Meat and bone meal biochar released large amounts of calcium into solution (Fig. 4.2), which when combined with strong pH buffering at pH 6.3

(observed during pH adjustments), suggested the presence of a soluble calcium mineral or compound. Given that the pKa_1 of H_2CO_3 is 6.35 (Lindsay, 1979), and that carbonate substitution in HAP was identified as a component of the MBM biochar in Chapter 3, this is most likely a result of the CO_3 component solubilizing from the MBM biochar.

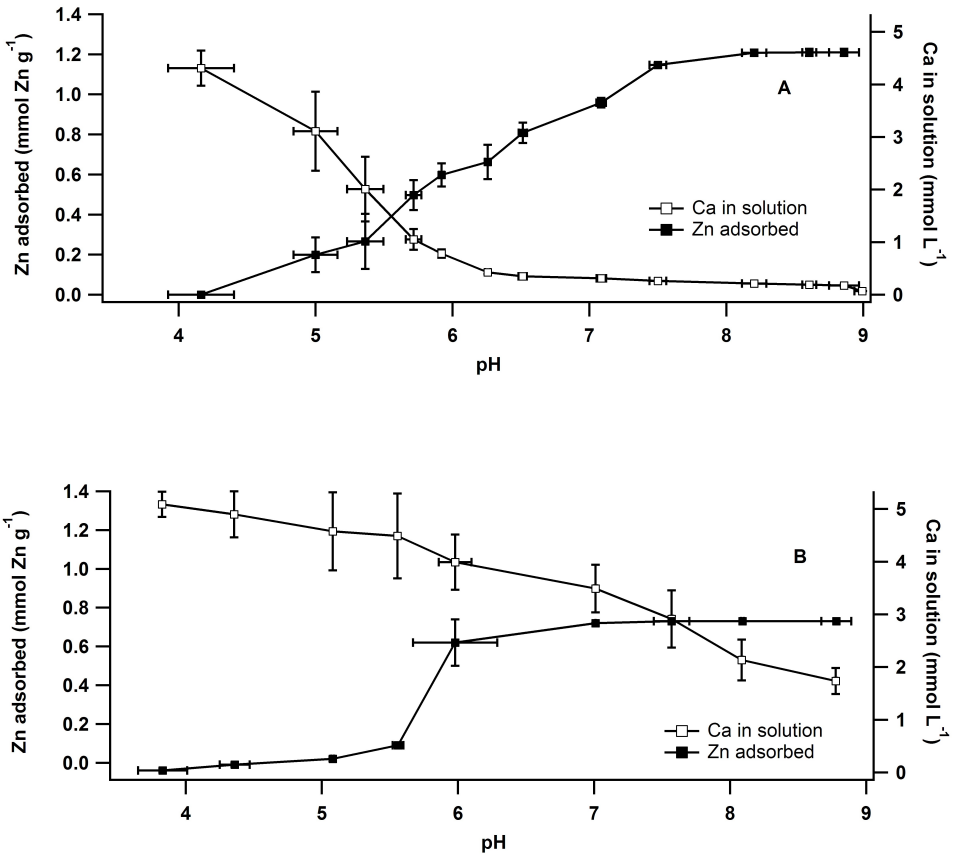

Figure 4.2. Adsorbed Zn (black squares) and Ca concentration in solution (white squares) are displayed as the mean of replicates with error bars of 1 standard deviation. The untreated pH envelope (A) shows gradual Zn adsorption over the pH range 4.0–8.0. Measurement of Ca in the untreated pH envelope suggests that a Ca-mineral is stable at high pHs but dissolves below pH 6.3. When MBM biochar had acidification pre-treament, Ca concentration is high in solution over the entire pH range. Under the acidified conditions, Zn sorption is very different and is steeply removed from solution at pH 5.5.

Pretreatment of the MBM biochar strongly influenced the pH dependence of Zn adsorption (Fig 4.3, black squares). The untreated pH edge (Fig 4.3A) shows a wide range of pH-dependent adsorption (i.e., 4.0–8.0), whereas acidified MBM biochar (Fig 4.3B) has a steep pH edge, showing near-complete Zn removal between pH 5.0 and 6.0. The discrepancy

in total Zn concentration between the two treatments is due to a difference in the concentration of the Zn spike and not a chemical effect.

The acidification pre-treated envelope may be a result of Zn sorption occurring after a portion of the HAP in MBM biochar has dissolved. Solubility of HAP has been observed at pH 5.0 (Cheung et al., 2002), making the pre-treatment at pH 3.5 for 24 h well below solubility of this mineral and HAP dissolution a likely outcome. Dissolution of HAP is supported by the high concentration of dissolved Ca present over the entire pH range of this experiment (Fig 4.2A). Dissolution is also supported by the negative q values at pH 3.8 and 4.5 (Fig 4.2B) due to a higher concentration of Zn in solution than the amount added. This could possibly be from the Zn content in the MBM biochar itself being released after mineral dissolution. Meat and bone meal biochar was shown to contain 113.7 mg Zn kg^{-1} by total elemental analysis (Chapter 3) whose release into solution with mineral dissolution would cause a Zn concentration higher than the amount added, thus the negative adsorption.

This dissolution may explain the difference in pH edges between the two methods. If mineral dissolution were occurring, large amounts of Ca^{2+} and PO_4^{2-} would be released and could explain the Ca^{2+} present in solution. If PO_4^{2-} activity were to exceed the solubility of a Zn-phosphate mineral (e.g., hopeite), precipitation would be a likely outcome. This is consistent with the results of Chen and co-workers (1997) who used XRD to confirm that hopeite precipitation after HAP dissolution occurred at pH 6.5.

Zinc and Ca measured in untreated pH envelope showed a molar uptake Zn to moles released Ca ratio of 1.4:1 between pH 6.2 and 8.0 (Fig 4.2A). Several researchers have interpreted mechanisms for Zn adsorption onto HAP as Zn ion exchange for Ca (Xu et al., 1994; Cheung et al., 2002; Smiciklas et al., 2008), in which case the Zn-uptake to Ca-release ratio should be 1:1. The higher ratio of Zn adsorption to Ca release (e.g., 1.4:1) observed during this study suggests that this may be occurring, but there are likely one or more other mechanisms responsible for Zn adsorption. For example, competition by Zn for surface adsorbed Ca could also give rise to Ca release, which could give rise to proportional release of Ca with Zn adsorption.

4.4.1.2 Adsorption kinetics. The kinetic adsorption data (q_t vs. time) were modeled using first-order kinetics and the Elovich, and power function models. Of these, the Elovich model [Eqn. 4.2] provided the best fit:

$q_t = (1/\beta) \ln(\alpha\beta) + (1/\beta)\ln(t)$ [Eqn. 4.2]

where q_t is the amount of sorbate per mass of sorbent at time t and the parameters α and β are constants specific to the experimental conditions. Although some studies have suggested that these constants can provide information about the adsorption kinetics, Sparks (2003) indicated that they are only useful as operationally-defined values. The Elovich model fit to the observed data had values of α= 0.427 and β = 6.390 and an r^2=0.93.

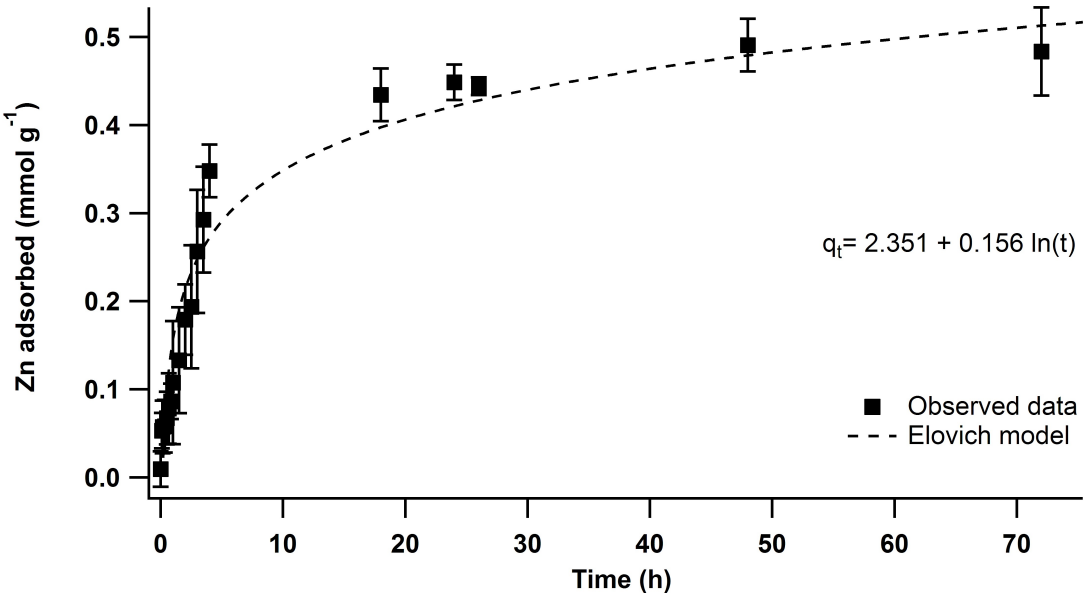

Figure 4.3. The reaction of MBM biochar with Zn is displayed as a function of time. Data is shown as Zn adsorbed (mmol g^{-1}) and error bars denote ±1 standard deviation from the mean (n=3). The Elovich model (dashed line) fit to the data is shown.

The Elovich equation has been used to infer a number of reaction mechanisms, including bulk and surface diffusion. The Elovich model describes reactions that are bi-phasic, with an initial, rapid reaction followed by a slower, secondary accumulation. This is observed in many sorption reactions, and may imply reactions limited by diffusion (Sparks, 2003). This would be the case if the external surface sites become saturated and particle aggregation necessitates the diffusion of Zn into the particle. Cheung et al. (2000) interpreted

the mechanism of Zn sorption onto a bone char fit with an Elovich equation to be diffusion through pores.

Other studies have found a more rapid rate of reaction (30 m to 1 h) compared to the slower rate found with MBM biochar (5 h) (Cheung et al., 2000; Sheha et al., 2007). This supports the theory that the adsorption of Zn is diffusion limited due to the surface properties of MBM biochar.

A near 1:1 stoichiometric exchange of Zn^{2+} for H^{+} was observed in the kinetics experiments based on observations of volume of acid dispensed from the autotitrator compared to the moles sorbed of Zn at each time point. This has previously been used as an indicator of the paired reaction of simultaneous surface deprotonation and inner-sphere Zn adsorption to surface sites [Eqn. 4.3] (Xu et al., 1994):

$$SOH + Zn^{2+} \leftrightarrow SO–Zn^{+} + H^{+} \qquad \text{[Eqn. 4.3]}$$

where 'S' denotes a generic surface with protonated oxygen groups.

4.4.1.3 Adsorption isotherms. Effect of pretreatment on Zn adsorption was evaluated in suspensions maintained at pH 6.1. Interestingly, the degree of variability followed the order: sonication > no pre-treatment > acidification (0.1, 0.03, 0.01 mmol Zn g^{-1}, respectively). Sonication was expected to produce a more homogenous and higher surface area solid and result in a lower deviation than untreated MBM biochar, so this current result is unexpected. One possible explanation is that 72 h of reaction time in the isotherms allows for re-aggregation and flocculation of the MBM biochar, and this colloidal process may be somewhat variable.

The adsorption experiments and their isotherm models are presented in Figure 4.4. No pre-treatment showed the lowest adsorption capacity and sonication or acid pre-treatment both increased to the adsorption capacity. Results were tested against the Langmuir and Freundlich models. The Langmuir equation is given:

$$q = kcb/(1+kc) \qquad \text{[Eqn. 4.4]}$$

where 'q' is the amount of adsorption (adsorbate per unit mass of adsorbent in mmol kg^{-1}), 'c' is the final Zn concentration (mmol L^{-1}), 'k' is a constant related to the binding strength,

and ‘b’ is the maximum amount of adsorbate that can be adsorbed assuming monolayer coverage (Sposito, 1984).

The Freundlich equation is given:

$$q = K_f C^n \qquad \text{[Eqn. 4.5]}$$

where q and c were previously defined and K_f and n are coefficients (Sposito, 1984).

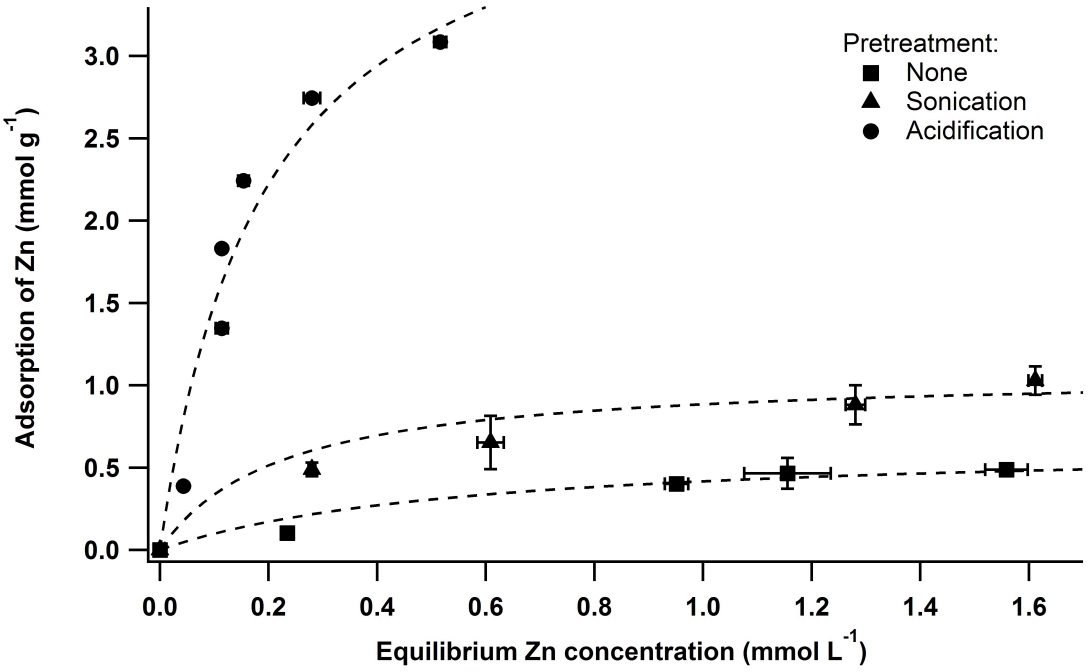

Figure 4.4. Zn adsorption experiments varying concentration of the adsorbate (Zn) at pH 6.1 ± 0.1 with a variety of surface pretreatments of the MBM biochar. The adsorption experiments are plotted as sorption capacity (q) as a function of the final adsorptive concentration remaining in solution (c). Data points and error bars are mean values and 1 standard deviation of results.

All adsorption isotherm results were best fit with the Langmuir model. Results from isotherm modeling, coefficient of determination (R^2) and derived maximum adsorption capacities are reported in Table 4.1.

Table 4.1. List of Langmuir model parameters, adsorption capacities and their coefficient of determination (R^2)

MBM pretreatment	K	1/b	q_{max}	R^2
			mmol g^{-1}	
None	1.783	1.539	0.65	0.68
Sonication	4.526	0.926	1.08	0.94
Acidification	5.213	0.230	4.35	0.65

It should be noted that despite the Langmuir providing the best fit to the observed data, many assumptions are necessary to use the Langmuir equation accurately. Most of these assumptions are not valid for the heterogeneous surfaces known to be in the MBM biochar. The material is a composite of willow, meat and bone waste after pyrolysis, so the assumption of a homogenous surface cannot be met. As a result, the Langmuir equation may fit the data well, but model results should only be used for purely qualitative and descriptive purposes.

As a general observation, MBM biochar is difficult to study in traditional adsorption experiments. The non-uniform surface coating from aggregation of meat, bone and willow and the solubility of the mineral itself in the MBM biochar material cause complications of surface homogeneity. The decision to use MBM biochar as it would be applied in the field (<2-mm size fraction) as opposed to grinding and sieving to achieve a smaller particle size made sorption experiments more difficult and more variable. Based on the Langmuir equation, the maximum adsorption capacity was 0.65 mmol Zn g^{-1}. Sonicating the MBM increased Zn adsorption and precision. Based on the wellness of fit the Elovich equation described adsorption kinetics, the increased adsorption capacity of the sonicated MBM biochar may be explained by a reduction in diffusion and increase in surface area, although this was not directly measured. The slower adsorption kinetics observed for MBM biochar compared to similar bone sorbents in other studies also suggests diffusion is an important limitation for MBM biochar.

Modeling the adsorption data with the Langmuir equation yielded an adsorption capacity of 1.08 mmol Zn g^{-1} for the sonicated MBM biochar. Acidification of the MBM (pH

5.0 for 24 h) further increased reproducibility, but yielded a maximum adsorption capacity that was 4–7 times greater than isotherm models from other MBM treatments (Table 4.1). Likewise, the adsorption capacity for the acidification pre-treated MBM was greater than the values reported for synthetic HAP (Xu et al., 1994; Cheung et al., 2000; Smiciklas et al., 2008), suggesting that a different mechanism—most likely Zn precipitation—was involved after acidification.

Sheha and collegues (2007) sorbed Zn onto synthetic HAP at a comparable pH (6.0 ± 0.5) and calculated an adsorption capacity of 1.56 mmol Zn g^{-1}, comparable to that of the sonicated MBM biochar. Given that Sheha et al., (2007) studied a synthetic hydroxyapatite with a higher surface area (76.6 m^2 g^{-1}) than the present study that used MBM biochar (35 m^2 g^{-1}), the lower sorption capacities found in the present study are reasonable.

Some reported Zn adsorption capacities for bone or synthetic HAP are lower than the capacities found in this study, ranging from 0.530–0.574 mmol Zn g^{-1} (Xu et al. 1994; Cheung et al. 2000; Smiciklas et al. 2008). But, these other adsorption experiments were performed at pH 5.5, or below. A decrease in pH would either increase or decrease the adsorption capacity, depending on the stability of the HAP being studied. For example, a lower pH could induce competitive adsorption effects between Zn and protons, thereby decreasing the adsorption capacity (seen in pH envelope). Alternatively, dissolution of the HAP could increase Zn removal from the suspension by producing a Zn-phosphate precipitate. Direct comparison of MBM biochar adsorption to other studies is difficult because it contains other components (i.e., organics), unique pyrolysis conditions (i.e., short heating at 900°C) and the mineral is not a pure HAP, but rather has carbonate substitution. This would affect the buffering pH and result in a higher pH of dissolution. Meat and bone meal biochar suspensions are buffered to pH 6.3, where a release of Ca was seen in pH envelopes. This is close to the pKa_1 of H_2CO_3 at 6.367 (Loos et al., 2004).

The Zn adsorption maximum observed for the acid washed MBM was 4.49 mmol Zn g^{-1}, which is well outside of the range generally observed for similar systems. The pretreatment of MBM biochar by acidifying to pH 5.0 for 24 h may have caused dissolution of the HAP, which was followed by Zn-phosphate precipitation at pH 6.0. This large (one order of magnitude) discrepancy of the adsorption maximum for isotherms has previously been interpreted as indicative of precipitation in Smiciklas et al. (2008). Lee et al. (2005)

measured XAS on a Zn and synthetic HAP adsorption solid sample where this was the case and measured the spectra of hopeite, which was also confirmed by XRD. Methods involving acidification of the MBM biochar (to pH 3.5 or 5.0) were the only experiments in this study where the solubility of HAP may have been exceeded, and were also the only experiments to exhibit very different sorption results—all of which suggest Zn-phosphate precipitation.

4.4.1.4 Willow biochar adsorption. An analogue to the willow biochar component in the MBM biochar material was obtained from the same company. A steep pH edge at pH 7.0 in the adsorption envelope indicated the only Zn adsorption. Only a $ZnCO_3$ precipitate was observed at pH 7.0 as indicated by the steep pH edge from an adsorption experiment. From a pH envelope and Zn K-edge XAS speciation (Appendix B), it was determined that willow biochar did not directly adsorb Zn.

4.4.2 Zn K-edge XAS

The EXAFS region of Zn K-edge XAS of MBM samples and relevant reference standards were multi-shell theoretical EXAFS modeled in WinXAS 3.1 using the theoretical scattering paths computed by FEFF (Ressler, 1998). Experimental data is shown with model fits in Fig. 4.5; the modeling parameters (i.e., CN, shell distance, elements in shell) are summarized in Table 4.2.

All MBM biochar adsorption samples were fit with similar parameters regardless of time of reaction or concentration of Zn. This indicates that the same adsorption species results under all the conditions tested; i.e., whether the equilibration time was 2 h or 48 h or the Zn concentration was 1.45 or 2.25 mM. Likewise, the interatomic distances (R) and coordination numbers (CN) between the Zn adsorbed HAP standard and the MBM biochar adsorption samples are within one standard deviation, so are not significantly different (Table 4.2).

A Zn-O distance of 1.95–1.98 Å has been found by EXAFS spectroscopy for tetrahedral coordination of Zn (Elzinga and Reeder, 2002; Roberts et al., 2002; Roberts et al., 2003). In contrast, Zn in an octahedral environment (e.g. aqueous Zn^{2+}) has a much longer Zn-O distance of 2.07 ± 0.02 Å (Roberts et al., 2003).

The k^3-weighted EXAFS spectrum of hopeite (Fig. 4.5A) has a distinctive feature at 8 $Å^{-1}$ that was captured by the scattering model. A similar peak pattern is weakly visible in the EXAFS of both 48 h reacted samples, although out of phase in energy. However, given our

experimental data quality we did not improve the fit with models that added Zn-P-P or Zn-Zn pathways observed in hopeite in our 48 h sorption samples.

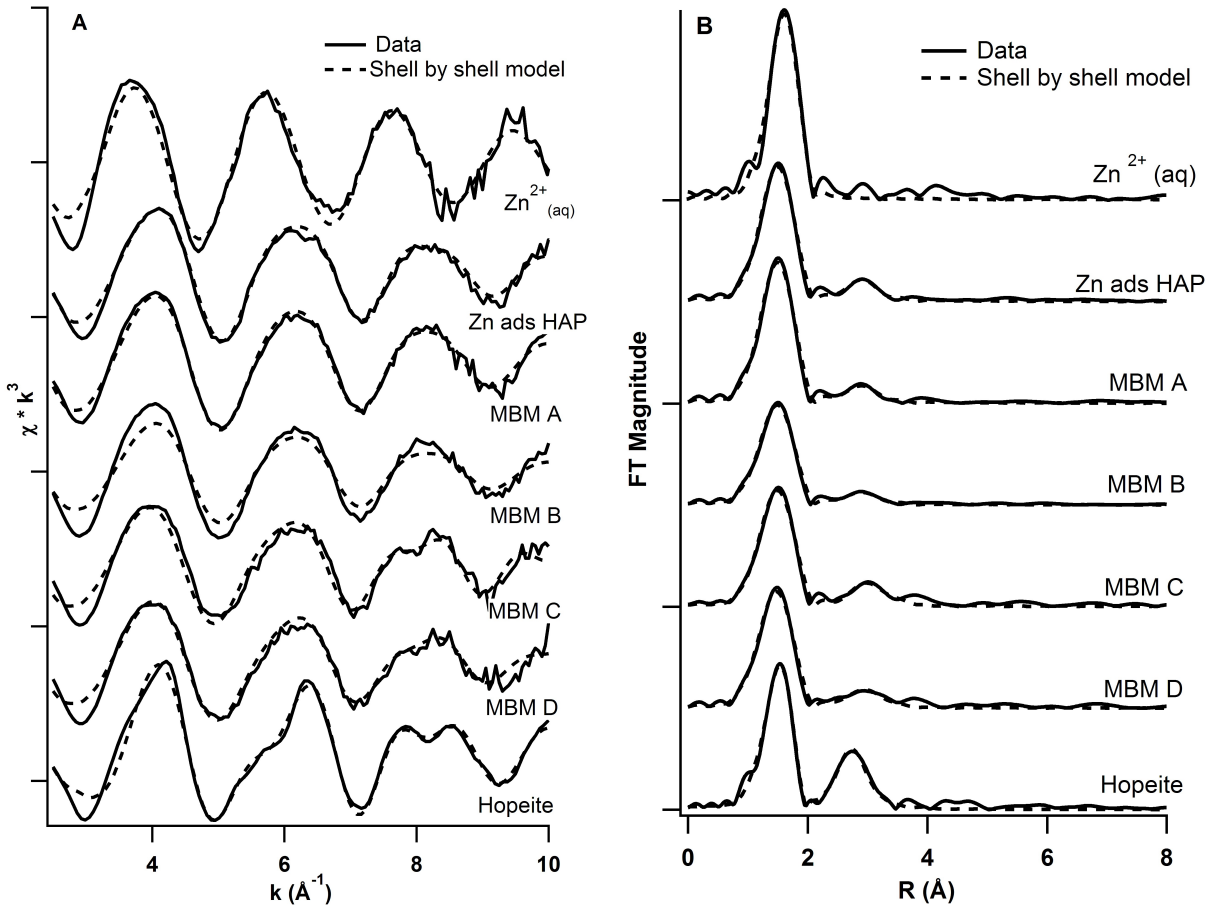

Figure 4.5. Zinc K-edge XAS of MBM samples (MBM A–D) and standards are shown in the extended x-ray absorption fine structure (EXAFS) region with k^3-weighting (A) and Fourier transformations (FT) of that region (B). Samples MBM A–D vary in reaction time or sorbate concentration and their conditions of preparation are detailed in Table 4.3 The multi-shell theoretical EXAFS models (dashed line) fit to the observed data (solid line) show that Zn speciation is not significantly different between all MBM biochar adsorption samples and the Zn adsorbed to hydroxyapatite (HAP) mineral. Hopeite mineral is distinctly different from all MBM biochar samples.

Table 4.2. Characteristics and multi-shell theoretical EXAFS models of Zn adsorbed on meat and bone meal (MBM) biochar and standards

Sample ID	[Zn]tot mmol Zn	Sample loading mmol Zn g^{-1}	pH	Reaction time (h)	Shell	CN†	R(Å)‡	σ^2(Å^2)§
Zn (aq)	0.76	-¶	1.0	-	Zn-O	6.0	2.09	-
Zn adsorbed HAP	1.0	0.33	6.30	2	Zn-O	5.0	1.97	0.009
					Zn-P	2.3	3.49	0.012
MBM A	1.45	0.27	6.30	2	Zn-O	5.0	1.97	0.009
					Zn-P	1.9	3.50	0.012
MBM B	2.25	0.40	6.17	2	Zn-O	4.0	1.97	0.010
					Zn-P	1.5	3.51	0.012
MBM C	1.45	0.38	6.25	48	Zn-O	4.5	1.98	0.010
					Zn-P	0.9	3.53	0.001
MBM D	2.25	0.46	6.24	48	Zn-O	4.2	1.96	0.009
					Zn-P	1.7	3.53	0.009
hopeite	-	-	-	-	Zn-O	5.2	1.97	0.009
					Zn-P	1.0	3.10	0.004
					Zn-Zn-P	5.9	3.46	0.003

†The model errors for coordination numbers (CN) are ± 15% for the first shell and ±>25% for second and third shells

‡ The model errors for radial distances (R) are ±0.02 Å for the first shell and ±0.05 Å for second and third shells

§The Debeye-Waller term (σ^2), is the absorber-backscatterer mean-square relative displacement

¶ (-) indicates a non-applicable value

If substitution of Zn for Ca was an important mechanism in the MBM samples, a shrinkage in the lattice from Ca-O held by 4 bonds at a distance of 2.3 Å with Zn at 1.96 Å would be expected (Tang et al., 2009; Hu et al., 2012). The replacement of Ca for Zn reduces the bond distance by at least 20% (Hu et al., 2012). Therefore, the Zn-O distance in our samples cannot distinguish between a substitution species and a tetrahedral adsorbed species. However, the Zn-P interatomic distance of 3.51–3.53 Å is much longer than the reported values for Zn substitution into HAP. In contrast, Tang et al. (2009) found two P shells at a distance of ~2.85–3.07 Å and two higher Ca shells at ~3.71–4.02 Å. These scattering pathways for Zn-P and Zn-Ca gave poor fits to the observed data.

The Zn-P distance of 3.53 Å also is too long for bidentate bonding (Lee et al., 2005) and the second shell would not be expected at this distance for outer-sphere adsorption. Instead, the Zn-O and Zn-P interatomic distances are most consistent with a monodentate bond to the oxygen of a phosphate group, which can be visualized in Fig. 4.6.

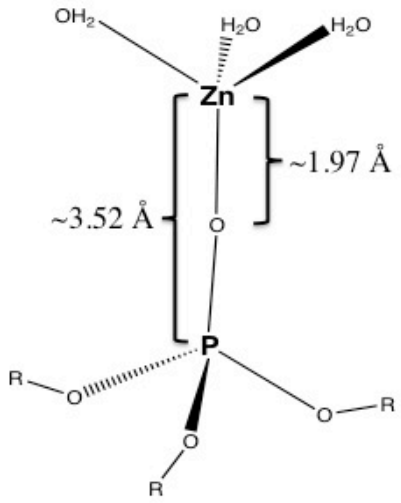

Figure 4.6. Visualization of monodentate bonding to a phosphate group with atomic distances as multi-shell theoretical EXAFS fits estimated. R groups indicate a lattice continuation in the solid.

4.5 Conclusions

Although MBM biochar contains 10% w/w willow biochar, adsorption experiments and Zn speciation on an analogous willow biochar showed only $ZnCO_3$ precipitation at pH 7.0 and no adsorption at the pH used in this study (Appendix A). Thus, only a minor and indirect reaction with Zn is expected with the willow component of the MBM; instead, the major sorbent for Zn in the MBM was HAP.

In this study, the evidence for surface complexation in the short time-scale reaction is strong. Solution acidification was observed in the first 5 h of the kinetics experiment, which is consistent with surface de-protonation and subsequent Zn bonding at active complexation sites. The EXAFS of MBM biochar samples were best fit with shells corresponding to inner-sphere monodentate complexation between Zn and a phosphate group. This was also seen in the Zn adsorbed HAP standard.

After 5 h of reaction, a slower adsorption rate takes place (Fig. 4.3). The kinetics of adsorption demonstrate a bi-phasic reaction, and the data was best fit with the Elovich equation. The combination of XAS and adsorption data suggests that the mechanism(s) taking place in the second reaction is/are diffusion past the surface coatings on MBM biochar and possibly diffusion through the pores in bone.

All adsorption experiments were reacted for 72 h, resulting in the second rate of reaction observations. When the MBM biochar was not pre-treated, the adsorption capacity was highly variable, particularly in experiments where Zn concentration was varied. Adsorption capacity of the MBM biochar was predicted to be 0.65 mmol Zn g^{-1} from Langmuir model but pre-treatment by sonication increased adsorption capacity to 1.08 mmol Zn g^{-1}. The slower rate of adsorption may be explained by diffusion of Zn through porous or aggregate structure of the MBM biochar. The differences in Zn adsorption capacity after sonication may be caused by a reduction of diffusion-limiting processes or an increase in surface area.

Although some research on Zn sorption on synthesized HAP suggests ion exchange for Ca, this study had a few phenomena to suggest this mechanism, but it is unlikely to be a major mechanism for Zn sorption on MBM biochar. Multi-shell theoretical EXAFS modeling of MBM biochar EXAFS spectra at 48 h was still best modeled using the adsorption model from 2 h of reaction although there was a poorer fit to the experimental data by giving

physically unrealistic parameters. The 48 h reaction showed a slight increase of the Zn-P second shell at 3.53 Å, but this was still within model error (0.02 Å). The 48 h models failed to completely reproduce an experimental EXAFS feature at 8 $Å^{-1}$ (Fig. 4.5) but attempts at adding scattering pathways to reproduce this feature were not successful. Weak nucleation of a hopeite mineral could explain the features in both the EXAFS and Fourier transform (FT) of the 48 h reacted MBM biochar, but the fits using Zn-Zn or Zn-P-P shells were not justified given the data quality.

The acidification pre-treatement showed evidence of Zn precipitation in adsorption experiments where pH or adsorbate were varied; the Langmuir model isotherm of the acid pre-treated experiment had a maximum adsorption capacity one order of magnitude larger than all other observed isotherms in this study (Table 4.2). The pH envelope showed precipitation of a Zn mineral at pH 6.0 when HAP has dissolved prior to adsorption. In contrast, the untreated pH envelope showed dissolution of the carbonate-substituted hydroxyapatite can occur below pH 6.3 using the conditions of experiment.

Because FT-IR data described the majority of P-O vibrations as being that of a carbonated apatite (Chapter 3) and Zn EXAFS showed bonding to phosphate groups (Table 4.3), the hypothesis of direct Zn bonding to the hydroxyapatite is confirmed. Bonding to organic-P is a possibility, but surface coverings of organic material are likely to only inhibit the observed adsorption given the diffusion-limited reaction rate and higher sorption capacity after sonication.

In summary, the MBM biochar displays a moderately-high affinity for Zn adsorption at pH 6.1 ± 0.1. Adsorption to MBM biochar was equivalent in capacity and mechanism to the HAP standard. Monodentate inner-sphere surface complexation occurred from 0–5 h of reaction and is responsible for the majority of the adsorption capacity. After 5 h, adsorption continues via the same mechanism, but is limited by diffusion. Dissolution of MBM biochar is likely below a pH of 6.3 and precipitation of Zn may occur in conditions where HAP is unstable. MBM biochar stability is, as expected, highly sensitive to pH and will buffer the solution to 6.3.

5.0 SPECIATION CHANGE OF ZINC IN SMELTER-IMPACTED SOILS WHEN AMENDED WITH MEAT AND BONE MEAL (MBM) BIOCHAR

5.1 Preface

After the meat and bone meal (MBM) biochar was characterized (Chapter 3) and its reactivity with Zn in a model system assessed (Chapter 4), the effects of MBM on Zn speciation in smelter-impacted soils were evaluated. It was previously shown that MBM adsorbs Zn via monodentate, inner-sphere complexation with phosphate groups (Chapter 4). Linear combination (LC) modeling on spectra from Zn K-edge x-ray absorption spectroscopy (XAS) of MBM biochar treated soil samples were used to identify the presence of MBM biochar adsorption as a significant mechanism in reacted soil samples. Additional wet chemical and micro-scale synchrotron techniques were also employed on the soils before and after treatment to give supporting evidence for a speciation change. Laboratory-based chemical analysis (total and extractable Zn) was performed on both control and reacted soils to give macroscopic information on Zn mobility changes. Spatially resolved, synchrotron-based x-ray microprobe techniques (i.e., micro x-ray fluorescence (μXRF) maps and micro x-ray absorption near edge structure (μXANES) spectroscopy on points of interest) were employed to further aid identification of single Zn species in the bulk-soil XAS.

5.2 Introduction

HudBay Minerals Inc., formerly Hudson Bay Mining and Smelting Co. Ltd., has been mining and processing copper (Cu), cadmium (Cd) and zinc (Zn) in Flin Flon, Manitoba /Creighton, Saskatchewan since 1930 and recently closed Cu smelting operations in 2010. After 80 years of operation, there has been significant loss of vegetation in the area around the smelting stack—reflecting both natural and anthropogenic stress that are common to non-ferrous smelters (Kozlov and Zvereva, 2007). At a similar smelter-impacted landscape in Sudbury, Ontario, the manual application of ground limestone to the soil surface detoxified the soil sufficiently for spontaneous colonization by seedlings of birch, poplar and willow (Winterhalder 1995, Gunn et al., 1995). In 1999, a community-based greening program was

initiated to test whether the same liming technique would work in the Flin Flon/Creighton area. The approach was less successful at some Flin Flon/Creighton locations than others, providing the impetus for further research into other factors on plant stress. To facilitate forest revegetation, HudBay Minerals Inc. and the University of Saskatchewan Department of Soil Science developed a multi-disciplinary project to assess revegetative options for the impacted landscape. The project commenced in 2008 with a soil survey of the area.

The soil is naturally acidic in the Flin Flon/Creighton area from the boreal shield parent material (Johnson et al., 1995), but addition of metals such as Zn, Cu, lead (Pb), arsenic (As), Cd and mercury (Hg) as aerially-deposited sulphides (Stothart, 2002; Jones and Henderson, 2006) has further reduced pH to levels that increase plant stress (pH 3.5–4.5). Under such acidic conditions, many of the metals from the sulphide ore become more mobile and plant-available in solution. Zinc is one of the most soluble and mobile trace metal cations (McBride, 1994), making it a highly phytotoxic element (Chaney, 1993). Therefore, understanding the plant-available pool of Zn in multi-metal contaminated soils is crucial to reduce plant toxicity and successfully revegetate this landscape.

In 2010, a screening trial was performed to determine the effect of several soil amendments on plant growth. Soil was collected from three Flin Flon/Creighton areas classified as: lime responsive with low total metals; lime unresponsive with high total metals; and lime responsive with high total metals. Each amendment was applied with a base treatment of granular fertilizer and dolomitic limestone and included: montmorillonite; glauconite; zeolite; manure based compost; municipal compost; oat hull biochar; willow biochar and a meat and bone meal (MBM) biochar. Treatments were applied to three soils and two separate plantings of tufted hairgrass (*Deschampsia cespitosa*) and American vetch (*Vicia americana*) grown from seed (Farrell, unpublished data, 2010). Meat and bonemeal biochar was the most promising amendment, likely due to its phosphate content.

Phosphorus materials have been studied extensively as amendments for metal contaminated soils because they can either form insoluble minerals (Ruby et al., 1994; Li et al., 2000; Basta et al., 2004; Kumpiene et al., 2008; Park et al., 2011) or adsorption complexes that effectively reduce metal mobility in the soil solution (Hodson et al., 2000; Panfili et al., 2005). The calcium phosphate mineral component of bone, hydroxyapatite (HAP), is of particular interest as a soil amendment because of its moderate solubility and

surface reactivity with multiple trace metals (Chen et al., 1997; Boisson 1999; Chen et al., 2010). Some researchers have suggested that bone is best applied to very acidic soils that can facilitate its dissolution (Sneddon et al., 2008). Sources of meat and bone meal (MBM) provide readily available sources of biological HAP (Deydier et al., 2005), and a MBM biochar has been proven to be especially effective as a Zn sorbent (Chapter 4).

In model adsorption experiments, MBM biochar adsorbs Zn rapidly (5 h) by forming a monodentate inner-sphere complex with phosphate groups (Chapter 4); yielding a sorption capacity of 0.65 mmol Zn g^{-1}. Below pH 6.3, however, the MBM biochar dissolves; phosphate is released and can form a Zn-phosphate precipitate (e.g., hopeite) (Chen et al., 1997; Ndiba et al., 2008; Dybowska et al., 2009; Baker et al., 2012). However, it is not yet known whether MBM biochar is able to still adsorb Zn in the presence of competing reactions in contaminated soil systems or be reactive with the species present in the soil.

For Zn speciation in heterogeneous samples (e.g. soil), the relative abundance of co-occurring species in XAS experiments is quantified through linear combination (LC) modeling. The recognized weakness of LC modeling is that an incomplete library can result in poorly fit models (Manceau et al., 2002). Nevertheless, this technique has been used successfully in amended soils involving Pb-P sorption species (Hashimoto et al., 2009) and Zn mineral and sorption species (Panfili et al., 2005; Baker et al., 2012). A recent study by Baker and colleagues (2012), used EXAFS to show that either hopeite or scholzite (a Zn-Ca-PO_4 mineral) formed in smelter-impacted soils amended with phosphate, but some of these species were undetectable in micro-scale x-ray diffraction (μXRD), which suggests either poor-crystallinity of the minerals or adsorption species. Poorly-crystalline or adsorbed Zn species have also been interpreted by other studies using bone meal or HAP to treat soil (Panfili et al., 2005; Sneddon et al., 2006). The uncertainty in the conclusions by Baker et al. (2012) may be explained by the lack of a suitable phosphorus adsorption standard. A similar study involved measuring Zn K-edge XAS on HAP-treated sediments (Panfili et al., 2005). The results showed a significant portion of Zn adsorbed to HAP in all soils, particularly after plants had grown in them.

This chapter investigates whether adsorption of Zn onto the meat and bone meal (MBM) biochar will occur in soils representative of the Flin Flon/Creighton area. The overall objective of this study was to determine whether the MBM biochar reacts with Zn in

contaminated soil, either through adsorption or precipitation with phosphate as observed in Chapter 4. Selected soils from the Flin Flon/Creighton site were mixed with MBM biochar under conditions favorable to reaction in adsorption experiments (Chapter 4). The observation of either hopeite or Zn-MBM adsorption complexes after amendment with Zn K-edge XAS would provide evidence of a direct influence of MBM biochar on Zn speciation in the soils. The specific goals of this study were to: (1) screen a series of smelter contaminated soils from the Flin Flon area for reactivity with MBM biochar and (2) determine if the MBM biochar treatment results in the formation of a Zn-phosphate mineral or direct adsorption of Zn to the biochar.

5.3 Materials and Methods

5.3.1 Study site

Soil cores were collected in locations adjacent to field amendment and tree planting trials at the HudBay Minerals Inc. site in Creighton, SK/Flin Flon, MB (Specht, unpublished, 2012). Sites were renamed as "1, 2, 3 and 4" for discussion in this study. The top 10-cm of soil were collected by pressing an aluminum core (3-cm diameter and 10-cm depth) at a location directly adjacent to the tree planting study (approximately 10-cm upslope of control plot). Control sampling locations were chosen to be an untreated (i.e., no lime, fertilizer, seeds or amendments) proxy for the soil used in the tree planting study. The soil cores were individually air-dried, sieved to pass a 2-mm sieve and well-mixed prior to all analyses. Site soil characteristics of soil organic carbon (OC, mg/mg), texture, and color were measured as part of the tree planting study (Specht, unpublished) and soil pH was measured as a part of this thesis. The combined results are compiled in Table 5.1. Photographs and brief site descriptions can be found in Appendix B.

5.3.2 Soil characterization

Soil pH was measured using a modified method of Conyers and Davey (1988). Briefly, a 1:4 (w/v) soil to 0.01 M $CaCl_2$ suspension (5.0 g to 20-mL $CaCl_2$) was stirred for 30 m. Solid was allowed to settle for 1 h and the pH measured using an accuTupH rugged-bulb, electrode with double-junction reference filled with KCl (Fisher Scientific, Singapore, Singapore) which had been calibrated to pH 4.0 and 7.0 using buffer solutions. Soil pH was

performed in batches with one duplicate per ten samples and a method check of extraction solution. Both method check and sample were ± 0.01 pH units of their duplicate values.

Table 5.1. Soil characteristics of core taken from each tree planting site.

Site	Soil pH	Organic Carbon (g C kg soil^{-1}) †	Texture†	Soil Color†
1	3.90	7.3 ± 0.1‡	sandy loam	2.5YR 7/1
2	3.94	114.3 ± 0.2	sandy clay loam	10YR 4/2
3	3.97	15.3 ± 0.04	sandy loam	10YR 6/4
4	3.34	53.5 ± 0.6	clay loam	2.5YR 7/2

† Source of data, Specht, unpublished (2012)

‡ Measurement of subsamples (n=3)

Total Zn was prepared in solution for each of the soils using a standard method for microwave-assisted acid digestion (US EPA method 3051) and a Milestone Ethos EX digestor (Milestone Inc., Shelton, Connecticut, USA). Briefly, 0.5 g of soil (< 45-μm) was weighed into Teflon vessels from an SK-10 high-pressure rotor (Milestone, Shelton, Connecticut USA). After addition of soil, 9.0 mL of 12 M HCl and 3.0 mL of 16 M HNO_3 were added to each vessel. Each vessel was closed and introduced into the rotor segment; the rotor was tightened by torque wrench and inserted into the microwave cavity. Vessels were heated in the microwave at a rate of 20°C min^{-1} for 10 min and held at a 200°C for 15 min. After the vessels were allowed to cool to room temperature, they were opened, transferred into 50-mL volumetric flasks, and brought to volume with double deionized water (18 mΩ).

Each sample was passed through a Whatman 0.45-μm pore size disposable filter, and the filtrate was stored in 15-mL polypropylene centrifuge tubes at 4°C. Zinc concentration was quantified by atomic absorbance spectrometry (AAS) (SpectrAA 220 Atomic Absorption Spectrometer, Varian Australia Pty Ltd., Australia) using standard operating methods for Zn measurement (Varian Inc., 1989). Instrument configuration required an Air/Acetylene flame (oxidant and fuel, respectively) and a 'Zn' hollow cathode lamp (Varian Inc., Mulgrave, Victoria, Australia), which emits light at 213.9 nm.

Prior to Flame-AAS measurement, the samples were diluted with $LaCl_3$ (0.72 mmol L^{-1}) at a sample to $LaCl_3$ solution ratio to ensure that Zn concentration was within the linear range of absorbance measured on calibration standards. Lanthanum solution was used as a

releasing agent to prevent phosphate mineral precipitation when measuring Zn (Baker and Amacher, 1982; Cantle, 1982). Samples were measured in duplicate (instrument replicate) and the mean absorbance used to calculate concentration using the slope of the calibration curve (concentration vs. absorbance).

5.3.3 Suspensions of soils with MBM biochar

The MBM biochar (0.3 g) was mixed with 3.0 g of sieved (<2-mm), air-dried soil and added to 200-mL deionized water in 250-mL polypropylene bottle. This will be referred to as the 'MBM/soil suspension'. The 'MBM/soil suspension' was performed in triplicate (n=3) for all four soils sampled. The suspensions were then shaken at 160 rpm on a gyratory shaker (New Brunswick Scientific, Model G10, Manasquan, New Jersey USA) for 30 d with regular checks of the pH using an accuTupH rugged-bulb, electrode with double-junction reference filled with KCl (Fisher Scientific, Singapore, Singapore). The solution pH of MBM/soil suspension was adjusted to be 6.1 ± 0.1 with either 0.1 M NaOH or 0.1 M HNO_3 as needed. Due to logistical constraints with checking and adjusting solution pH, one replicate from each site was pH adjusted using a Metrohm 716 Stat Titrino auto-titrator (Metrohm, Herisau, Switzerland) and the two corresponding replicates were manually pipetted with an identical volume of the titrating solution.

These conditions were selected to facilitate reaction between Zn and the MBM biochar based on previous observations of MBM biochar reactivity (Chapter 4) and from plant response in screening trials (Farrell, unpublished, 2010). The ratio of MBM biochar to soil (1:10, w/w) was previously used in an amendment screening trial of Flin Flon/Creighton area soils and yielded significantly higher plant root and shoot biomass in two out of three soils tested (Farrell, unpublished, 2010). The pH (6.1 ± 0.1) and low suspension density (1.5 g MBM biochar L^{-1}; 15.0 g soil L^{-1}) had previously been shown to result in moderately-high affinity of Zn adsorption onto MBM biochar (0.65 mmol Zn g^{-1}) during adsorption experiments (Chapter 4). The 30-d reaction time was well-past the rapid rate of adsorption observed in Chapter 4, but allowed for competition with kinetically-slower reactions of Zn that are common in smelter-impacted soils; for example, Zn-Al layered double hydroxide mineral is a potentially-important control on Zn mobility in soils, but requires 800 h for formation under suspension mixing conditions (Roberts et al., 2003). A suspension density of 15.0 g L^{-1} low solid to solution ratio (with low ionic strength) also promotes adsorption

processes by diluting cationic activity near the solid surfaces, which makes excess of adsorption sites more likely.

5.3.4 Extractable Zn

In the absence of an appropriate plant bioassay, chemical extractions have been proposed as a proxy for determining the plant-available fraction of metals in soil (Hendershot et al., 2008). Extractable Zn was measured on air-dried, sieved (<2-mm) soil from the sampled core and on soil recovered from the reacted soil/MBM suspensions. Control soil was extracted in triplicate (n=3), but the recovered 30-d reaction soil could only be extracted singly, due to errors in maintaining triplicate soil/MBM suspensions to pH 6.1 ± 0.1. The extraction solution consisted of 0.1 M $CaCl_2$, adjusted to the pH of the control soil with 0.1 M HCl (Waterlot et al., 2011). The extraction method of Waterlot et al., (2011) was modified to use a lower soil to extracting solution ratio to match the solid to solution ratio as the 30-d suspensions. Because the effect of solid to solution ratio has shown to not significantly affect Ca-Na ion exchange on a montmorillonite clay in the range of 25 g L^{-1} to 2.5 g L^{-1} (Tertre et al., 2011), the ratio used for this study (15.0 g L^{-1}) is expected to provide a conservative estimate of extractable Zn because the replenishment of extracting solution would not limit Zn extraction. In a 250-mL polypropylene vessel, 3.0-g of soil was added to 200-mL 0.1 M $CaCl_2$ (15 g L^{-1}) and the suspension shaken on a gyratory shaker for 2 h (Boisson et al., 1999; Basta and Gradwohl, 2000).

Prior to analysis, each sample was passed through a Whatman 25 mm, 0.45-µm pore size disposable filter. Filtrate was acidified with 10-µL of 8 M HNO_3 and stored in 15-mL polypropylene centrifuge tubes at 4°C. Detailed methods were discussed previously in Section 5.3.2.

5.3.5 Zn K-edge XAS

Zinc K-edge XAS spectra were collected at the HXMA beamline (06ID-1) of the Canadian Light Source (Saskatoon, SK). Measurements were performed using a Si(220) monochromator with detuning of 40–50% for harmonic rejection at 12k eV. The beamline was calibrated to the Zn K-edge (9659 eV) using transmission measurements of a reference Zn metal foil located between the I_1 and I_2 ion chambers (after the sample). This allows for calibration of spectra to the Zn K-edge for each measurement. All soil spectra were collected in fluorescence mode using a solid-state, 32-element detector (Canberra) with a 6-µm Cu

filter and Sollar slits to remove fluorescence arising from lower atomic number elements and scatter, respectively. Multiple scans were collected to ensure adequate signal to noise ratio for analysis; individual spectra were calibrated and averaged using the Athena EXAFS analysis software package (Ravel et al., 2005).

Zinc K-edge EXAFS were collected on control soil (before suspension) and reacted soil (after suspension for 30 d with 10% w/w MBM biochar) for all four sites. The control soils were mounted into Teflon holders as air-dry, <2-mm sieved soil and held in place with Kapton tape (an inert polyimide film). Reacted soils were recovered from the reaction vessels by vacuum filtration, mounted as a moist paste onto Teflon holders, and held in place with Kapton tape.

Zinc K-edge EXAFS of Zn standard reference materials were collected at the HXMA beamline as part of a previous study (Hamilton, unpublished data, 2013). Collected standards were: franklinite [$ZnFe_2O_4$], sphalerite [ZnS], Zn-Al layered double hydroxide (LDH), Zn hydroxyl interlayered phyllosilicate mineral (HIM), hopeite [$Zn_3(PO_4)_2$], smithsonite [$ZnCO_3$], willemite [Zn_2SiO_4], zincite [ZnO], zinc hydroxide [ZnOH], Zn sulphate [$ZnSO_4$], Zn substituted HAP, Zn sorbed to Goethite, Zn sorbed to montmorillonite, Zn adsorbed birnessite (MnO_2), Zn adsorbed to MBM biochar ('MBM C' from Chapter 4), Zn sorbed citrate and Zn^{2+}.

Quantitative XAS speciation analysis of unknown samples was performed using a LC technique of modeling the soil spectra to a combination of chemically plausible Zn reference standards using the Athena software package (Ravel et al., 2005). The margin of error in similar studies has been estimated to be ~10% on each fitted component and was assumed to be similar for this study (Manceau et al., 2000; Nachtegaal et al., 2005). The R-factor and χ^2 are measures of wellness-of-fit, but are only relative to a single sample. It is difficult to quantify the number of 'independent measurements' in an XAS spectrum, as this would be equal to the number of Zn atoms in the spot size during spectrum reading. The Athena software uses the number of data points as a conservative estimate to calculate a reduced χ^2. Therefore, the reduced χ^2 was used only in selecting the best-fit model for a single sample (Ravel et al., 2005).

5.3.6 X-Ray microprobe measurements

Synchrotron-based x-ray microprobe measurements of the soils were also performed, using μXRF and μXANES, at the VESPERS beamline (07B2-1) at the Canadian Light Source (Saskatoon, SK). Soil and MBM suspensions were measured in the same Teflon holders that had been prepared for Zn K-edge XAS at the HXMA beamline (06ID-1). Soil from the cores (air-dried, < 2-mm), were ground in an agate mortar and pestle and passed through a 750-μm sieve to achieve better sample homogeneity. The sieved soils were spread thinly across Kapton tape and held in place with a second piece of tape. Each sample was mounted at a 45° angle to the incident beam and all data were collected in fluorescence mode using a four-element, Vortex-ME4 detector (Hitachi High-Technologies Science America, Inc., Northridge, California, USA). Measurements were taken at a resolution of 5 μm^2 per pixel. Zinc K-edge μXANES were measured with the same four-element vortex detector and a spot size of 5 μm on selected spots of the map.

5.4 Results and Discussion

5.4.1 Chemical analysis

Characterization of the soil cores revealed trends of total Zn: Site 2 > Site 4 > Site 1 ≈ Site 3. However, the exchangeable Zn in soils exhibited a very different trend: Site 1 > Site 2 > Site 4 ≈ Site 3. This highlights the need for assessment of plant-available Zn, either through extractions or direct XAS measurement, as there can be high extractable Zn in a soil even with low total Zn concentration.

The unreacted soil from Site 1 was highest in extractable Zn despite having the lowest total Zn (Table 5.2). Site 1 soil had 38% of the total Zn (Table 5.2) in the extractable fraction, compared to 1–4% for the other three soils. After suspension reaction with MBM biochar, all soils showed a reduction in exchangeable Zn, but Site 1 was the most pronounced (Table 5.2). After reaction, filtrate Zn levels from all four soils were very dilute, ranging 50–60 μM Zn across all four soils. Although reductions in the $CaCl_2$-extractable Zn fraction were apparent after treatment, additional replicates would greatly improve the certainty of conclusions concerning Zn mobility. The experimental design had included triplicate treatment for all four sites, but after 23 d of reaction, the samples that had undergone manual titration were buffered to pH 5.5 whereas the auto-titrated samples that had been maintained

at pH 6.1 ± 0.1 and they could no longer be used as replicates. Despite this, reaction conditions in the single, auto-titrated replicates were well controlled and still provide valuable chemical information about the sample that was studied with Zn K-edge XAS.

Table 5.2. Zinc concentrations of the soil from a 10-cm depth core (air-dried, <2-mm) from each site location. Total digest zinc (Zn) (n=4) and $CaCl_2$ extractable Zn on soil before (n=3) and after mixed suspension with MBM biochar (n=1).

Site	Total soil digest before suspension	$CaCl_2$-extractable fraction in soil before suspension	$CaCl_2$-extractable fraction in soil after suspension †
	mg Zn kg soil^{-1}		
1	1150 ± 33.4	441 ± 37.6	82.2
2	9160 ± 322	193 ± 3.8	119
3	871 ± 55.9	34.5 ± 0.9	18.4
4	5840 ± 217	69.6 ± 3.3	34.4

† Single measurement from $CaCl_2$ extraction on soil and MBM biochar recovered after 30-d suspension.

5.4.2 Bulk XAS results

Visual inspection of the Zn XANES and EXAFS spectra (Fig. 5.1A and 5.1B, respectively) revealed that one of the samples (Site 1) clearly changed after treatment; and the other three (Site 2, 3, and 4) had only minor changes after 30 d of reaction. All soil samples contained a major component of franklinite [$ZnFe_2O_4$], evidenced by the triple peak adsorption features in the XANES, as well as features in the EXAFS. This Zn-bearing mineral is commonly observed throughout the smelter-affected area of Flin Flon (Hamilton, unpublished data, 2013) as a result of aerial deposition from the smelter. The strong scattering of franklinite often complicates observation of minor species changes, particularly those associated with subtle adsorption features (Jacquat et al., 2009), and limits the utility of visual fingerprinting in this study.

For quantitative analysis, LC modeling was performed on the EXAFS results. From the standards tested, only the following were found to be significant components in the models: franklinite [$ZnFe_2O_4$], sphalerite [ZnS], Zn-Al layered double hydroxide (LDH), Zn-Al hydroxyl interlayered phyllosilicate mineral (HIM), hopeite [$Zn_3(PO_4)_2$], Zn adsorbed to birnessite (MnO_2), Zn adsorbed to MBM biochar and Zn sorbed to montmorillonite. Based upon those preliminary results, models generally were in agreement with visual

interpretation; Sites 1, 2, 3, and 4 all show some change in Zn speciation after reaction, with Site 1 being the most pronounced.

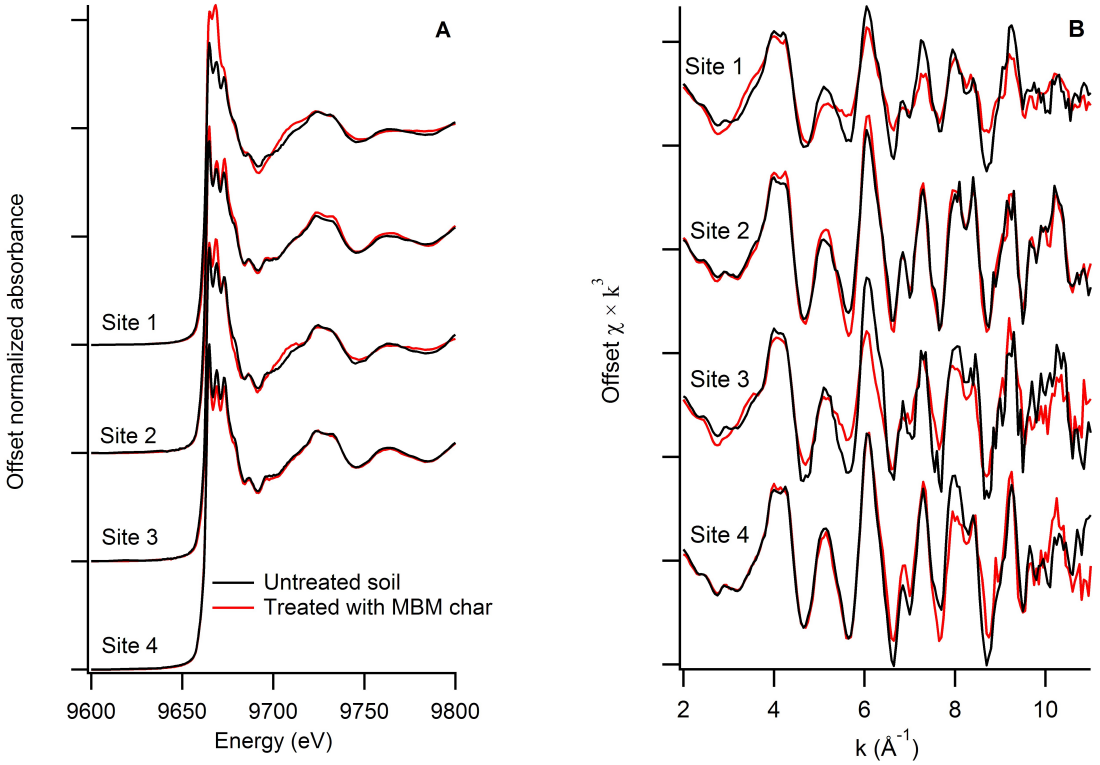

Figure 5.1. Zinc XAS into the EXAFS region were measured on unreacted control soils (black) and the same soil recovered after shaken in suspension with MBM biochar at pH 6.1 ± 0.1 for 30 d (red). All soils share a common, major component of franklinite. After shaken in suspension, changes can be seen in the XANES (A) and EXAFS (B) region of Site 1 but Site 2, 3, and 4 show only minor difference from the untreated control.

Linear combination modeling of the Site 2, 3, and 4 reacted and unreacted soils did not provide a single unique solution that was able to explain the results to the degree needed for definitive quantitative speciation. However, categories of Zn species types were observed such as: smelter-related minerals (e.g., franklinite and sphalerite), adsorption complexes and secondary precipitates (e.g., Zn-Al HIM). Site 2 was dominantly smelter-related minerals, with almost no change after treatment. Site 3 and 4 each contained a mixture of smelter-related minerals, adsorption complexes and secondary precipitates. Both site 3 and 4 soils

contained a larger fraction of adsorption complexes and secondary precipitates after reaction, but no interactions with MBM biochar. It is possible that the pH increase to pH 6.1 ± 0.1 resulted in an increase in adsorption and secondary precipitates of Zn among soil components naturally present. These results are consistent with earlier work performed on soils from the same sampling locations (Hamilton, unpublished 2013).

Of primary interest to this study, when the standards MBM biochar or hopeite were used, they both yielded poor fits (i.e., high X^2 relative to other models of the same spectrum) for Sites 2, 3, and 4; this indicated Zn speciation change unrelated to the MBM biochar. Therefore, the MBM biochar did not directly react with Zn in the soils from Sites 2, 3, or 4.

In contrast, the treated Site 1 sample showed clear changes in both the XANES and the EXAFS regions after treatment. Linear combination modeling required a component of either hopeite or the Zn adsorbed to MBM biochar standards, but either standard provided an approximately equal quality model (minor difference in X^2 and features in spectrum). For this reason, identification of single species at the micron spatial scale by microprobe measurements was used to refine the LC model of the Site 1 reacted soil.

5.4.3 Synchrotron microprobe

Micro scale XRF maps were measured to spatially-resolve semi-quantitative elemental concentrations in the samples. From elemental correlations of interest, μXANES were measured to identify Zn species on a 5 μm^2 spot. Zinc-MBM biochar adsorption sample previously analyzed via bulk EXAFS (Chapter 4) to observe the elemental correlations between Zn and MBM biochar in a sample without soil and to compare bulk XANES with spatially-resolved μXANES to determine any changes in self-absorption that may occur when using the VESPERS beamline. Results are shown in Figure 5.2; μXANES showed signs of self-absorption indicated by the reduced edge fluorescence, but all of the feature positions aligned with the bulk-XANES from the same sample. This indicates that μXANES measured at the VESPERS beamline may be affected by self-absorption in "hot spots" of local high concentration.

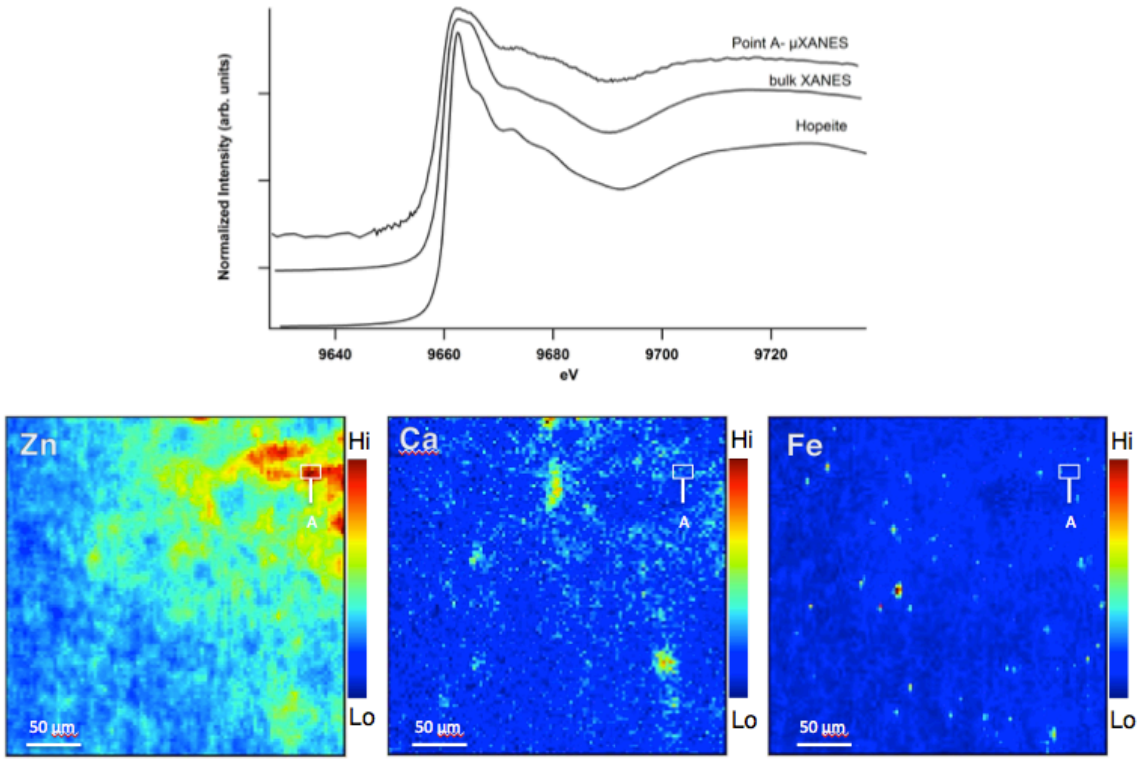

Figure 5.2. A 350 x 350 µm area of MBM biochar sample after reaction with Zn. Three single element maps (Zn, Ca, and Fe) are displayed in fluorescence-dependent color (blue to red) relative to the semi-quantitative concentrations within each single-element area. Micro-scale XANES were collected at the point of interest (Point A). This point was chosen to test for possible Zn mineral formation, which was plausible given the high density of fluorescence. Micro-scale XANES closely matched the bulk-EXAFS of the sample but difference in feature intensity are due to self-absorption in the sample (top). Point A µXANES did not match the hopeite standard and instead was the same species as the bulk sample, evidenced by the identical XANES feature positions (top).

X-ray fluorescence maps were collected on the MBM biochar treated Site 1 soil to support identification of minor Zn components (Fig. 5.3). The Zn to Ca spatial correlation over the map area (point A) suggests the possibility of a Zn/MBM biochar association, because rather than occurring in discrete, high-fluorescence-density areas common to minerals, the correlation area is diffuse in the sample. The spatial correlation of Zn and Ca in the top (point A) suggests a possible adsorption species as was seen in the Zn adsorbed, MBM biochar sample (Figure 5.3). Unfortunately, the concentration of Zn was too low to yield enough fluorescence counts for µXANES on the co-located Zn and Ca areas (Point A in Fig. 5.3). Spatial correlations between Zn and Ca in the whole map area (Figure 5.3, top left)

shows a linear relationship at high Zn fluorescence counts and low Ca, suggesting a high concentration Zn species in an association with Ca, possibly a mineral. Instead, μXANES were collected on a different point of interest (Point B in Fig. 5.3). This point was chosen to measure a non-franklinite species, because high-density Zn concentration in this spot was not co-located with Fe. The μXANES did not resemble any single standard species. Instead, LC modeling was employed and best fit the μXANES using a mixture of franklinite, hopeite and Zn-Al-HIM.

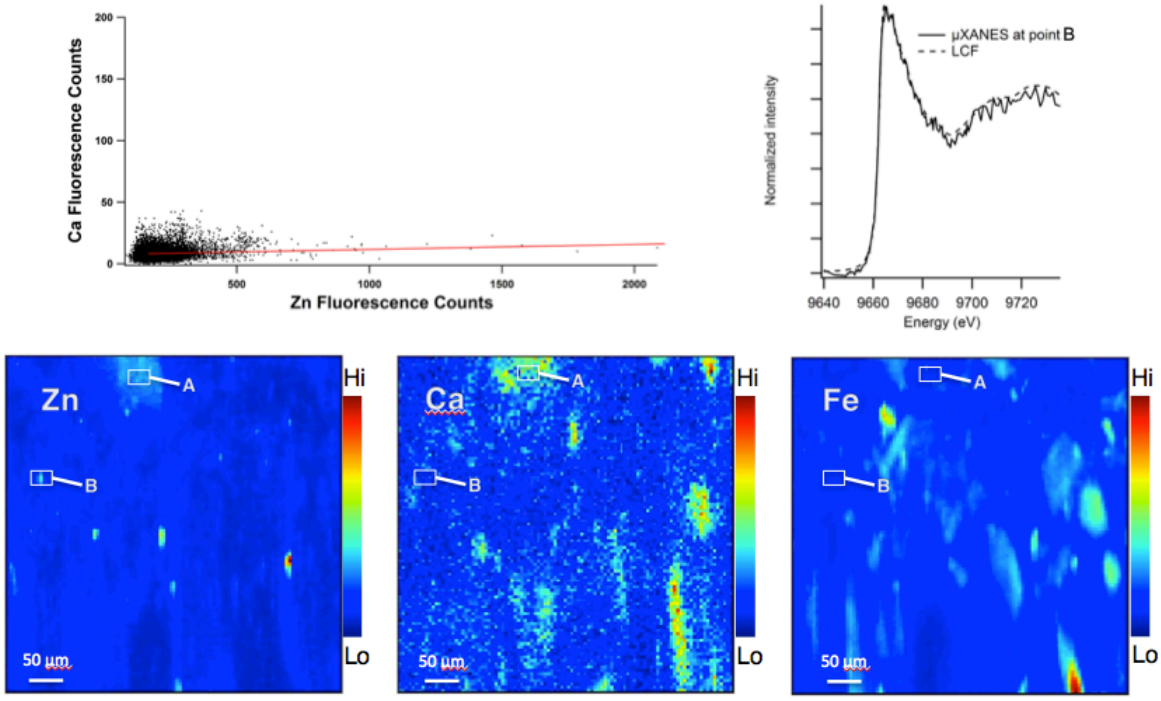

Figure 5.3. A 500 x 500 μm x-ray fluorescence (XRF) map was measured on the MBM biochar treated Site 1 soil. Three single-element maps (Zn, Ca, and Fe) of the same spatial area displayed in fluorescence-dependent color (low to high counts are blue to red, respectively) relative to the concentrations within each single element area. Points A and B indicate positions of interest where μXANES were measured. Point A did not have enough fluorescence for μXANES. A high concentration of Zn at point B was another position of interest. Micro scale XANES were measured at point B (top right). The features suggest a mixture of species best fit with a LC model (dashed line) including the three standards: franklinite, hopeite, and Zn-hydroxy interlayered mineral (HIM). The LC model parameters are shown in Table 5.3.

Zinc-Aluminum HIM is a clay mineral that has been found to co-precipitate Zn with Al and may substantially impact Zn mobility in acidic soils (Scheinost et al., 2002; Manceau et al., 2004; Jacquat et al., 2009).

Based on the results from microprobe techniques and bulk chemical analyses, LC speciation was refined and fit well to the data (Figure 5.4). Contribution of components in LC models are given in (Table 5.3). After reaction with MBM biochar, ore species (e.g., franklinite and sphalerite) were a much smaller component than in the untreated soil and sphalerite was no longer a component of the model. After treatment, Zn-Al HIM also formed, which is known to occur in acidic, smelter-impacted soils (Scheinost et al., 2002). These speciation changes are consistent with the results by earlier Zn K-edge XAS measurements and LC modeling on soils from the same tree-planting locations as part of a separate thesis (Hamilton, unpublished, 2013).

The choice of MBM biochar standard versus hopeite standard in linear combination models was difficult to distinguish because of similar XANES (Figure 5.2, top) and EXAFS features and a general difficulty in modeling minor Zn components in the presence of franklinite (Jacquat et al., 2009). Hopeite provided the best fit in the μXANES, but the μXANES measurement was also restricted to areas of high density fluorescence to ensure sufficient data quality; this may also be more likely to measure hopeite. In the LC modeling of EXAFS, the use of Zn adsorbed on MBM as a standard provided similar fit to a combination of hopeite and Zn adsorbed on montmorillinite as an outer-sphere complex. The increased contribution of Zn on montmorillonite necessary when using hopeite standard is not consistent with the decrease in $CaCl_2$-extractable Zn after treatment; this was the justification for favoring a Zn adsorbed MBM component. Because both standards are so similar, both species may indeed be present in the reacted soil and this should be considered a possibility. The use of either standard indicates the direct interaction between Zn and phosphate, thus confirming that the MBM reacted directly with Zn in the Site 1 soil.

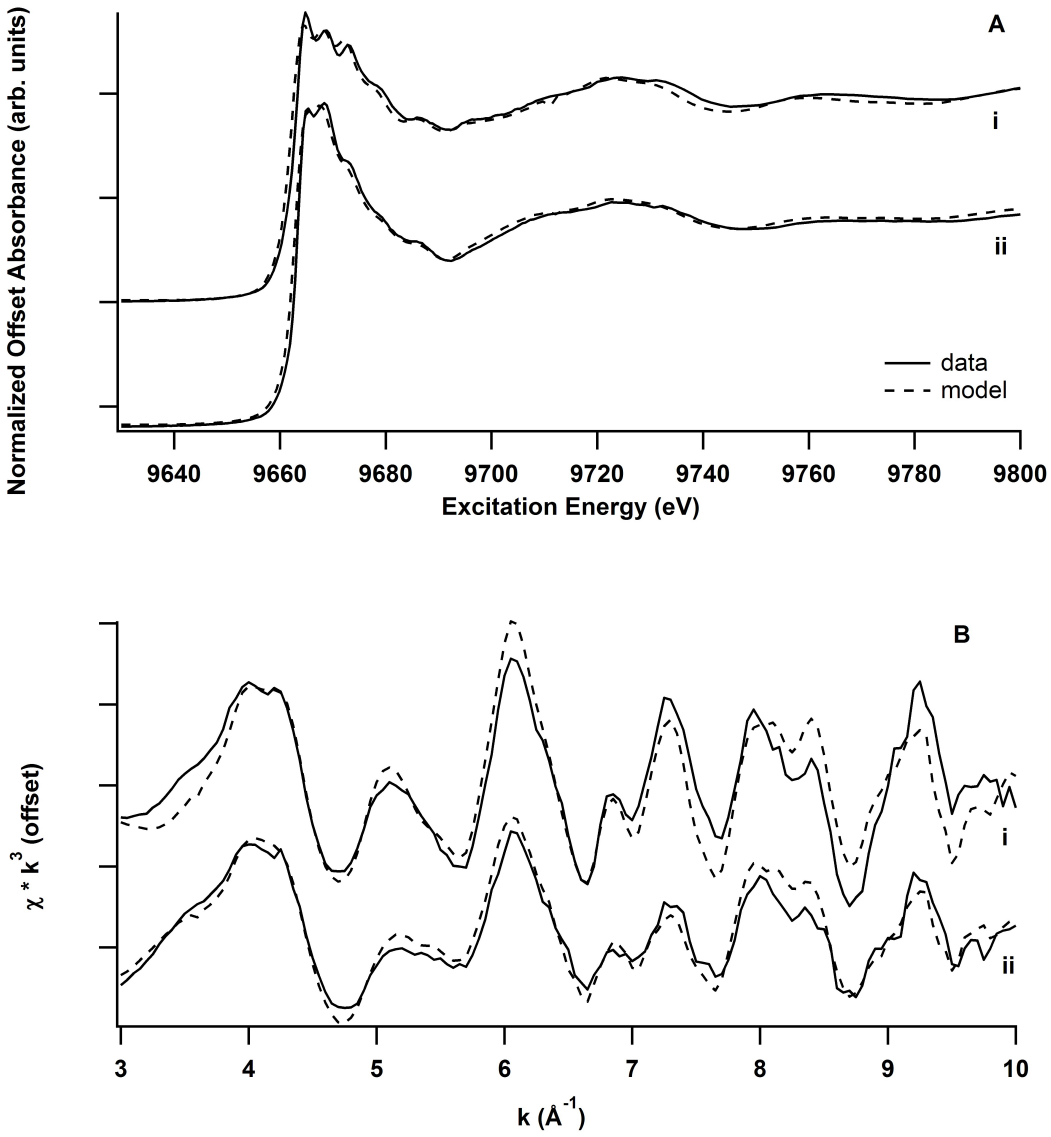

Figure 5.4. Site 1 soil K-edge x-ray absorption spectroscopy (XAS) are displayed with the best fit linear combination (LC) model. The x-ray absorption near-edge structure (XANES) (A) is displayed for the Site 1 unreacted (i) and MBM biochar reacted (ii) soils. The x-ray absorption extended fine structure (EXAFS) region (B) is displayed for the same Site 1 unreacted (i) and MBM biochar reacted (ii) soils. Linear combination model parameters are given in Table 5.3.

Table 5.3. Percent contributions of components in linear combination (LC) models of EXAFS from Site 1 soil before and after reaction with meat and bone meal (MBM) biochar at pH 6.1 ± 0.1 for 30 d.

Soil Core	Zn species						
	Franklinite	Sphalerite	Hopeite	Ads. MBM biochar	Zn-Al HIM	Ads. Mont.	Sum of components
	%†						
Site 1	66	17	-	-	-	15	98
Site 1 treated	44	-	-	25	18	15	102
Site 1 treated, uXANES Point B	34	-	40	-	26	-	100

† LC modeling was performed using a maximum of four standards in χ (k) space, allowing components to not be constrained to 100%.

The choice of MBM biochar standard versus hopeite standard in linear combination models was difficult to distinguish because of similar XANES (Figure 5.2, top) and EXAFS features and a general difficulty in modeling minor Zn components in the presence of franklinite (Jacquat et al., 2009). Hopeite provided the best fit in the μXANES, but the μXANES measurement was also restricted to areas of high density fluorescence to ensure sufficient data quality; this may also be more likely to measure hopeite. In the LC modeling of EXAFS, the use of Zn adsorbed on MBM as a standard provided similar fit to a combination of hopeite and Zn adsorbed on montmorillinite as an outer-sphere complex. The increased contribution of Zn on montmorillonite necessary when using hopeite standard is not consistent with the absence of change in $CaCl_2$-extractable Zn after treatment; this was the justification for favoring a Zn adsorbed MBM component. Because both standards are so similar, both species may indeed be present in the reacted soil and this should be considered a possibility. The use of either standard indicates the direct interaction between Zn and phosphate, thus confirming that the MBM reacted directly with Zn in the Site 1 soil.

5.5 Conclusion

After being shaken in suspension with MBM biochar, Zn speciation changed in three of the four soils studied (Sites 1, 3, and 4), but only Site 1 showed a direct Zn-PO_4 association via XAS. So, despite suspension conditions at a pH, aqueous Zn concentration

and reaction time optimal for adsorption onto MBM biochar (Chapter 4), the MBM biochar did not adsorb Zn or induce precipitation of hopeite in the soils from Site 2, 3, or 4. Extractable Zn in the three control soils showed a trend: Site 1 > Site 2 > Site 4 ≈ Site 3. This higher mobility of Zn in the Site 1 soil may be an important factor for its reaction with the MBM biochar.

Linear combination modeling of the Site 1 reacted soil was best fit with a ~25% Zn adsorbed MBM component. Despite some uncertainty between the Zn species in treated soil between hopeite and MBM biochar adsorption, there is convincing evidence that one or both species are significant component(s) after treatment with MBM biochar. This confirms the presence of a direct reaction of MBM biochar with Zn in Site 1 soil from the Flin Flon/Creighton area.

6.0 SYNTHESIS AND CONCLUSIONS

HudBay Minerals Inc., formerly Hudson Bay Mining and Smelting Co. Limited, have been operating smelter facilities in the Flin Flon/Creighton area from 1930 until closure in 2010. The smelting and refining complex extracted copper (Cu), zinc (Zn) and cadmium (Cd) through heating and chemical treatments of sulphide ore, producing emissions of sulfur dioxide (SO_2) and particulates containing Zn, Cu, lead (Pb), arsenic (As), Cd and mercury (Hg). The landscape surrounding the smelting stack has experienced vegetation loss common to non-ferrous smelters due to natural and anthropogenic sources of stress (Kozlov and Zvereva, 2007). The Department of Soil Science at the University of Saskatchewan, together with HudBay Minerals Inc., initiated a multi-disciplinary project to assess options for revegetating the impacted landscape surrounding the smelter. The project commenced in 2008 with a soil survey of the area and began to develop soil treatment strategies to increase revegetation success.

A locally-sourced meat and bone meal (MBM) biochar was of interest because of its proven plant growth response in preliminary screenings (Farrell, unpublished, 2011) and potential for metal immobilization due to the phosphate content of its minerals (Hodson et al., 2001; Smiciklas et al., 2008; Dybowska et al., 2009). Meat and bone meal (MBM) has been suggested for re-use as a readily available source of the calcium phosphate mineral, hydroxyapatite (HAP) (Deydier et al., 2005), which has shown immobilizing effects on multiple metals (Zn, Cu, Cd, Pb) in metal contaminated soil and water (Hodson et al., 2001; Smiciklas et al., 2008; Dybowska et al., 2009).

At high concentrations and acidic soil conditions, Zn can be highly toxic to plants due to its mobility in soil solution (Chaney, 1993). This property of Zn combined with the high total soil Zn concentrations and acidic conditions of Flin Flon/Creighton soil gave reason to test the phytotoxicity of Zn and its mobility in soils despite the common co-contamination of Cu, Cd, As, and Pb. Soil toxicity studies weighed the influence of each contaminant in the

smelter-impacted soils and identified Zn as the primary restriction to plant growth (Sicilano, unpublished 2010).

The overall objective of this thesis is to identify whether the MBM biochar is directly influencing Zn speciation after its amendment to a smelter-impacted soil. The first objective was characterization of the MBM biochar and identification of the main mineral and organic components. Based on knowledge of the physico-chemical characteristics of MBM biochar, this knowledge of the material allows for it to be studied as an adsorbent and to explain the reactivity as a function of pH, Zn concentration, and time. Measurement of x-ray absorption spectroscopy (XAS) spectra allow for mechanistic interpretation of the adsorption reaction by using multi-shell theoretical EXAFS modeling. The mechanistic knowledge enables its use as a standard spectrum for use in modeling Zn speciation in more heterogeneous systems such as soils. The technique of K-edge XAS was used to identify Zn speciation change in soils treated with MBM biochar and inclusion of the previously measured mechanism can serve as proof for the presence/absence of direct interaction between Zn and MBM biochar.

The MBM biochar used in this study was sourced from industrial partner, Titan Clean Energy, Inc. (Craik, SK). Meat and bone meal biochar was produced using pyrolysis conditions by heating a MBM material at 20°C min^{-1} to a highest heating temperature of 900°C and then immediately cooling the residue at 40°C min^{-1} by running cool water through adjacent pipes. This produced a MBM biochar with physicochemical characteristics such as the material's high external surface area, charred organics and presence of minor carbonate substitution in the HAP mineral.

The main component of MBM biochar was the mineral HAP, which has been found for heat-treated residues of similar MBM sources (Deydier et al., 2005; Etok et al., 2007; Coutand et al., 2008; Sobczak et al., 2009). When MBM biochar was maintained in a strong-electrolyte-washed suspension (0.1 M $NaNO_3$), the solution was generally alkaline, forming a solution pH of 8.6. Meat and bone meal biochar stability is highly sensitive to pH and will buffer the solution to pH 6.3. The adsorption pH experiments demonstrated that below pH 6.3, a Ca mineral in the MBM biochar will begin to dissolve, as evidenced by release of Ca into solution.

The pH buffering properties of MBM biochar has implications for its use as a soil amendment in the Flin Flon/Creighton area. When applied to the acidic soil (pH 3.5–4.5)

MBM biochar will act as a liming agent and may dissolve. After application of MBM biochar to soils in Chapter 5, pH was measured and adjusted to 6.1 ± 0.1 every 3 d and trends were observed. Initially, a strong liming effect necessitated the use of acid titration (0.1 M HNO_3), after 10 d, the pH remained stable near 6.1 ± 0.1, after 20 d of reaction, all soils required base (0.1 M NaOH) to be maintained at pH 6.1 ± 0.1 and after 23 d, only the single samples from each soil that had received base titration were maintained at 6.1, the other soils became buffered to 5.5. If the soil pH is maintained above MBM biochar solubility, the sorbent properties of MBM biochar become relevant and if the soil acidity exceeds the MBM biochar solubility, Zn phosphate minerals such as hopeite become relevant.

Adsorption experiments indicated that MBM biochar has a moderately-high affinity for Zn adsorption in a model system and reacted in a similar capacity and mechanism as the synthesized HAP. The kinetics indicate adsorption in a biphasic reaction, with adsorption to phosphate groups occurring rapidly, followed by diffusion-limited adsorption. This interpretation was supported by the increase in adsorption capacity after sonication pre-treatment to MBM biochar in adsorption experiments. The multi-shell theoretical EXAFS models of adsorption samples identified the mechanism of adsorption as monodentate bonding onto a phosphate group in a tetrahedral coordination. This mechanistic information is useful to predict the stability of the inner-sphere bond between Zn and phosphate. Adsorption of Zn on to the HAP surface may be the precursor to the widely reported Zn-phosphate precipitation in other amendment studies, but a reaction time longer than 3 d is needed to confirm this.

Recommendations for improving the adsorption properties of this MBM biochar include: (i) exclusion of the willow component and (ii) sonication or other dispersion pretreatment to disrupt aggregation, which will improve Zn adsorption capacity, possibly by reducing kinetic limitations and increasing the reactive surface area. Further studies should investigate whether field application utilizing these pretreatments on MBM biochar are (a) practical and (b) produce similar reduction of aqueous Zn as predicted from this study.

When a series of soils collected from Flin Flon were shaken in a suspension with MBM biochar (10% w/w) at pH 6.1 ± 0.1 for 30 d, three of the four soils showed a significant change in Zn speciation, but only one showed a Zn speciation change related to Zn-phosphorus interactions. Site 1 did show a definite association between Zn and

phosphorus, thus confirming the hypothesis that MBM biochar will directly react with Zn when added to soil at a pH of 6.1 ± 0.1. The mechanism of this reaction is less clear because μXRF mapping and μXANES only identified hopeite in the soil. It should be considered that each species is present but MBM biochar is the main species. The only soil that reacted with MBM biochar had a large component of weathered Zn species at depth (Hamilton, unpublished data, 2013), which is supported by the large fraction of $CaCl_2$-exchangeable Zn in a bulked soil from the same core (10-cm of core sampling would include both surface and depth measured in Hamilton's thesis). This reactive soil was separate from the others tested due to the fact that it had more than 200 mg L^{-1} extractable Zn and more than 10% of the total Zn in the $CaCl_2$-extractable fraction. This suggests that there may be a threshold of labile Zn that Site 1 exceeded (while the others did not) that allowed for reaction with MBM biochar. The co-occurance of a hopeite precipitate and adsorption onto MBM char is possible because at pH 6.1 ± 0.1, a Zn phosphate mineral was interpreted to precipitate when MBM biochar had acidification pre-treatment but an adsorption species occurred when the MBM biochar was untreated, indicating two possible mechanisms at pH 6.1 ± 0.1 depending on the surface alteration of MBM biochar by low pH.

The results of this study suggest that a more complicated reaction is occurring in soil than adsorption experiments with the MBM biochar can predict in single-element sorption systems. A full explanation of causative factors for reactivity between soils and MBM biochar is outside the scope of this project, but trends have been noticed in the soil characteristics that should be studied in future work. Site 1 (reactive site) had a lower percent organic carbon (OC), higher extractable Zn pool and low clay content. The low cation exchange capacity (low OC and low clay) may leave a cation exchange deficit that MBM biochar can supplement. Soils that were not MBM biochar reactive, on the other hand, either had more clay or a greater percentage of OC, or the Zn was primarily in forms that were insoluble (e.g., the smelter derived minerals franklinite and sphalerite). Site 3 and 4 each showed minor change in Zn speciation but the speciation shift to clay mineral associations indicate that this is a result of raising the pH to 6.1 ± 0.1 instead of any relation to the MBM biochar. Zn-phosphate standards provided poor LC fits to both Site 3 and 4 reacted soils.

It is possible that additional standards would improve the LC fits, despite this study's efforts to include novel sorption standards. Future studies would benefit from including a

MBM biochar sample that has been reacted with Zn for the same reaction time as the soil treatments, instead of the relatively short-term of 48-h used in this study. The Ca-Zn phosphate mineral, scholzite, has also been used as a standard in similar studies and may be useful in this study as a relevant standard (Baker et al., 2012).

Future work should also consider a control treatment to each soil where pH is adjusted to 6.1 ± 0.1 without MBM biochar addition. This would allow isolation of pH effects and could clarify any direct Zn interactions with MBM biochar. A large amount of outer-sphere Zn was observed in the bulk Zn XAS of the soil; performing bulk Zn speciation after a $CaCl_2$ extraction may improve results because removal of outer-sphere Zn will allow other sorption species to be more apparent in XAS.

The reactivity of MBM biochar at each site has implications for Zn speciation at the tree planting locations. The immobilization of Zn at Site 1 may result in reduced Zn uptake by the trees and lower metal stress may result in healthier tree establishment. Future work should involve soil sampling from the tree plantings to measure Zn speciation as Zn-MBM adsorption species or hopeite species may form.

In conclusion, MBM biochar has a moderately-high affinity for Zn adsorption in a model system and reacted much like a synthesized HAP (i.e., by monodentate adsorption to phosphate). This suggests that the MBM biochar has potential as a soil amendment for use in accelerating revegetation in the smelter-impacted soils of Flin Flon, MB and Creighton, SK.

REFERENCES

Adams, P.B. and W.O. Passmore. 1966. Critical factors in the determination of alkaline earth elements in glass by atomic absorption spectrometry. Anal. Chem. 38:630-633.

Adriano, M.V. 2001. Zinc in Plants. In: R. Amils, C. Ellis-Evans and H. Hinghofer-Szalkay, editors. Life in Extreme Environments. Springer Netherlands, New York, NY. p. 644–651.

Al-Maydama, H.M.A., P.J. Gardner, and I.W.McAra. 1992. The standard enthalpies of formation of zinc orthophosphate and its hydrates. Thermochimic Acta 194:117–127.

Anderson, J.A.H., M.J. Hooper, J.C. Zak and S.B. Cox. 2009. Characterization of the structural and functional diversity of indigenous soil microbial communities in smelter impacted and nonimpacted soils. Environ. Toxicol. Chem. 28:534–541.

Arias M., C. Perez-Novo, E. Lopez and B. Soto. 2006. Competitive adsorption and desorption of copper and zinc in acid soils. Geoderma 133:151–159.

Atanassova, I. 1999. Competitive effect of copper, zinc, cadmium and nickel on ion adsorption and desorption by soil clays. Water Air Soil Poll. 113:115–125.

Ayllon, M., G. Gea, M.B. Murillo, J.L. Sanchez and J. Arauzo. 2004. Kinetic study of meat and bone meal pyrolysis: An evaluation and comparison of different possible kinetic models. J. Anal. Appl. Pyrol. 74:445–453.

Ayllon, M., M. Aznar, J.L. Sanchez, G. Gea and J. Arauzo. 2006. Influence of temperature and heating rate on the fixed bed pyrolysis of meat and bone meal. Chem. Eng. J. 121:85–96.

Babel, S. and T.A. Kurniawan. 2003. Low-cost adsorbents for heavy metals uptake from contaminated water: a review. J. Hazard. Mater. 97:219–243.

Baddiel, C.B. and E.E. Berry. 1966. Spectra structure correlations in hydroxyl and fluorapatite. Spectrochim. Acta 22:1407–1416.

Baes, C.F. and R.E. Mesmer. 1976. The hydrolysis of cations. Wiley. New York, NY. p.489.

Baig, A.A., J.L. Fox, R.A. Young, Z. Wang, J. Hsu, W.I. Higuchi, et al. 1999. Relationships among carbonated apatite solubility, crystallite size, and microstrain parameters. Calcif. Tissue Int. 64:437–449.

Baker, D. E. and M. C. Amacher. 1982. Nickel, copper, zinc, and cadmium. Pages 323–336 in A. L. Page, R. H. Miller, and D. R. Keeney, eds. Methods of soil analysis. Part 2. Chemical and micro-biological properties. Agronomy Monograph no. 9. 2nd ed. ASA-SSSA. Madison, WI.

Baker, L.R., G.M. Pierzynski, G.M. Hettiarachchi, K.G. Scheckel and M. Newville. 2012. Zinc speciation in proximity to phosphate application points in a lead/zinc smelter-contaminated soil. J. Environ. Qual. 41:1865–1873.

Barrea, R.A., C.A. Perez, A.Y. Ramos, H.J. Sanchez and M. Grenon. 2003. Distribution and incorporation of zinc in biological calcium phosphates. X-Ray Spectrom. 32:387–395.

Basta, N. and R. Gradwohl. 2000. Estimation of Cd, Pb, and Zn bioavailability in smelter-contaminated soils by a sequential extraction procedure. J. Soil Contam. 9:149–164.

Basta, N.T. and S.L. McGowen. 2004. Evaluation of chemical immobilization treatments for reducing heavy metal transport in a smelter-contaminated soil. Environ. Pollut. 127:73–82.

Basta, N.T., R. Gradwohl, K.L. Snethen and J.L. Schroder. 2001. Chemical immobilization of lead, zinc, and cadmium in smelter-contaminated soils using biosolids and rock phosphate. J. Environ. Qual. 30:1222–1230.

Bazin, D., X. Carpentier, I. Brocheriou, P. Dorfmuller, S. Aubert, C. Chappard, et al. 2009. Revisiting the localisation of Zn2+ cations sorbed on pathological apatite calcifications made through X-ray absorption spectroscopy. Biochimie 91: 1294–1300.

Beesley, L. and M. Marmiroli. 2011. The immobilisation and retention of soluble arsenic, cadmium and zinc by biochar. Environ. Pollut. 159:474–480.

Beesley, L., E. Moreno-Jimenez and J.L. Gomez-Eyles. 2010. Effects of biochar and greenwaste compost amendments on mobility, bioavailability and toxicity of inorganic and organic contaminants in a multi-element polluted soil. Environ. Pollut. 158:2282–2287.

Beesley, L., E. Moreno-Jimenez, J.L. Gomez-Eyles, E. Harris, B. Robinson and T. Sizmur. 2011. A review of biochar's potential role in the remediation, revegetation and restoration of contaminated soils. Environ. Poll. 159:3269–3282.

Bhatnaga.V.M. 1967. IR-spectra of fluorapatite and fluorchlorapatite. Experientia 23:10–12.

Boisson, J., A. Ruttens, M. Mench and J. Vangronsveld. 1999. Evaluation of hydroxyapatite as a metal immobilizing soil additive for the remediation of polluted soils. Part 1. Influence of hydroxyapatite on metal exchangeability in soil, plant growth and plant metal accumulation. Environ. Pollut. 104:225–233.

Bradl, H.B. 2004. Adsorption of heavy metal ions on soils and soils constituents. J. Colloid Interf. Sci. 277:1–18.

Cances, B., M. Ponthieu, M. Castrec-Rouelle, E. Aubry and M.F. Benedetti. 2003. Metal ions speciation in a soil and its solution: experimental data and model results. Geoderma 113:341–355.

Cantle, J.E. 1982. Atomic absorption spectrometry. Vol. 5. Elsevier,New York: Elsevier Science Limited. p. 70.

Cao, R.X., L.Q. Ma, M. Chen, S.P. Singh and W.G. Harris. 2003. Phosphate-induced metal immobilization in a contaminated site. Environ. Pollut. 122:19–28.

Cao, X.D., L.Q. Ma, M. Chen, S.P. Singh and W.G. Harris. 2002. Impacts of phosphate amendments on lead biogeochemistry at a contaminated site. Environ. Sci. Technol. 36:5296–5304.

Carlos Moreno, J., R. Gomez and L. Giraldo. 2010. Removal of Mn, Fe, Ni and Cu Ions from wastewater using cow bone charcoal. Materials 3:452–466.

Carroll, S.A., P.A. O'Day and M. Piechowski. 1998. Rock−water interactions controlling zinc, cadmium, and lead concentrations in surface waters and sediments, U.S. tri-state mining district. 2. geochemical interpretation. Environ. Sci. Technol. 32:956–965.

Chaala, A. and C. Roy. 2003. Recycling of meat and bone meal animal feed by vacuum pyrolysis. Environ. Sci. Technol. 37:4517–4522.

Chaney, R.L. 1993. Proceedings of the International Symposium on 'Zinc in Soils and Plants' Held at The University of Western Australia, 27–28 September, 1993 pgs. 136–139. Editor A.D. Robson.

Chaney, R.L. 1993. Zinc phytotoxicity. In: A.D. Robson, editor, Zinc in soils and plants. Kluwer Academic, Dordrecht, the Netherlands. p. 135–150.

Chaney, R.L., M. Malik, Y.M. Li, S.L. Brown, E.P. Brewer, J.S. Angle, and A.L.M. Baker. 1997. Phytoremediation of soil metals. Curr. Opin. Biotech.. 8:279–284.

Chen, J.-H., Y.-J. Wang, D.-M. Zhou, Y.-X. Cui, S.-Q. Wang and Y.-C. Chen. 2010. Adsorption and desorption of Cu(II), Zn(II), Pb(II), and Cd(II) on the soils amended with nanoscale hydroxyapatite. Environ. Prog. Sustain. Energy 29:233–241.

Chen, S.B., Y.G. Zhu, Y.B. Ma and G. McKay. 2006. Effect of bone char application on Pb bioavailability in a Pb-contaminated soil. Environ. Pollut. 139:433–439.

Chen, X.B., J.V. Wright, J.L. Conca and L.M. Peurrung. 1997. Effects of pH on heavy metal sorption on mineral apatite. Environ. Sci. Technol. 31:624–631.

Chen, X.B., J.V. Wright, J.L. Conca and L.M. Peurrung. 1997. Evaluation of heavy metal remediation using mineral apatite. Water Air Soil Poll. 98:57–78.

Cheung, C.W., J.F. Porter and G. McKay. 2000. Sorption kinetics for the removal of copper and zinc from effluents using bone char. Sep. Purif. Technol. 19:55–64.

Cheung, C.W., J.F. Porter and G. McKay. 2002. Removal of Cu(II) and Zn(II) ions by sorption onto bone char using batch agitation. Langmuir 18:650–656.

Choy, K.K.H., D.C.K. Ko, C.W. Cheung, J.F. Porter and G. McKay. 2004. Film and intraparticle mass transfer during the adsorption of metal ions onto bone char. J. Colloid Interf. Sci. 271:284–295.

Chrysochoou, M., D. Dermatas and D.G. Grubb. 2007. Phosphate application to firing range soils for Pb immobilization: The unclear role of phosphate. J. Hazard. Mater. 144:1–14.

Conyers, M.K. and B.G. Davey. 1988. Observations on some routine methods for soil-pH determination. Soil Sci. 145:29–36.

Corami, A., S. Mignardi and V. Ferrini. 2007. Copper and zinc decontamination from single- and binary-metal solutions using hydroxyapatite. J. Hazard. Mater. 146:164–170.

Cotter-Howells, J. and S. Caporn. 1996. Remediation of contaminated land by formation of heavy metal phosphates. Appl. Geochem. 11:335–342.

Coutand, M., M. Cyr, E. Deydier, R. Guilet and P. Clastres. 2008. Characteristics of industrial and laboratory meat and bone meal ashes and their potential applications. J. Hazard. Mater. 150:522–532.

Das, S. and M.J. Hendry. 2011. Changes of crystal morphology of aged goethite over a range of pH (2–13) at 100 °C. Appl. Clay Sci. 51:192–197.

de Jong, W., G. Di Nola, B.C.H. Venneker, H. Spliethoff and M.A. Wojtowicz. 2007. TG-FTIR pyrolysis of coal and secondary biomass fuels: Determination of pyrolysis kinetic parameters for main species and NOx precursors. Fuel 86:2367–2376.

Degryse, F., A. Voegelin, O. Jacquat, R. Kretzschmar and E. Smolders. 2011. Characterization of zinc in contaminated soils: Complementary insights from isotopic exchange, batch extractions and XAFS spectroscopy. Eur. J. Soil Sci. 62:318–330.

Deydier, E, R. Guiliet and P. Sharrock. 2003. Beneficial use of meat and bone meal combustion residue: “An efficient low cost material to remove lead from aqueous effluent”. J. Hazard. Mater. 101:55–64.

Deydier, E., R. Guilet, S. Sarda and P. Sharrock. 2005. Physical and chemical characterisation of crude meat and bone meal combustion residue: "Waste or raw material?". J. Hazard. Mater. 121:141–148.

Dimovic, S., I. Smiciklas, I. Plecas, D. Antonovic and M. Mitric. 2009. Comparative study of differently treated animal bones for Co(II) removal. J. Hazard. Mater. 164:279–287.

Dudka, S. and D.C. Adriano. 1997. Environmental impacts of metal ore mining and processing: a review. J Environ Qual 26:590–602.

Dybowska, A., D.A.C. Manning, M.J. Collins, T. Wess, S. Woodgate and E. Valsami-Jones. 2009. An evaluation of the reactivity of synthetic and natural apatites in the presence of aqueous metals. Sci. Total Environ. 407:2953–2965.

Elzinga, E.J. and R.J. Reeder. 2002. X-ray absorption spectroscopy study of Cu(II) and Zn(II) adsorption complexes at the calcite surface: Implications for site-specific metal incorporation preferences during calcite crystal growth. Geochim. Cosmochim. Ac. 66:3943–3954.

Etok SE, Valsami-Jones E, Wess TJ, Hiller JC, Maxwell CA, Rogers KD, 2007. Structural and chemical changes of thermally treated bone apatite. J. Mater. Sci. 42:9807–9816.

Fellet, G., L. Marchiol, G. Delle Vedove and A. Peressotti. 2011. Application of biochar on mine tailings: Effects and perspectives for land reclamation. Chemosphere 83:1262–1267.

Feng, X.H., L.M. Zhai, W.F. Tan, F. Liu and J.Z. He. 2007. Adsorption and redox reactions of heavy metals on synthesized Mn oxide minerals. Environ. Pollut. 147:366–373.

Fleet, M.E. and X.Y. Liu. 2009. Calcium L-2,L-3-edge XANES of carbonates, carbonate apatite, and oldhamite (CaS). Am. Mineral. 94:1235–1241.

Fleet, M.E., X.Y. Liu and P.L. King. 2004. Accommodation of the carbonate ion in apatite: An FTIR and X-ray structure study of crystals synthesized at 2–4 GPa. Am. Mineral. 89:1422–1432.

Franzin, W.G., G.A. McFarlane and A. Lutz. 1979. Atmospheric fallout in the vicinity of a base metal smelter at Flin Flon, Manitoba. Environ. Sci. Technol. 13:1513–1522.

Ginocchio, R. 2000. Effects of a copper smelter on a grassland community in the Puchuncavi Valley, Chile. Chemosphere 41:15–23.

Gunn, J., W. Keller, J. Negusanti, R. Potvin, P. Beckett and K. Winterhalder. 1995. Ecosystem recovery after emission reductions: Sudbury, Canada. Water Air Soil Poll. 85: 1783–1788.

Gunn, J., W. Keller, J. Negusanti, R. Potvin, P. Beckett, and K. Winterhalder. 1995. Ecosystem recovery after emission reductions: Sudbury, Canada. Water Air Soil Poll. 85:1783–1788.

Hashimoto, Y., M. Takaoka, K. Oshita and H. Tanida. 2009. Incomplete transformations of Pb to pyromorphite by phosphate-induced immobilization investigated by X-ray absorption fine structure (XAFS) spectroscopy. Chemosphere 76:616–622.

Hendershot W.H, H. Lalande and M. Duquette. 2008. Ion exchange and exchangeable cations. In M.R. Carter and E.G Gregorich, eds. Soil sampling and methods of analysis. 2nd ed. CRC Press LLC, Boca Raton, FL. p.197–205.

Henderson, P.J., I. McMartin, G.E. Hall, J.B. Percival and D.A. Walker. 1998. The chemical and physical characteristics of heavy metals in humus and till in the vicinity of the base metal smelter at Flin Flon, Manitoba, Canada. Environ. Geol. 34:39–58.

Henke, B.L., E.M. Gullikson and J.C. Davis. 1993. X-ray interactions—Photoabsorption, scattering, transmission, and reflection at E=50–30,000 EV, Z=1–92. Atom. Data Nucl. Data 54:181–342.

Himpsel F.J., U.O. Karlsson, J.F. Morar, D. Rieger and J.A. Yarmoff. 1986. Determination of interface states for CaF_2/Si(111) from near-edge x-ray-absorption measurements. Phys. Rev. Lett. 56:1497–1500.

Hodson, M.E., E. Valsami-Jones and J.D. Cotter-Howells. 2000. Bonemeal additions as a remediation treatment for metal contaminated soil. Environ. Sci. Technol. 34:3501–3507.

Hodson, M.E., E. Valsami-Jones, J.D. Cotter-Howells, W.E. Dubbin, A.J. Kemp, I. Thornton and A. Warren. 2001. Effect of bone meal (calcium phosphate) amendments on metal release from contaminated soils—a leaching column study. Environ. Pollut. 112:233–243.

Hu, W., J. Ma, J.L. Wang and S.M. Zhang. 2012. Fine structure study on low concentration zinc substituted hydroxyapatite nanoparticles. Mat. Sci. Eng. C. 32:2404–2410.

HudBay Minerals Inc. 2010. HudBay Minerals 2010 Corporate Social Responsibility Report.

Ishikawa, K., P. Ducheyne and S. Radin. 1993. Determination of the Ca/P ratio in calcium-deficient hydroxyapatite using x-ray diffraction analysis. J. Mater. Sci. - Mater. Med. 4:165–168.

Jacquat, O., A. Voegelin and R. Kretzschmar. 2009. Local coordination of Zn in hydroxy-interlayered minerals and implications for Zn retention in soils. Geochim. Cosmochim. Ac. 73:348–363.

Jacquat, O., A. Voegelin, F. Juillot and R. Kretzschmar. 2009. Changes in Zn speciation during soil formation from Zn-rich limestones. Geochim. Cosmochim. Ac. 73:5554–5571.

Jaynes, W.F., P.A. Moore and D.M. Miller. 1999. Solubility and ion activity products of calcium phosphate minerals. J. Environ. Qual. 28:530–536.

Jenner, G.A., H.P. Longerich, S.E. Jackson and B.J. Fryer. 1990. ICP-MS – A powerful tool for high-precision trace-element analysis in earth sciences—Evidence from anaylsis of selected USGS reference samples. Chem. Geol. 83:133–148.

Johnson, D., L. Kershaw, A. MacKinnon, and J. Pojar. 1995. Plants of the Western Boreal Forest & Aspen Parkland Lone Pine Publishing, Edmonton, Alberta.

Jones, G. and V. Henderson. 2006. Metal concentrations in soil and produce from gardens in Flin Flon, Manitoba, 2002. Habitat Management and Ecosystem Monitoring Section, Wildlife and Ecosystem Protection Branch, Manitoba Conservation. Winnipeg, MB. Manitoba Conservation Report No. 2006–01. 81 pp.

Joseph, S.D., M. Camps-Arbestain, Y. Lin, P. Munroe, C.H. Chia, J. Hook, L. van Zwieten, S. Kimber, A. Cowie, B.P. Singh, J. Lehmann, N. Foidl, R.J. Smernik, and J.E. Amonette. 2010. An investigation into the reactions of biochar in soil. Aust. J. Soil Res. 48:501–515.

Kabata-Pendias, A. 2004. Soil-plant transfer of trace elements-an environmental issue. Geoderma 122:143–149.

Kabata-Pendias, A. and H. Pendias, 2000. Trace elements in soils and plants. CRC Press, Boca Raton, Florida, USA. P. 132–136.

Kiikkila, O. 2003. Heavy-metal pollution and remediation of forest soil around the Harjavalta Cu-Ni smelter, in SW Finland. Silva Fenn. 37:399–415.

Klug, H.P. and L.E. Alexander. 1974. X-ray diffraction procedures: For polycrystalline and amorphous materials, 2nd Edition., Wiley-Interscience, New York, NY.

Knox, A.S., D.I. Kaplan and M.H. Paller. 2006. Phosphate sources and their suitability for remediation of contaminated soils. Sci. Total Environ. 357:271–279.

Ko, D.C.K., J.F. Porter and G. McKay. 2004. Multicomponent mass transport model for the sorption of metal ions on bone char. Aiche J. 50:2130–2141.

Kozlov, M.V. and E.L. Zvereva. 2007. Industrial barrens: Extreme habitats created by non-ferrous metallurgy. Rev. Environ. Sci. Biotechnol. 6:231–259.

Kumar, G.S., E.K. Girija, A. Thamizhayel, Y. Yokogawa and S.N. Kalkura. 2010. Synthesis and characterization of bioactive hydroxyapatite-calcite nanocomposite for biomedical applications. J. Colloid Interf. Sci. 349:56–62.

Kumpiene, J., A. Lagerkvist and C. Maurice. 2008. Stabilization of As, Cr, Cu, Pb and Zn in soil using amendments—A review. Waste Manage. 28: 215–225.

Lanfranco, A.M., P.F. Schofield, P.J. Murphy, M.E. Hodson, J.F.W. Mosselmans and E. Valsami-Jones. 2003. Characterization and identification of mixed-metal phosphates in soils: the application of Raman spectroscopy. Mineral. Mag. 67:1299–1316.

Lee, Y.J., E.J. Elzinga and R.J. Reeder. 2005. Sorption mechanisms of zinc on hydroxyapatite: Systematic uptake studies and EXAFS spectroscopy analysis. Environ. Sci. Technol. 39:4042–4048.

Legeros, R.Z., O.R. Trautz, E. Klein and J.P. Legeros. 1969. Two types of carbonate substitution in apatite structure. Experientia 25:5–7.

Lehmann, J., J. Gaunt, and M. Rondon. 2006. Bio-char sequestration in terrestrial ecosystems – A review. Mitig. Adapt. Strat. Global Change. 11:403–427.

Li, Y.M., R.L. Chaney, G. Siebielec and B.A. Kerschner. 2000. Response of four turfgrass cultivars to limestone and biosolids-compost amendment of a zinc and cadmium contaminated soil at Palmerton, Pennsylvania. J. Environ. Qual. 29:1440–1447.

Lindsay, W.L. 1972. Zinc in soils and plant nutrition. Adv. Agron. 24:147–186.

Lindsay, W.L. 1979. Chemical equilibria in soils. John Wiley and Sons Ltd. Chichester, Sussex, UK. p. 210–242.

Longerich, H.P., G.A. Jenner, B.J. Fryer and S.E. Jackson. 1990. Inductively coupled plasma-mass spectrometric analysis of geological samples – A critical evaluation based on case studies. Chem. Geol. 83:105–118.

Loos, D., C. Pasel, M. Luckas, K.G. Schmidt and J.D. Herbell. 2004. Experimental investigation and modelling of the solubility of calcite and gypsum in aqueous systems at higher ionic strength. Fluid Phase Equilibr. 219:219–229.

Ludbrook, J. 1991. On making multiple comparisons in clinical and experimental pharmacology and physiology. Clin. Exp. Pharmacol. P. 18:379–392.

Ma, Q.Y., S.J. Traina, T.J. Logan and J.A. Ryan. 1994. Effects of aqueous Al, Cd, Cu, Fe(II), Ni, and Zn on Pb immobilization by hydroxyapatite. Environ. Sci. Technol. 28:1219–1228.

Manceau, A., B. Lanson and V.A. Drits. 2002. Structure of heavy metal sorbed birnessite. Part III: Results from powder and polarized extended x-ray absorption fine structure spectroscopy. Geochim. Cosmochim. Ac. 66:2639–2663.

Manceau, A., B. Lanson, M.L. Schlegel, J.C. Harge, M. Musso, L. Eybert-Berard, J.-L. Hazemann, D. Chateigner and G.M. Lamble. 2000. Quantitative Zn speciation in smelter-contaminated soils by EXAFS spectroscopy. Am. J. of Sci. 300:289–343.

Manceau, A., M.A. Marcus, N. Tamura, O. Proux, N. Geoffroy and B. Lanson. 2004. Natural speciation of Zn at the micrometer scale in a clayey soil using x-ray fluorescence, absorption, and diffraction. Geochim. Cosmochim. Ac. 68:2467–2483.

McBride, M. B. 1994. Trace and toxic elements in soil. In: Environmental chemistry of soils. Oxford University Press, New York. p.308–332.

McGowen, S.L., N.T. Basta and G.O. Brown. 2001. Use of diammonium phosphate to reduce heavy metal solubility and transport in smelter-contaminated soil. J. Environ. Qual. 30:493–500.

McMartin, I., P.J. Henderson and E. Nielsen. 1999. Impact of a base metal smelter on the geochemistry of soils of the Flin Flon region, Manitoba and Saskatchewan. Can. J. Earth Sci. 36:141–160.

McMartin, I., P.J. Henderson, A. Plouffe and R.D. Knight. 2002. Comparison of Cu–Hg–Ni–Pb concentrations in soils adjacent to anthropogenic point sources: Examples from four Canadian sites. Geochem-Explor. Env. A. 2:57–73.

Miyaji, F., Y. Kono and Y. Suyama. 2005. Formation and structure of zinc-substituted calcium hydroxyapatite. Mater. Res. Bull. 40:209–220.

Moore, D.M. and R.C. Reynolds. 1989. X-ray diffraction and the identification and analysis of clay minerals. Oxford University Press, Oxford, UK. p. 5–14.

Moreno-Pirajan, J.C., L. Giraldo and V.S. Garcia-Cuello. 2011. Study of the textural properties of bovine bones char under different conditions. J. Water Resource Prot. 3:176–181.

Mycock, A. 2011. Characterizing organic matter and nutrient status in smelter-affected soils. M.Sc. thesis. University of Saskatchewan, Saskatoon, Saskatchewan.

Nachtegaal, M., M.A. Marcus, J.E. Sonke, J. Vangronsveld, K.J.T. Livi, D. Van der Lelie, et al. 2005. Effects of in situ remediation on the speciation and bioavailability of zinc in a smelter contaminated soil. Geochim. Cosmochim. Ac. 69:4649–4664.

Naftel, S.J., T.K. Sham, Y.M. Yiu and B.W. Yates. 2001. Calcium L-edge XANES study of some calcium compounds. J. Synchrotron Radiat. 8:255–257.

Narasaraju, T.S.B. and D.E. Phebe. 1996. Some physico-chemical aspects of hydroxylapatite. J. Mater. Sci. 31:1–21.

Ndiba, P., L. Axe and T. Boonfueng. 2008. Heavy metal immobilization through phosphate and thermal treatment of dredged sediments. Environ. Sci. & Technology 42:920–926.

Newville, M. 2001. IFEFFIT: Interactive XAFS analysis and FEFF fitting. J. Synchrotron Rad. 8:322–324.

Nriagu, J.O. 1973. Solubility equilibrium constant of alpha-hopeite. Geochim. Cosmochim. Ac. 37:2357–2361.

Panfili, F.R., A. Manceau, G. Sarret, L. Spadini, T. Kirpichtchikova, V. Bert, et al. 2005. The effect of phytostabilization on Zn speciation in a dredged contaminated sediment using scanning electron microscopy, x-ray fluorescence, EXAFS spectroscopy, and principal components analysis. Geochim. Cosmochim. Ac. 69: 2265–2284.

Pang, Y.X. and X. Bao. 2003. Influence of temperature, ripening time and calcination on the morphology and crystallinity of hydroxyapatite nanoparticles. J. Eur. Ceram. Soc. 23:1697–1704.

Park, J.H., N. Bolan, M. Megharaj and R. Naidu. 2011. Comparative value of phosphate sources on the immobilization of lead, and leaching of lead and phosphorus in lead contaminated soils. Sci. Total Environ. 409: 853–860.

Paschke, M.W., E.F. Redente and D.B. Levy. 2000. Zinc toxicity thresholds for important reclamation grass species of the western United States. Environ. Toxicol. Chem. 19:2751–2756.

Peak, D., G.W. Luther and D.L. Sparks. 2003. ATR-FTIR spectroscopic studies of boric acid adsorption on hydrous ferric oxide. Geochim. Cosmochim. Ac. 67:2551–2560.

Peng, C. and M.J. Apps. 1999. Modelling the response of net primary productivity (NPP) of boreal forest ecosystems to changes in climate and fire disturbance regimes. Ecol. Model. 122:175–193.

Peters, F., K. Schwarz and M. Epple. 2000. The structure of bone studied with synchrotron x-ray diffraction, x-ray absorption spectroscopy and thermal analysis. Thermochim. Acta 361:131–138.

Porter, S.K., K.G. Scheckel, C.A. Impellitteri and J.A. Ryan. 2004. Toxic metals in the environment: Thermodynamic considerations for possible immobilization strategies for Pb, Cd, As, and Hg. Crit. Rev. Env. Sci. Tec. 34:495–604.

Posner, A.S. 1969. Crystal chemistry of bone mineral. Physiol. Rev. 49:760–789.

Preston, C.M. and M.W.I. Schmidt. 2006. Black (pyrogenic) carbon: a synthesis of current knowledge and uncertainties with special consideration of boreal regions. Biogeosciences 3:397–420.

Ravel, B. 2001. ATOMS: crystallography for the x-ray absorption spectroscopist. J. Synchrotron Rad. 8:314–316.

Ravel, B. and M. Newville. 2005. ATHENA, ARTEMIS, HEPHAESTUS: data analysis for x-ray absorption spectroscopy using IFEFFIT. J. Synchrotron Radiat. 12:537–541.

Ressler, T. 1998. WinXAS: a program for x-ray absorption spectroscopy data analysis under MS-Windows. J Synchrotron Rad. 5:118–122.

Rey, C., B. Collins, T. Goehl, I.R. Dickson and M.J. Glimcher. 1989. The carbonate environment in bone mineral – A resolution-enhanced fourier-transform infrared-spectroscopy study. Calcif. Tissue Int. 45:157–164.

Rey, C., V. Renugopalakrishnan, B. Collins and M.J. Glimcher. 1991. Fourier-transform infrared spectroscopic study of the carbonate ions in bone-mineral during aging. Calcif. Tissue Int. 49:251–258.

Roberts, D.R., A.C. Scheinost and D.L. Sparks. 2002. Zinc speciation in a smelter-contaminated soil profile using bulk and microspectroscopic techniques. Environ. Sci. Technol. 36:1742–1750.

Roberts, D.R., R.G. Ford and D.L. Sparks. 2003. Kinetics and mechanisms of Zn complexation on metal oxides using EXAFS spectroscopy. J. Colloid Interf. Sci. 263:364–376.

Rogers K.D. and P. Daniels. 2002. An x-ray diffraction study of the effects of heat treatment on bone mineral microstructure. Biomaterials 23:2577–2585.

Ruby, M.V., A. Davis and A. Nicholson. 1994. In-situ formation of lead-phosphates in soils as a method to immobilize lead. Environ. Sci. Technol. 28:646–654.

Ryser, A.L., D.G. Strawn, M.A. Marcus, S. Fakra, J.L. Johnson-Maynard and G. Moller. 2006. Microscopically focused synchrotron x-ray investigation of selenium speciation in soils developing on reclaimed mine lands. Environ. Sci. Technol. 40:462–467.

Sarret, G., A. Manceau, L. Spadini, J.C. Roux, J.L. Hazemann, Y. Soldo, L. Eybert-Berard and J.-J. Menthonnex. 1998. Structural determination of Zn and Pb binding sites in Penicillium chrysogenum cell walls by EXAFS spectroscopy. Environ. Sci. Technol. 32:1648–1655.

Sarret, G., J. Balesdent, L. Bouziri, J.M. Garnier, M.A. Marcus, N. Geoffroy, F. Panfilli and A. Manceau. 2004. Zn speciation in the organic horizon of a contaminated soil by micro-x-ray fluorescence, micro- and powder-EXAFS spectroscopy, and isotopic dilution. Environ. Sci. Technol. 38:2792–2801.

Scheidegger, A.M., G.M. Lamble and D.L. Sparks. 1997. Spectroscopic evidence for the formation of mixed-cation hydroxide phases upon metal sorption on clays and aluminum oxides. J. Colloid Interf. Sci. 186:118–128.

Scheinost, A.C., R. Kretzschmar, S. Pfister and D.R. Roberts. 2002. Combining selective sequential extractions, x-ray absorption spectroscopy, and principal component analysis for quantitative zinc speciation in soil. Environ. Sci. Technol. 36:5021–5028.

Schnitzer, M. 1969. Reactions between fulvic acid, a soil humic Compound and inorganic soil constituents. Soil Sci. Soc. Am. J. 33:75–81.

Sheha, R.R. 2007. Sorption behavior of Zn(II) ions on synthesized hydroxyapatites. J. Colloid Interf. Sci. 310:18–26.

Sigg, L. and W. Stumm. 1981. The interaction of anions and weak acids with the hydrous goethite (alpha-FeOOH) surface. Colloid. Surface. 2:101–117.

Smiciklas, I., A. Onjia, S. Raicevic, D. Janackovic and M. Mitric. 2008. Factors influencing the removal of divalent cations by hydroxyapatite. J. Hazard. Mater. 152:876–884.

Smiciklas, I., S. Dimovic, M. Sljivic and I. Plecas. 2008. The batch study of Sr(II) sorption by bone char. J. Environ. Sci. Health A Tox. Hazard Subst. Environ. Eng. 43:210–217.

Sneddon, I.R., M. Orueetxebarria, M.E. Hodson, P.F. Schofield and E. Valsami-Jones. 2006. Use of bone meal amendments to immobilise Pb, Zn and Cd in soil: A leaching column study. Environ. Pollut. 144:816–825.

Sneddon, I.R., M. Orueetxebarria, M.E. Hodson, P.F. Schofield and E. Valsami-Jones. 2008. Field trial using bone meal amendments to remediate mine waste derived soil contaminated with zinc, lead and cadmium. Appl. Geochem. 23:2414–2424.

Sobczak, A., Z. Kowalski and Z. Wzorek. 2009. Preparation of hydroxyapatite from animal bones. Acta Bioeng. Biomech. 11:23–28.

Sohi, S.P., E. Krull, E. Lopez-Capel and R. Bol. 2010. A review of biochar and its use and function in soil. Adv. Agron. 105:47–82.

Sparks, D.L. 2003. Sorption Phenomena on Soils. *In*: C.R. Crumly Editor. Environmental Soil Chemistry. Elsevier Press, San Diego, CA. p. 147–152.

Sparks, D.L., T.H. Carski, S.E. Fendorf and C.V. Toner. 1996. Methods of Soil Analysis Part 3 Chemical Methods. In: J.M. Bartels et al., eds. SSSA Book Series:5. Soil Science Society of America, Inc. Madison, WI. p.1275–1285.

Sposito, G. 1989. Inorganic and Organic Solute Adsorption in Soils. *In*: E.A. Paul and F.E. Clark, editors. The Surface Chemistry of Soils. Oxford University Press, New York, NY. p. 234–241.

Stauffer, M.R. 1974. Geology of Flin Flon area—New look at Sunless City. Geosci. Can. 1:30–35.

Stefanova, V., V. Kmetov and A. Canals. 2003. Application of internal standardization in ICP–QMS through discrete sample introduction methodologies. J. Anal. Atom. Spectrom. 18:1171–1174.

Stoetzel, C., F.A. Mueller, F. Reinert, F. Niederdraenk, J.E. Barralet and U. Gbureck. 2009. Ion adsorption behaviour of hydroxyapatite with different crystallinities. Colloid. Surface. B. 74:91–95.

Storm, G.L., G.J. Fosmire and E.D. Bellis. 1994. Persistence of metals in soil and selected vertebrates in the vicinity of the Palmerton Zinc smelters. J. Environ. Qual. 23:508–514.

Stothart, P. 2011. Facts and figures of the Canadian mining industry. The Mining Association of Canada.

Syme, E.C., S.B. Lucas, A.H. Bailes and R.A. Stern. 1999. Contrasting arc and MORB-like assemblages in the Paleoproterozoic Flin Flon Belt, Manitoba, and the role of intra-arc extension in localizing volcanic-hosted massive sulphide deposits. Can. J. Earth Sci. 36:1767–1788.

Tang, Y.Z., H.F. Chappell, M.T. Dove, R.J. Reeder and Y.J. Lee. 2009. Zinc incorporation into hydroxylapatite. Biomaterials 30:2864–2872.

Terra, J., M. Jiang and D.E. Ellis. 2002. Characterization of electronic structure and bonding in hydroxyapatite: Zn substitution for Ca. Philos. Mag. A. 82:2357–2377.

Tertre, E., D. Pret and E. Ferrage. 2011. Influence of the ionic strength and solid/solution ratio on Ca(II)-for-Na(I) exchange on montmorillonite. Part 1: Chemical measurements, thermodynamic modeling and potential implications for trace elements geochemistry. J. Colloid Interf. Sci. 353:248–256.

Thompson, T.J.U., M. Islam and M. Bonniere. 2013. A new statistical approach for determining the crystallinity of heat-altered bone mineral from FTIR spectra. J. Archaeol. Sci. 40:416–422.

Uchimiya, M., I.M. Lima, K.T. Klasson, and L.H. Wartelle. 2010. Contaminant immobilization and nutrient release by biochar soil amendment: Roles of natural organic matter. Chemosphere 80:935–940.

Uchimiya, M., S. Chang and K.T. Klasson. 2011. Screening biochars for heavy metal retention in soil: Role of oxygen functional groups. J. Hazard. Mater. 190:432–441.

US EPA method 3051. 1994. Microwave-assisted acid digestion of sediments, sludges, soils and oils, Washington, DC.

US EPA report. 2007. The use of soil amendments for remediation, revitilization and reuse. Solid waste and emergency response. Washington, DC.

Van Damme, A., F. Degryse, E. Smolders, G. Sarret, J. Dewit, R. Swennen, et al. 2010. Zinc speciation in mining and smelter contaminated overbank sediments by EXAFS spectroscopy. Geochim. Cosmochim. Ac. 74:3707–3720.

Varian Inc., 1989. Flame atomic absorption spectrometry—Analytical methods. Publication no. 85-100009-00.

Vespa, M., M. Lanson and A. Manceau. 2010. Natural attenuation of Zinc pollution in smelter-affected soil. Environ. Sci. Technol. 44:7814–7820.

Viventsova, E., J. Kumpiene, L. Gunneriusson, and A. Holmgren. 2005. Changes in soil organic matter composition and quantity with distance to a nickel smelter—a case study on the Kola Peninsula, NW Russia. Geoderma 127:216–226.

Vodyanitskii, Y.N. 2010. Zinc forms in soils (Review of publications). Eurasian Soil Sci. 43:269–277.

Voegelin, A., O. Jacquat, S. Pfister, K. Barmettler, A.C. Scheinost and R. Kretzschmar. 2011. Time-dependent changes of zinc speciation in four soils contaminated with zincite or sphalerite. Environ. Sci. Technol. 45:255–261.

Voegelin, A., S. Pfister, A.C. Scheinost, M.A. Marcus and R. Kretzschmar. 2005. Changes in zinc speciation in field soil after contamination with zinc oxide. Environ. Sci. Technol. 39:6616–6623.

Warren, G.P., J.S. Robinson and E. Someus. 2009. Dissolution of phosphorus from animal bone char in 12 soils. Nutr. Cycl. Agroecosys. 84:167–178.

Waterlot, C., C. Pruvot, H. Ciesielski and F. Douay. 2011. Effects of a phosphorus amendment and the pH of water used for watering on the mobility and phytoavailability of Cd, Pb and Zn in highly contaminated kitchen garden soils. Ecol. Eng. 37:1081–1093.

Williams, A.G.B., K.G. Scheckel, G. McDermott, D. Gratson, D. Neptune and J.A. Ryan. 2011. Speciation and bioavailability of zinc in amended sediments. Chem. Spec. Bioavailab. 23:143–154.

Winterhalder, K. 1995. Dynamics of plant communities and soils in revegetated ecosystems: A Sudbury case study, p. 173–182, In J. M. Gunn, ed. Restoration and recovery of an industrial region. Springer-Verlag New York Inc., New York.

Winterhalder, K. 2003. Minimeal amelioration as appropriate technology in the Green Flin Flon/Creighton Project Sudbury 2003 Mining and the Environment, Laurentian University, Sudbury, Ontario Canada.

Xu, Y.P., F.W. Schwartz and S.J. Traina. 1994. Sorption of Zn(II) and Cd(II) on hydroxyapatite surface. Environ. Sci. Technol. 28:1472–1480.

Zasoski R.J. and R.G. Burau. 1978. A technique for studying the kinetics of adsorption in suspensions. Soil Sci. Soc. Am. J. 42:372–374.

Zoltai, S.C. 1988. Distribution of base metals in peat near a smelter at Flin-Flon, Manitoba. Water Air Soil Poll. 37:217–228.

APPENDIX A

A.1 Zn Sorption on Willow Biochar

A willow biochar comparable to that in the MBM biochar (Titan Clean Energy Inc.) was assessed for Zn adsorption as a function of pH in order to assess its importance as a Zn sorbant. A pH envelope for the willow biochar indicated Zn sorption only above pH 7.0 (Fig. A.1), which is in contrast to sorption behavior of Zn on MBM biochar. Both Zn K-edge XANES and EXAFS measured on recovered willow biochar from willow pH adsorption experiments were identified as purely $ZnCO_3$ species (Fig. A.2). Zinc carbonate formation above pH 7.0 has been observed in adsorption experiments with no sorbent (Sheha et al., 2007).

The absence of Zn sorption below pH 7.0 on willow biochar could be attributed to the strong electrolyte (0.1 M $NaNO_3$). If the willow biochar has a low affinity for adsorption, outer-sphere complexation of relatively dilute Zn^{2+} (1.0 mM) may be out-competed by the more concentrated Na^+ ions (0.1 M).

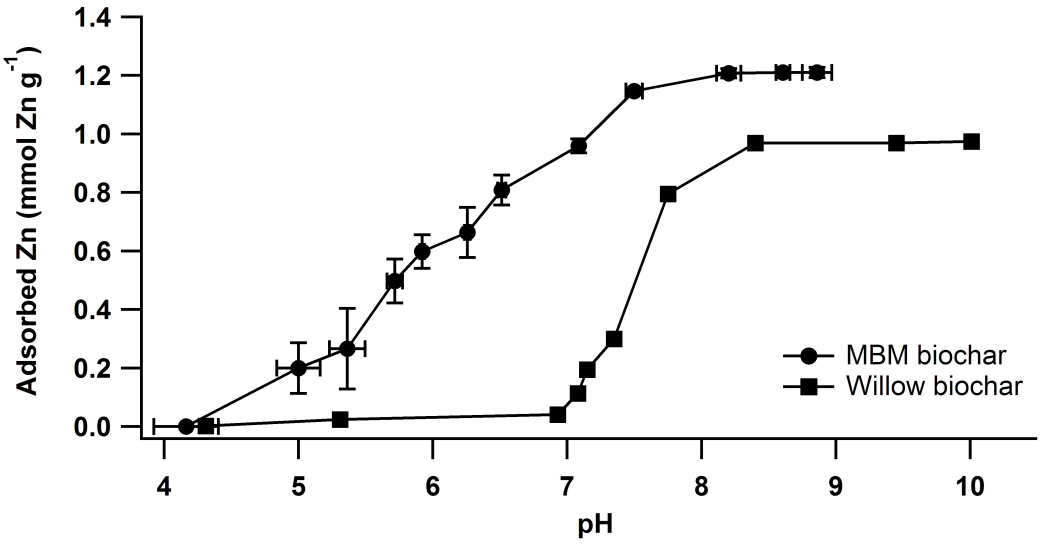

Figure A.1. An adsorption pH envelope showing MBM biochar in solid down arrow points and willow biochar in crosses. Initial Zn concentration in system was 1.0 mM $Zn(NO_3)_2$. Zinc sorption in the willow biochar system is very low until pH 7.0 and reaches complete removal by pH 8.5.

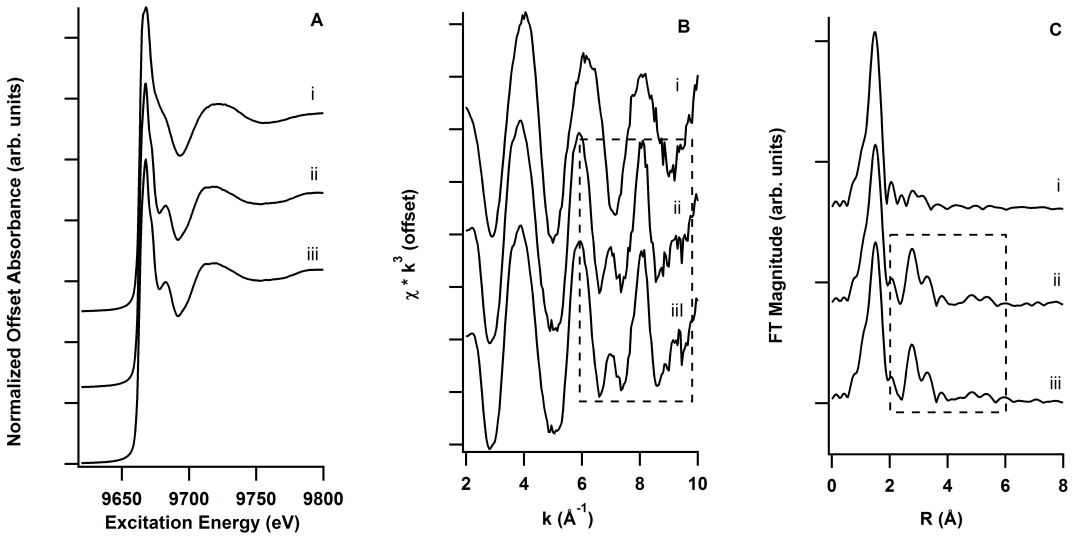

Figure A.2. Zinc K-edge x-ray absorption near edge spectra (XANES) (A), extended x-ray absorption fine structure (EXAFS) and Fourier transform (FT) displaying meat and bone meal (MBM) biochar (i), willow biochar (ii) and a $ZnCO_3$ standard (iii). Each biochar sample was solid recovered from sorption experiments; MBM biochar (pH 6.1) and willow biochar (pH 7.0). Zinc species in willow biochar was identified as purely Zn CO_3 due to the feature match (dashed lines) in the EXAFS and FT spectrum (B,C).

A.2 Hydroxyapatite (HAP) Synthesis

The synthetic HAP prepared for this study was positively identified as HAP by the comparison of their x-ray diffraction patterns (Fig. A.3).

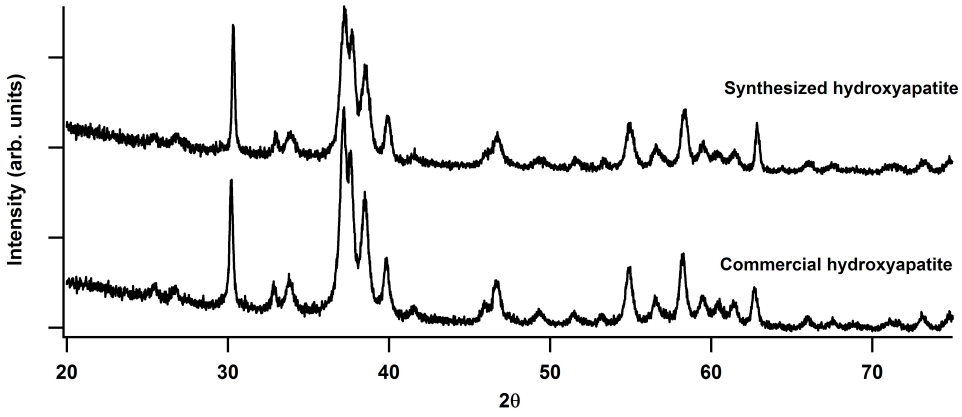

Figure A.3. An x-ray diffraction spectrum of synthetic hydroxyapatite (HAP) prepared in this study and commercial HAP. Synthetic HAP displays peak positions identical to the commercial HAP standard.

APPENDIX B

B.1 Site Photographs

Figure B.1. Site 1. The area had 80% vegetative ground cover consisting of colonial bent grass (*Agrostis capillaris)*. Position was mid-slope on a 2% slope

Figure B.2. Site 2. The area had 0% vegetation cover. Position was in a local depression with occasional water with poor drainage (Specht unpublished data, 2012).

Figure B.3. Site 3. The area had 15% vegetation cover consisting of colonial bent grass (*Agrostis capillaris)*. Position was on mid-slope shoulder (Specht unpublished data, 2012).

Figure B.4. Site 4. The area had a 15% vegetation cover consisting of colonial bent grass (*Agrostis capillaris)*. Postion was a local depression near the top of slope.